

# **Origin of Exocytotic Fusion Pore Dynamics**

Benjamin S. Stratton

Submitted in partial fulfillment of the  
requirements for the degree of  
Doctor of Philosophy  
in the Graduate School of Arts and Sciences

COLUMBIA UNIVERSITY  
2015

© 2015

Benjamin S. Stratton

All rights reserved

## ABSTRACT

### Origin of Exocytotic Fusion Pore Dynamics

Benjamin S. Stratton

Vesicular membrane fusion involves the release of contents in a broad array of biological systems, such as intracellular trafficking, secretion, fertilization, and development. It is also a critical step in the infection of cells by membrane enveloped viruses such as HIV, influenza, and Ebola. SNARE proteins form the core of the fusion machinery in nearly all intracellular fusion processes. The initial complete connection between two fusing membranes is the fusion pore. There is considerable evidence that both the fusion machinery and the biophysical properties of the membranes themselves affect contents release, lipid mixing, and fusion kinetics, but the mechanisms are poorly understood. Flickering of fusion pores during exocytotic release of hormones and neurotransmitters is well documented, but without assays that use biochemically defined components and measure single pore dynamics the contributions from different influences are almost impossible to separate. This thesis examines the biophysical mechanisms by which SNAREs and lipid composition control fusion rates and fusion pore kinetics.

First, we studied fusion pore flickering *in vitro*. We used total internal reflection fluorescence (TIRF) microscopy to quantify fusion pore dynamics *in vitro* and to separate the roles of SNARE proteins and lipid bilayer properties. To interpret the experimental measurements quantitatively, we developed a mathematical model to describe the diffusion of labelled lipids from a vesicle, through a flickering fusion pore, and into a supported bilayer. When small unilamellar vesicles (SUV) bearing neuronal v-SNAREs fused with planar bilayers (SBL) reconstituted with cognate t-SNAREs, lipid transfer rates were

severely reduced, suggesting that pores flickered. We developed an algorithm which included a complete description of fluorophores in the TIRF field. We accounted for the intensity decay of the evanescent TIRF wave normal to the SBL, the polarization of the evanescent TIRF wave, and any potential quenching effects. In general, the first two effects are coupled. This algorithm allowed us to measure the sizes of docked vesicles using fluorescent microscopy.

From the lipid release times we used the model to compute pore openness, the fraction of the time the pore is open, which increased dramatically with cholesterol. For most lipid compositions tested SNARE-mediated and non-specifically nucleated pores had similar openness, suggesting that pore flickering was controlled by lipid bilayer properties. However, with physiological cholesterol levels SNAREs substantially increased the fraction of fully open pores and fusion was so accelerated that there was insufficient time to recruit t-SNAREs to the fusion site, consistent with t-SNAREs being pre-clustered by cholesterol into functional docking and fusion platforms. Our results suggest that cholesterol opens pores directly by reducing the fusion pore bending energy, and indirectly by concentrating a number of SNAREs into individual fusion events.

In the second part of the thesis, I describe my contributions to a project in which a mathematical model was developed to describe the behavior of SNAREpins connecting SUVs of different sizes to a planar membrane. It was necessary to quantify the membrane-membrane and SNAREpin-membrane interaction forces. By combining the well-known van der Waals, electrostatic, and steric-hydration membrane forces with the SNAREpin-membrane-electrostatic interactions I developed a complete description of the membrane forces involved in SUV-SBL fusion. We then combined the description of the interactions

with experimentally measured SNARE zippering energies. We find that the predominant driving forces for membrane fusion, once the SNAREpins have completely zippered, are steric-hydration forces among the SNAREpins and membranes. These forces enlarge a SNAREpin cluster, which in turns pulls the membranes together due to curvature effects.

# CONTENTS

<b>LIST OF FIGURES.....</b>	<b>iv</b>
<b>LIST OF TABLES.....</b>	<b>v</b>
<b>CHAPTER 1- INTRODUCTION.....</b>	<b>1</b>
I- EXOCYTOSIS AND THE FUSION MACHINERY .....	1
II- THE DYNAMIC FUSION PORE .....	7
<b>CHAPTER 2- CHOLESTEROL INCREASES THE OPENNESS OF SNARE-</b>	
<b>MEDIATED FLICKERING FUSION PORES .....</b>	<b>15</b>
I-BACKGROUND .....	15
II-RESULTS .....	18
<i>Single event TIRF based fusion assay.....</i>	<i>18</i>
<i>Retarded lipid release suggests that fusion pores flicker .....</i>	<i>20</i>
<i>Fusion pore openness <math>P_o</math> is quantitatively related to the lipid release time <math>\tau_{release}</math> .....</i>	<i>21</i>
<i>SNARE-mediated fusion pores flicker or are permanently open .....</i>	<i>23</i>
<i>Cholesterol promotes the open state of the fusion pore.....</i>	<i>25</i>
<i>SNARE proteins have little effect on the fusion pore unless physiological levels of</i> <i>cholesterol are present.....</i>	<i>27</i>
<i>With physiological amounts of cholesterol fusion is so accelerated that there is</i> <i>insufficient time to recruit additional t-SNAREs to the fusion site after docking.....</i>	<i>28</i>
<i>Fluorescence reduction factor and vesicle size are unique functions of the docked</i> <i>vesicle intensity .....</i>	<i>30</i>
III-DISCUSSION .....	32

<i>The size of a docked vesicle can be directly inferred from the docked vesicle intensity in TIRFM</i> .....	32
<i>Fusion pores mediated by SNARE proteins flicker rapidly</i> .....	33
<i>Lipid membranes alone sustain flickering pores</i> .....	34
<i>Cholesterol opens fusion pores by lowering the pore bending energy</i> .....	34
<i>Cholesterol promotes fusion by direct membrane effects and by indirect promotion of SNARE-mediated fusion</i> .....	35
METHODS .....	38
APPENDIX- CHAPTER 2 .....	41
<i>Lipid compositions used in this study (details)</i> .....	41
<i>Decomposition of the docking-to-fusion delay time distribution into a fast and a slow component</i> .....	43
<i>Properties of single fluorescent lipids in the SBL</i> .....	46
<i>Analysis of individual fusion events</i> .....	49
<i>Dependence of fusion statistics on vesicle size</i> .....	51
<i>Calculation of relation between pore openness and lipid release time</i> .....	53
<i>Calculation of the number of SNARE complexes at the fusion pore using the t-SNARE recruitment model of ref. [77]</i> .....	61
<i>Dependence of the TIRF fluorescence reduction factor <math>\lambda_{TIRF}</math> on vesicle radius <math>R_{ves}</math>: coupled contributions from incident evanescent intensity decay and polarization effects</i> .....	63
<i>Quantitative model of the effect of cholesterol on the fusion pore bending energy</i> .	66

<b>CHAPTER 3- STUDY OF THE PHOSPHOLIPID MEMBRANE INTERACTIONS IN THE PRESENCE OF SNAREPINS.....</b>	<b>70</b>
I-BACKGROUND.....	70
II-SNAREPIN AND MEMBRANE INTERACTIONS.....	72
III-COLLABORATIVE RESULTS .....	77
<b>BIBLIOGRAPHY .....</b>	<b>82</b>

## List of Figures

<b>Figure 1.1-</b> .....	3
<b>Figure 1.2-</b> .....	7
<b>Figure 1.3-</b> .....	8
<b>Figure 2.1-</b> .....	19
<b>Figure 2.2-</b> .....	26
<b>Figure 2.3-</b> .....	29
<b>Figure 2.4-</b> .....	31
<b>Figure 2.5-</b> .....	36
<b>Figure S1-</b> .....	44
<b>Figure S2-</b> .....	51
<b>Figure S3-</b> .....	53
<b>Figure S4-</b> .....	54
<b>Figure S5-</b> .....	60
<b>Figure S6-</b> .....	67
<b>Figure 3.1-</b> .....	75
<b>Figure 3.2-</b> .....	79
<b>Figure 3.3-</b> .....	80

## List of Tables

<b>Table S1-</b> .....	41
<b>Table S2-</b> .....	42
<b>Table S3-</b> .....	48

## ACKNOWLEDGEMENTS

I would like to thank my advisor, Ben O'Shaughnessy, for all of his time and effort in guiding me in my research. His guidance has been invaluable in completing this work. In the O'Shaughnessy group I have been fortunate to work with Dr. Jason Warner and Dr. Matt Stachowiak for several years, and more recently to work closely with Sathish Thiyagarajan and Hakhamanesh Mostafavi. Thanks to all of them for many fruitful discussions.

I am also in debt to Dr. Erdem Karatekin and his group as a consistent source of experimental data, ideas, and discussion. I would also like to thank members of the Rothman group for discussion of their experimental methods and their experimental data. The experimental work of all of our collaborators made my work much more fruitful.

Finally, thank you to my friends and family. You have all been incredibly supportive and encouraging. Thanks to my parents, thanks to my brother. Thanks especially to Madeline, for your support and understanding throughout this process.

*To my family and friends, who have all supported me in this work.*

## **Chapter 1- Introduction**

Membrane fusion, the merging of two opposing membranes into a single continuous lipid bilayer, is critical for many biological processes such as secretion, fertilization, and intracellular transport [1-3]. In neurotransmission, synaptic vesicles fuse with the plasma membrane and release neurotransmitter across the synapse [4, 5]. During fertilization, cortical granules fuse with the plasma membrane of the egg [6, 7] and acrosomal vesicles fuse with the sperm [7]. Endocrine cells secrete hormones by fusion of granules with the plasma membrane, for example pancreatic beta cells release insulin [8]. A complex protein fusion machinery mediates intracellular fusion events, and **Soluble NSF Attachment Receptor (SNARE)** proteins form the core of the fusion machinery in nearly all of these systems [1, 8]. A key step in infection by membrane-enclosed viruses such as HIV, influenza, Ebola is membrane fusion [9]. A critical step in all of these processes is the formation of a fusion pore which connects membrane enclosed compartments and is essential for contents release. It has been demonstrated that the fusion pore is a dynamic structure.

### **I- Exocytosis and the fusion machinery**

SNAREs constitute the core of the cell's fusion machinery [1, 10-12], and have been shown to be the minimal machinery for fusion [13]. The neuronal SNAREs are the vesicle associated v-SNARE synaptobrevin (syb, VAMP), and the target membrane associated t-SNAREs syntaxin (stx) and SNAP-25 which form the t-SNARE acceptor complex [11]

**(Figure 1.1).** Fusion is driven by N- to C- terminal complexation (“zippering”) of the v-SNARE with the t-SNARE acceptor complex to form a 4- $\alpha$ -helical SNAREpin [1, 11, 13-16], though the mechanism by which the formation of a SNAREpin drives fusion is unclear. VAMP and syntaxin contribute one helix each, and SNAP25 contributes 2 helices to the 4- $\alpha$ -helical SNAREpin bundle. Post fusion, the SNAREs form the highly stable cis complex [15, 17-20], which is then disassembled by ATP-driven NSF and SNAP [21, 22]. Both syntaxin and synaptobrevin are anchored by transmembrane domains in the plasma membrane and the vesicular membrane respectively [11, 15], while SNAP-25 is attached to the plasma membrane by palmitoylation of cysteine residues in the linker region between the two SNARE domains [23-26]. Syntaxin has a three helix N-terminal regulatory domain, known as the H<sub>abc</sub> domain. Prior to the formation of the t-SNARE acceptor complex, the H<sub>abc</sub> domain folds back upon the SNARE domain of syntaxin, resulting in the closed conformation [27-32].

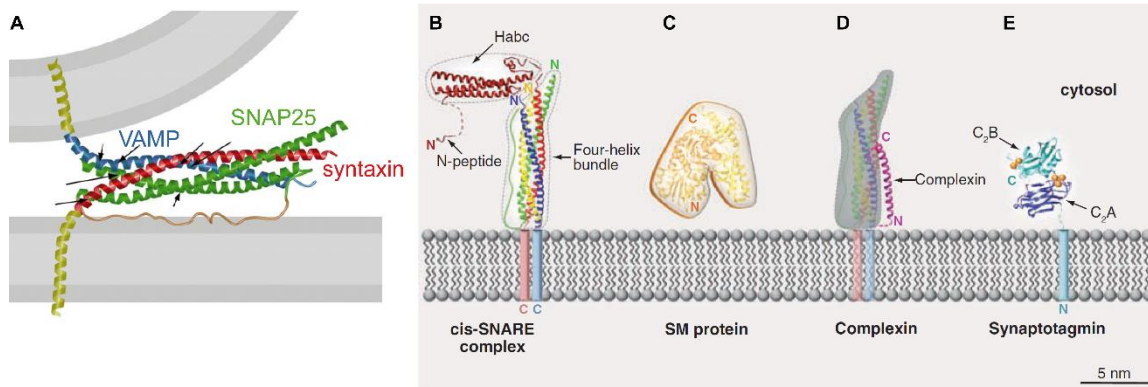


**Figure 1.1-**

The crystal structures of the fusion machinery. (A) The trans-SNARE complex, consisting of VAMP (blue), syntaxin (red), and SNAP25 (green). VAMP and syntaxin are anchored by transmembrane domains. (B). The cis-SNARE complex, shown with the regulatory H<sub>abc</sub> domain of syntaxin. (C) An example of the regulatory SM protein, here Munc18-1, which highlights the clasp structure which binds to syntaxin. (D) A cis-SNARE complex bound by complexin (magenta). (E) The structure of synaptotagmin, highlighting the Ca<sup>2+</sup> binding domains. Panel (A) Taken from ref. [11]. Panels (B-E) taken from ref. [27].

In addition to SNAREs, two of the most extensively studied components of the fusion machinery are complexin and synaptotagmin, which are critical for coordinating fusion with the arrival of an action potential to the synapse [33-38]. Both complexin [33-42] and synaptotagmin [43-51] are critical for regulation of SNARE mediated fusion in vivo [52]. Complexin inhibits basal and spontaneous fusion [37, 38, 42], but promotes synchronous neurotransmitter release [40], two seemingly contradictory roles. Complexin is thought to prevent SNARE complexation by “clamping” the v-SNARE synaptobrevin in the partially zipped onto the fully formed t-SNARE acceptor complex [35]. It has recently been shown that the accessory helix of complexin clamps the neighboring partially zipped SNAREpin, and many SNARE-complexin units form a “zigzag” array [37, 38]. Additional studies have suggested that this structure is physiologically relevant [38]. Synaptotagmin is the Ca<sup>2+</sup> sensor for exocytosis [23, 43-50, 53-64], and has two calcium binding domains,

C2A and C2B (**Figure 1.1**), that may insert into the membrane or interact with other accessory proteins after binding with  $\text{Ca}^{2+}$  [51]. The domains are connected by an unstructured linker domain. It has been suggested that upon  $\text{Ca}^{2+}$  binding, synaptotagmin may perturb the membranes to promote fusion. A functional form of complexin is required for synaptotagmin to effectively promote fusion in the presence of  $\text{Ca}^{2+}$  [37], but it is uncertain how these two accessory proteins interact with SNAREs to drive exocytosis.

Beyond these proteins, intracellular fusion is regulated by several additional accessory proteins. Multi-subunit tethering factors such as the yeast and mammalian exocysts help to spatially target vesicles to the active zone of the plasma membrane by interacting with the cytoskeleton [65]. Munc13/Rim-like proteins are thought to assist in vesicle priming and localization to active regions of the plasma membrane [14]. Munc13 has also been implicated in the opening of syntaxin and apparently plays a role in the plasticity of the synapse [14]. RIM1 $\alpha$  initially was shown to be a Rab3 effector [66, 67] and is critical for both long- and short-term plasticity [68]. Sec-1/Munc-18-like (S/M) proteins, while poorly understood, are essential for regulated membrane fusion, have been observed binding to the closed conformation of syntaxin in regulated exocytosis, and may assist in SNAREpin formation [14, 27, 32, 69-71].

Deficiencies in SNARE-mediated fusion, interactions between SNAREs and accessory protein, and SNARE expression have been implicated in a wide range of diseases. Abnormal aggregation of SNARE regulation protein  $\alpha$ -synuclein has been demonstrated in patients with dementia with Lewy body, and it was suggested that SNARE dysfunction is the cause [72, 73]. Abnormal syntaxin binding to Munc-18 has been implicated as a cause of immunological diseases such as familial hemophagocytotic lymphohistocytosis [74].

Reduced expression of syntaxin, synaptotagmin, and SNAP25 have been correlated with reduced insulin secretion from pancreatic islets from patients with type 2 diabetes [75]. Increased levels of SNAP25 expression have been demonstrated in patients with bipolar I disorder [76]. Even with significant evidence implicating SNAREs and exocytotic accessory proteins in various diseases, the fundamental mechanisms of SNARE-mediated exocytosis are not well understood, and thus the mechanisms by which SNAREs may directly or indirectly cause these diseases has not been identified.

Reconstituted in vitro studies have been essential in the efforts to interrogate and understand the mechanisms by which SNAREs drive fusion. The use of fluorescence microscopy has been central in the quest for the mechanisms of fusion and the role of SNARE proteins [13, 47, 77-85]. Individual fusion events can be tracked with total internal reflection fluorescence microscopy (TIRFM), a method that probes a thin layer near the target membrane [13, 47, 78-82]. Reconstituted fusion studies have helped to identify the role of individual components of the cell's fusion machinery. This strategy has revealed that SNAREs are the minimal fusion machinery [13], that 1-11 SNAREs are required to achieve fusion on biological timescales [77, 84, 85] and that, in the absence of auxiliary fusion proteins such as synaptotagmin, complexin, or SM proteins, SNAREs can drive fusion after delay times between docking and fusion ranging from  $\sim 30$  s [78, 79] to  $\sim 25$  ms [77, 81].

One of the primary motivations for studying membrane fusion and exocytosis is that nervous system uses exocytosis to communicate. The nervous system is highly complex. In the human brain, there are  $\sim 100$  billion neurons which form trillions of synaptic connections [5]. For essential function, the neurons must communicate across synapses.

Neurotransmission involves: 1) an input signal, such as the tapping of the knee to test one's reflexes. 2) electrical signal propagation. The neuron transmits a signal electrically in the form of an action potential, which depolarizes the plasma membrane [86-88]. 3) chemical signal propagation, by release of neurotransmitter into the synaptic cleft. When the action potential reaches the synapse,  $\text{Ca}^{2+}$  enters the presynaptic terminal and causes neurotransmitter, such as dopamine or acetylcholine, to be released into the synaptic cleft, for example to a neighboring neuron or muscle [4, 66, 89, 90]. The neurotransmitter can then either activate or inhibit the activity of the neighboring cells. While these basic steps are known, the specific mechanism of neurotransmitter release is not well understood.

Neurotransmitters are small molecules that transmit signals across a synapse from a neuron to the postsynaptic cell by binding to receptors on neurons or muscle cells [4, 66, 89, 90] (**Figure 1.2**). Neurotransmitters are typically stored in small, synaptic vesicles (~50 nm diameter), which are positioned at the active zone of the neuron [4]. Neurotransmitter release is triggered by the arrival of an action potential which depolarizes the cell membrane and opens  $\text{Ca}^{2+}$  channels in the presynaptic terminal [86-88, 91, 92]. These ion channels are more highly concentrated at the active zone [4]. The increase in calcium concentration activates the fusion machinery via synaptotagmin [45]. The fusion machinery then drives the formation of the initial connection between the vesicle lumen and the extracellular space, the nascent fusion pore [4, 45, 46, 49, 93]. The formation of the fusion pore is the essential initial step in the release of vesicular contents, such as neurotransmitters [94]. Extensive study of neurotransmission, as well as other forms of exocytosis, have suggested that the nascent fusion pore is a highly dynamic structure.

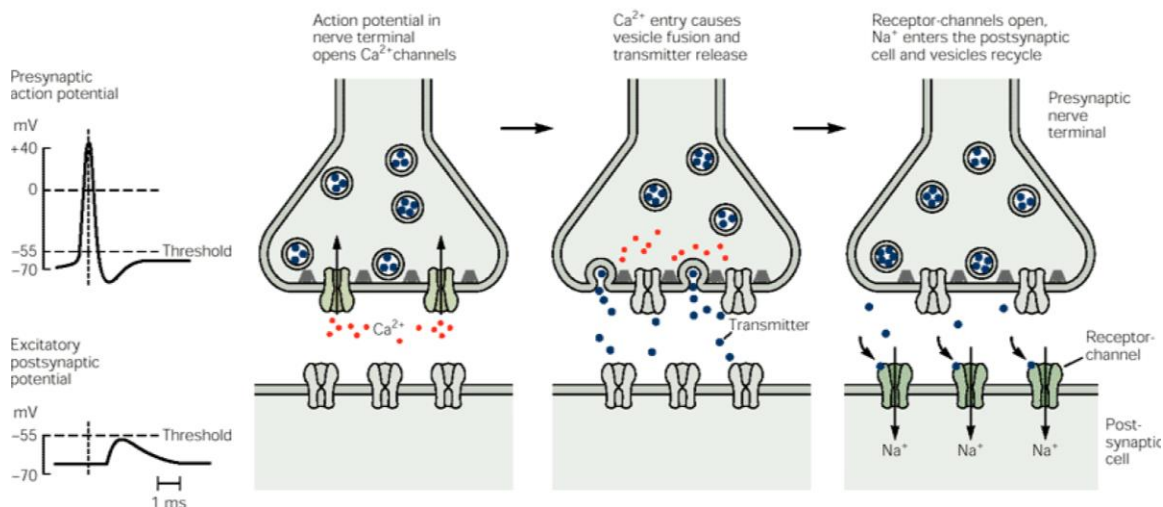


**Figure 1.2-**

The sequence of neurotransmitter release at the synapse, taken from ref. [5].  $\text{Ca}^{2+}$  (red) influx occurs upon activation by the presynaptic action potential. This activates the fusion machinery, which in turns opens the fusion pore and releases the neurotransmitter (blue). Neurotransmitter then binds to receptors on the postsynaptic cell.

## II- The dynamic fusion pore

Present understanding of the fusion pore is based primarily on live cell studies using electrophysiological methods such as amperometry and admittance to track fusion [94]. These studies suggest exocytotic fusion pores are highly dynamic structures that may control secretion [43, 56, 94-113], and that the pore dynamics consist of rapid transitions between several states (**Figure 1.3**): (i) Closed pore (unfused membranes); (ii) open pore (fused membranes, but the pore is so narrow that contents are slowly released); (iii) fully developed fusion pore (sufficiently expanded to initiate vesicle collapse).

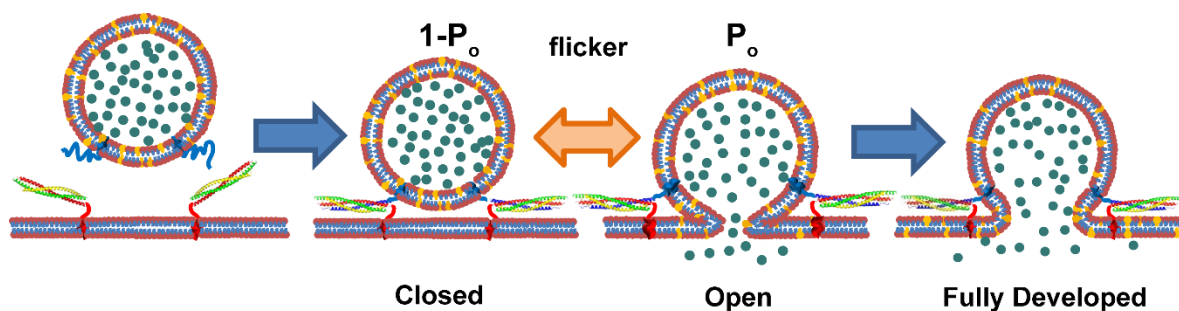


**Figure 1.3-**

Flickering dynamics of membrane fusion pores (schematic). A vesicle docks onto a planar membrane by complexation of vesicle v-SNAREs (blue) with t-SNAREs (red, yellow, green). Fusion of the membranes creates an open pore through which contents are released. Live cell electrophysiological studies show that fusion pores flicker rapidly and repeatedly between closed and open states, then dilating to become fully developed pores, or permanently closing. In chapter 2, we tracked flickering of fusion pores by monitoring release of labeled vesicle membrane lipids (yellow) into the planar membrane. Release is retarded because the pore is open only a fraction  $P_o$  of the time.

Flickering of the fusion pore between the open and closed states is indicated by signal flickering during the early portion of admittance and amperometric measurements. Pore flickering has been observed in fusion of vesicles of radius  $\sim 50 \text{ nm} - 1 \mu\text{m}$  [43, 94, 96, 97, 105, 107-112, 114, 115]. Amperometric measurements signal fusion by a sharp current spike as vesicular contents arrive and are oxidized at the electrode. Pore flickering is frequently indicated in amperometry by a small amplitude signal prior to the spike known as the pre-spike foot (PSF), which may exhibit signal fluctuations. The pre-spike foot duration ranges from  $\sim 30\text{-}500 \text{ ms}$  [96, 97].

Admittance measurements are typically broken into two components, conductance and capacitance. Capacitance measurements signal fusion by an increase from one stable signal level to another stable signal level [94, 107, 116], and the increase in signal represents the total membrane area added to the cell membrane. Conductance measurements signal fusion and fusion pore expansion by an off-scale signal increase [94, 97, 117], and the magnitude

of the transient signal represents the size of the fusion pore. Conductance and capacitance measurements display pore flickering prior to the development of the fusion pore, by either small amplitude signal fluctuations (conductance) or by rapid fluctuations between two different signal levels (capacitance) [94, 102, 107, 111].

During transient fusion events where the vesicle does not completely collapse into the target membrane (kiss-and-run), pore flickering has been observed using all measurement techniques [108-111, 113, 118, 119]. Flickering in kiss-and-run fusion occurs with varying durations and frequencies. For example, in the ventral midbrain neurons, kiss-and-run fusion was observed using amperometry. Approximately 80% of events were “simple” with one flicker, while the remainder were “complex” with 2-5 flickers. Each flicker lasted  $\sim 100 \mu\text{s}$  [106]. Both complete fusion with a clearly defined pre-spike foot and kiss-and-run fusion in catecholamine cells was observed using amperometry. Complete fusion occurred in  $\sim 80\%$  of events. Each kiss-and-run event lasted for  $\sim 150 \text{ ms}$ ,  $\sim 4$ -fold longer than the pre-spike foot in the same cell type [108]. Using admittance, large dense core vesicles and microvesicles of the posterior pituitary nerve terminal have been shown to predominantly undergo complete fusion, and  $\sim 5\%$  of the time undergo kiss-and-run fusion. The duration of kiss-and-run fusion of microvesicles ( $\sim 50 \text{ nm}$  diameter) is  $\sim 300 \text{ ms}$ , while that of large dense core vesicles ( $\sim 150 \text{ nm}$  diameter) is  $\sim 500 \text{ ms}$  [111].

The dynamics of the pore are physiologically regulated and determine the amount, the size and the kinetics of cargo release with important consequences for downstream events. In chromaffin cells, basal stimulation selectively releases only small cargo through flickering fusion pores, whereas increased stimulation leads to release of all cargo sizes through pores that rapidly dilate [113]. Although more challenging to detect, pore flickering also occurs

during exocytosis at the synapse [106, 110, 111] and may serve to regulate synaptic strength [120].

Fusion pore dynamics are altered by mutations in SNAREs and other components of the fusion machinery [43, 98, 121]. By replacing individual residues of the TMD of syntaxin with a tryptophan residue, the amplitude of the PSF was reduced by ~10-15% [98]. These are not residues which have been shown to interact with the TMD of the v-SNARE [15]. The duration of the PSF in cracked PC12 exocytosis was reduced by ~30% upon the introduction of a longer linker between the two calcium binding domains of synaptotagmin. The introduction of the extended linker disrupted the interaction between the t-SNARE and synaptotagmin [43]. In bovine chromaffin cells, deletion of C-terminal residues of SNAP25 results in a 3-fold increase in PSF duration and a ~50% decrease in PSF amplitude [121].

The fusion pore is also affected by the phospholipid composition of the fusing membranes. Cholesterol, a major constituent of eukaryotic plasma membranes (40% [122]), synaptic vesicles (~40% [12]), and secretory granules (25% [123]), is also a key modulator of fusion pore dynamics and rates of fusion. Pharmacological reduction of cholesterol lowered rates of exocytosis in hippocampal neurons [124], but shortened the duration of the pre-spike foot (PSF) in chromaffin cells, suggesting a faster transition to a fully developed pore [125]. The presence of oleic acid, with an inverted cone geometry similar to that of cholesterol, reduced the PSF duration in PC12 and chromaffin cells [126]. Introduction of ~40% cholesterol to liposome membranes increased the initial rates of fusion in a bulk liposome assay [127]. In cell-cell fusion mediated by the influenza fusion protein hemagglutinin, cholesterol accelerated and increased the incidence of fusion [128].

A bulk study of nanodiscs fusing with large unilamellar vesicles made an attempt to elucidate the role that SNAREs play in the formation and expansion of the fusion pore. Nanodiscs (ND) are circular lipoprotein discs of ~17 nm in diameter held together with the membrane scaffold protein apolipoprotein A1 [129-131]. By observing both lipid and contents mixing between the ND and the LUVs, it was suggested that 1 SNAREpin was sufficient to open the fusion pore, but 3 were necessary to open the pore sufficiently for contents release [85]. This is the most advanced study of the fusion pore in vitro that has been published, and it was not able to obtain information about individual fusion pores. Despite these advances, reconstituted studies have not been able to probe the dynamics of the fusion pore itself, and the role of SNAREs and the fusion machinery in regulating those dynamics.

Although there is much information about the effect of fusion machinery and lipid composition on fusion pore dynamics, not much is known about the mechanisms which control fusion pore dynamics. For example, questions remain about how the lipid composition might affect the duration and amplitude of the PSF. The main reason this has not been elucidated is that there has not been a biochemically defined assay with single fusion pore resolution. In vitro assays were important for the elucidation of the role of SNAREs in exocytosis and the formation of the fusion pore, but these assays have not been able to interrogate individual fusion pores [13, 47, 77-85]. Typically, the time resolution of fluorescence measurements of fusion are limited by the time it takes for lipids to diffuse a significant distance from the fusion site, which is too slow to interrogate the fusion pore dynamics [77]. Thus, the development of a biochemically defined assay that can observe individual fusion pores [77, 132], which is used in Chapter 2 of this thesis, was critical.

While reconstituted SNARE fusion assays have been extremely useful for studying fusion, there is a very long history of studying protein free membrane fusion. These studies typically use  $\text{Ca}^{2+}$  or another divalent cation as the fusogen. There is significant evidence from these studies that protein-free fusion passes through the hemifused intermediate, where only the outer leaflets have fused, while the inner leaflets form a new bilayer known as the hemifusion diaphragm (HD). Based on this work, a pathway to fusion was proposed: i) adhesion, ii) stalk formation, iii) expansion of the stalk to a growing HD, iv) fusion by rupture of the growing HD [105, 133-140]. Hemifusion may be a dead end state [141, 142]. A major mechanism for controlling the fusion pathway is the lipid composition of the fusing membranes, where positive curvature lipids promote rupture of the HD [105, 138, 139] and negative curvature lipids protect the HD from rupture and promote dead-end hemifusion [141, 143]. Flickering pores have been observed in the expanding HD [105], although these pores have a different structure from the fusion pore. These are simple pores, a lipid lined pore within one bilayer, rather than a pore which connects two discontinuous bilayers [105, 142, 144].

There is also significant evidence that hemifusion is an important fusion intermediate in intracellular fusion. Long-lived hemifused intermediates were detected on the fusion pathway in pneumotocytes and during yeast vacuole fusion [145, 146]. Electron microscopy revealed extended HDs between synaptic vesicles and the plasma membrane (~5 nm in diameter), between vesicles and the endothelium in rat blood capillaries (~30 nm), between vesicles and the plasma membrane of zoospores (~50 nm) and between cortical granules and sea urchin egg plasma membranes (~0.5  $\mu\text{m}$ ) [147-150]. However, there was no evidence for hemifusion as an observable intermediate in this work.

The approach for the work I describe in this thesis was to analyze the effects of SNAREs and the membranes, isolated from the complexities of the cell. To do this, we utilized a novel biochemically defined fluorescent assay developed by our collaborators [77, 132]. This assay uses TIRF to observe fusion of SUVs with a supported bilayer (SBL). Using a combination of mathematical modelling and quantitative image analysis we observed the flickering fusion pore in vitro for the first time. Because the system was well defined, we were able to isolate the effects of SNAREs and the biophysical properties of the membranes on fusion and the fusion pore separately. We developed a mathematical model of lipid release through the flickering fusion pore. We examined how the composition of the membranes affects the fusion rate and the fusion pore dynamics. We did not find any evidence of the hemifused intermediate in this assay. In additional work, we quantified how SNAREs and membranes interact with each other prior to formation of the fusion pore and in collaborative work this was one of the key components of a model developed by my colleagues to predict the waiting time for fusion and the effects of SNARE density at the fusion site.

In the first part of the thesis we used a novel single-event fusion assay to measure fusion pore flickering during reconstituted SNARE-mediated fusion of SUVs to a SBL using total internal reflection fluorescence (TIRF) microscopy. Here we utilized the unique properties of TIRF, which gives a signal increase as soon as a fluorescent lipid diffuses from the vesicle to the SBL and increases the time resolution to the acquisition time, rather than the diffusion time of lipids away from the diffusion site. We thus developed a mathematical model of lipid diffusion through a fusion pore. We found that the dynamics of the fusion pore are typically controlled by biophysical properties of the membranes, and that SNAREs

do not typically affect pore dynamics. We found that physiological levels (~45%) of cholesterol promotes the open state of the fusion pore and shortens docking-to-fusion delay time. These results suggest that high levels of cholesterol may drive t-SNARE complex clustering in the plasma membrane. In the second part of the thesis, we found that the predominant driving forces for membrane fusion, once the SNAREpins have completely zippered, are steric-hydration forces among the SNAREpins and membranes. These forces enlarge a SNAREpin cluster, which in turns pulls the membranes together due to curvature effects.

In the first part of the thesis, the experimental setup was developed by, and the experiments were performed by our collaborators in the Karatekin Lab at Yale University. Preliminary data analysis (calculating bleaching times, diffusion constants, etc.) was performed by myself. Development of the model of lipid release was done by Prof. O'Shaughnessy and myself. Fitting of all data to the model, analysis of the fits, and the remaining calculations was performed by myself. In the second part of the thesis, the model of the vesicle-vesicle, SNAREpin-SNAREpin, and SNAREpin-vesicle interactions was done by me. The initial development of the Monte Carlo simulation was done by Dr. Jason Warner, and Hakhamanesh Mostafavi and I further developed this simulation.

## Chapter 2- Cholesterol Increases the Openness of SNARE-Mediated Flickering Fusion Pores

### I-Background

A critical step in processes such as neurotransmitter or hormone release via exocytosis, intracellular trafficking, and enveloped virus infection is the creation of a fusion pore that connects membrane-enclosed compartments and allows contents to be released[94]. Most intracellular membrane fusion events, as well as exocytosis, are driven by *soluble N-ethylmaleimide-sensitive factor attachment protein receptor* (SNARE) proteins when vesicle-associated v-SNAREs form complexes with target membrane-associated t-SNAREs [27]. Exocytotic fusion pores are highly dynamic, and may flicker repeatedly between the open and closed states before either permanently closing or dilating [43, 96-98, 101, 102, 106-108] (Fig. 1.1).

Flickering dynamics of fusion pores are most directly measured using electrophysiological approaches. In amperometric traces of contents release, pore flickering causes fluctuations in the low amplitude PSF and in “stand alone feet” that signal transient events involving partial contents release without full pore enlargement [43, 96, 97, 106, 108]. Flickering is also manifested by fluctuations in pore conductance[97, 101] and in membrane capacitance[107, 111]. From such studies, fusion pores that flicker typically flicker ~2-10 times, at frequencies from 40 Hz in beige mast cells to 170 Hz in chromaffin cells to 4000 Hz in ventral midbrain neurons[97, 106, 108]. A pore height ~15 nm similar to that of a

gap-junction is commonly assumed, in which case measured conductances imply pore radii  $\sim 0.5 - 5\text{nm}$  [101, 107, 110, 111].

In small vesicles pores were measured to flicker between two discrete states, the closed state and an open state of fixed size that varies little within or between flickering episodes. In  $\sim 25\text{ nm}$  radius synaptic vesicles and microvesicles, conductance of fusion pores revealed  $\sim 10\text{-}20\text{ Hz}$  flickering between discrete open and closed states, with sharp transitions between the two and an almost constant conductance in the open state from one open event to another [110, 111]. In amperometric measurements of fusion pores in  $\sim 25\text{ nm}$  synaptic vesicles during exocytosis in ventral midbrain neurons the initial peak value in flickering sequences was consistent between events, suggesting a fixed fully open pore state [106]. In larger  $\sim 100\text{ nm}$  large dense-core vesicles in chromaffin cells, prior to dilation flickering pores in the fully open state had approximately constant conductance from flicker to flicker, whereas pores in  $\geq 1\text{ }\mu\text{m}$  sized large granules in beige mast cells show much more variable conductance in time during flickering [97, 117, 151].

A quantitative characteristic of a 2-state flickering pore is its openness  $P_o$ , the fraction of the time the pore is in the open state. The analogous concept is used in the study of ion channels [152]. The openness is closely related to the thermodynamic driving force for fusion,  $\Delta F_{\text{pore}}$ , the free energy difference between the open and closed states (Fig. 1.3). Using Boltzmann's distribution,  $P_o = e^{-\Delta F_{\text{pore}}/k_B T} / (1 + e^{-\Delta F_{\text{pore}}/k_B T})$  where  $T$  is temperature and  $k_B$  is Boltzmann's constant.  $\Delta F_{\text{pore}}$  presumably sums downhill contributions from SNAREs and other components that drive the pore to open, and uphill contributions from the lipid membranes that must bend to make the fusion pore [153]. In a natural generalization to a flickering pore whose size fluctuates through a continuum of

sizes,  $P_o$  is the time-averaged conductance relative to the conductance when fully open. Electrophysiological measurements suggest  $P_o \sim 0.3 - 0.8$ , i.e. small free energy differences  $\Delta F_{\text{pore}}$  of order  $kT$  [97, 102, 106, 108, 110, 111].

The mechanism that governs pore flickering is unknown, in part because methods to measure individual pore dynamics in reconstituted, biochemically defined systems have not been available. Here we developed such a method, using total internal reflection fluorescence (TIRF) microscopy to measure flickering pores during reconstituted SNARE-mediated fusion of small unilamellar vesicles (SUVs, comparable in size to synaptic vesicles) with supported bilayers (SBLs). Due to the evanescent wave excitation with a polarized laser beam [154], individual fusion events are signaled by a rapid increase in intensity as fluorescently labelled lipids diffuse from the vesicle membrane into the SBL membrane. Consistent with rapid ( $\geq 100$  Hz) pore flickering, lipids were released from the vesicle  $\sim 10$ -fold and in some cases up to a 100-fold more slowly compared to a continuously open pore (Supplementary Figure S1). From the lipid release time we calculated the pore openness  $P_o$  (Fig. 1.1) and vesicle size for each event. For most lipid compositions, lipid bilayers controlled pore flickering: SNAREs had little effect, and cholesterol increased pore openness, consistent with its ability to lower fusion pore membrane bending energy. With higher, physiological cholesterol levels in target membranes the presence of SNAREs dramatically opened flickering pores. Thus, in addition to its direct role, cholesterol synergistically facilitates pore opening by SNARE proteins. Our results suggest this effect derives from cholesterol-mediated clustering of t-SNAREs at the fusion site.

## **II-Results**

### **Single event TIRF based fusion assay**

We used a recently established TIRF microscopy (TIRFM) based fusion assay [77, 132, 155] to monitor fusion of individual, neuronal v-SNARE-containing SUVs with neuronal t-SNARE-reconstituted planar bilayers supported on a soft poly(ethylene glycol) (PEG) cushion in microfluidic flow channels, with 0.6-1% of the vesicle lipids fluorescently labeled (Fig. 2A).

Four membrane lipid compositions were tested (Tables S1 & S2): a model PC/PS mixture[77, 85, 132], and three compositions that included PIP2 (in SBL membranes), PE and varying amounts of cholesterol from 0% to 10%/45% and 45%/45% in the SUV/SBL membranes (PC/PS/PE/PIP2, PC/PS/PE/PIP2/Ch, PC/PS/PE/PIP2/Ch+, see Tables S1 & S2 and Methods). PE is found at levels up to 15% in synaptic vesicles, secretory granules, and plasma membranes[12], has negative spontaneous curvature and promotes fusion in model systems[156], but its physiological role is unclear. The signaling lipid PIP2 is present in small amounts in the inner leaflet of the plasma membrane (1-2%)[157] and interactions with the t-SNARE syntaxin concentrate PIP2 at docking and fusion sites[158]. Cholesterol has a facilitating role in biological and model fusion reactions that is well-documented[124, 127, 128], including its modulation of the fusion pore[125].

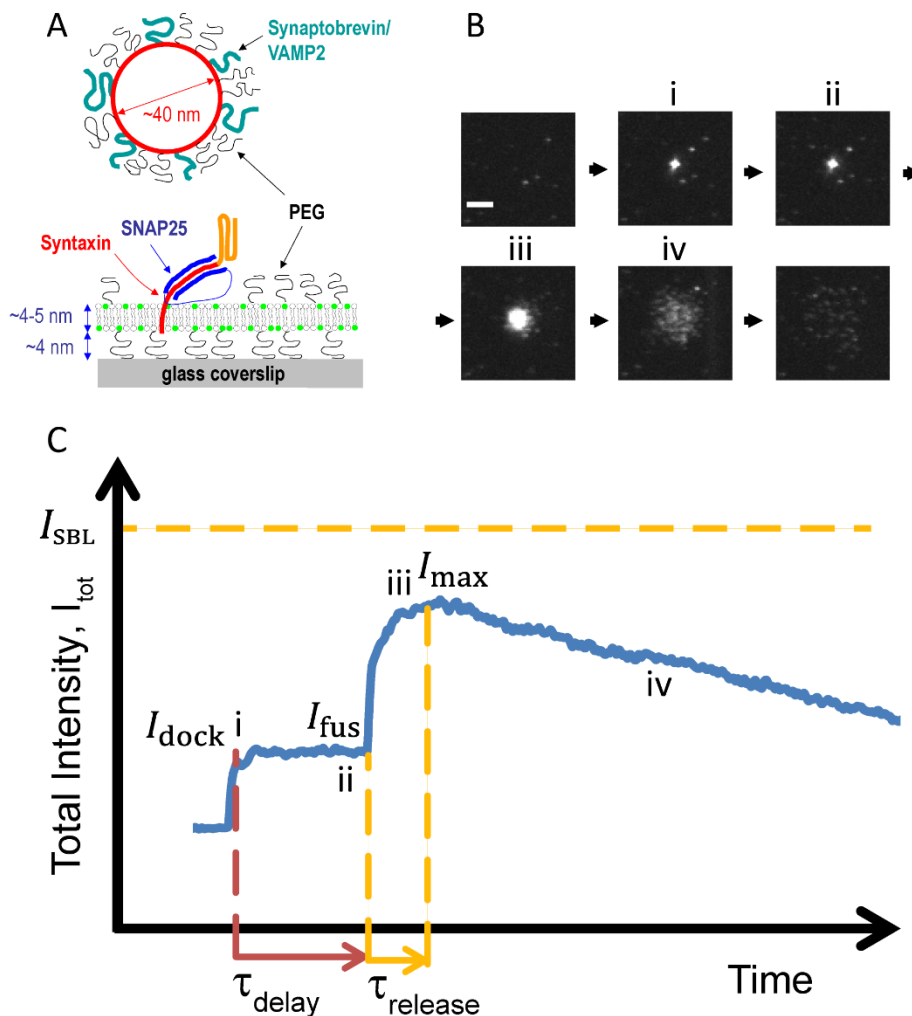


**Figure 2.1-**

Using TIRFM to measure fusion pore flickering dynamics. (A) Vesicles reconstituted with v-SNAREs (synaptobrevin/VAMP2) fuse with a target supported bilayer (SBL) reconstituted with cognate t-SNAREs (syntaxin and SNAP25). Membranes are PEGylated to prevent non-specific interactions and 0.6-1% of lipids are fluorescently labelled. (B) TIRF sequence during a typical fusion event, viewed from beneath coverslip in (A). When the vesicle docks onto the SBL a spot appears, (i). A time  $\tau_{delay}$  later fusion occurs, (ii), and the spot brightens as labeled lipids diffuse into the SBL, (ii)→(iii). Individual lipids are discernible by stage (iv). Box size 22 x 22  $\mu\text{m}$ , 82 x 82 pixels. Bar, 5  $\mu\text{m}$ . (C) Typical time course of total fluorescence intensity  $I_{tot}$  integrated over the box in (B), from which we extracted the lipid release time  $\tau_{release}$ . Following lipid release into the SBL,  $I_{tot}$  would increase to the value  $I_{SBL}$  were it not for bleaching, iii→iv ( $I_{max} < I_{SBL}$ ).

We recorded movies of docking and fusion events. For each fusion event we measured the total intensity versus time  $I_{tot}(t)$ , summed over all pixels in a box drawn around the fusing vesicle, Figure 2.2B, C. Following docking of a vesicle to the SBL when the intensity

increases to a value  $I_{\text{dock}}$ , after a delay time  $\tau_{\text{delay}}$  fusion is announced by a rapidly increasing intensity[81] as labeled lipids, initially in the vesicle membrane, begin to be released into the SBL through the bilayer walls of the fusion pore (Fig. 1.1). The intensity of labelled lipids in the vesicle is reduced by a certain average factor  $\lambda_{\text{TIRF}}$  because the evanescent excitation field, with a decay length  $\sim 68$  nm (Online Methods), decays with distance from the SBL and its polarization is a worse match for the dipole orientations of the fluorescent lipid labels when they reside in the spherical vesicle[154]. The delay time distributions revealed a fast-fusing SNARE-mediated population and a slowly fusing non-specific population[77] (Supplementary Fig. S2E & F, Appendix).

### **Retarded lipid release suggests that fusion pores flicker**

We used the fluorescence increase that accompanies diffusion of a labelled vesicle lipid into the SBL to track the release process and hence infer properties of the fusion pore. The fluorescence increases by the inverse of the mean intensity reduction factor for lipids in the vesicle,  $\lambda_{\text{TIRF}}$ . As the increase is instantaneous upon lipid transfer we could measure the fraction of lipids transferred with high sensitivity and with temporal resolution limited only by acquisition frame rates ( $\sim 100$  Hz). Individual lipid labels became discernible as they diffused away from the fusion site, eventually disappearing in single bleaching steps[155]. The release of lipids into the SBL occurred over a timescale  $\tau_{\text{release}}$ , when the intensity increased toward a plateau but then decreased due to bleaching (Fig. 2.1C).

Lipid release times were far greater ( $\sim 30 - 250$  ms, Supplementary Fig. S1) than expected for a permanently open pore ( $\sim 10$  ms, the lipid diffusion time on the scale of a

typical vesicle[159]). This suggested that fusion pores were flickering and spending only a fraction of the time in the open state, i.e. the pore openness  $P_0$  was significantly less than unity.

## **Fusion pore openness $P_0$ is quantitatively related to the lipid release time**

### **$\tau_{\text{release}}$**

Next we established a relationship that enabled us to deduce the pore openness  $P_0$  from the time for lipids to be released from the vesicle into the SBL,  $\tau_{\text{release}}$ , that we measured for each fusion event from the TIRFM intensity curve (Fig. 2C). A mathematical model of lipid release through a flickering pore showed that

$$P_0 = \frac{A_{\text{ves}} b}{2\pi r_p D_{\text{lip}} \tau_{\text{release}}} \quad 2.1$$

(see Appendix). For a 2-state (open/closed) pore  $P_0$  is the fraction of the time in the open state, but eq. 2.1 is equally valid for a flickering pore with a size varying continuously in time, when  $P_0$  is the time-averaged pore radius relative to the fully open radius. In eq. 2.1  $A_{\text{ves}}$  is the vesicle area and  $D_{\text{lip}}$  the lipid diffusivity which we measured directly (see below). We took a pore height  $b = 15$  nm, as is commonly assumed, and the radius of the fully open conducting pore was taken to be 1 nm as reported for smaller vesicles [101, 106, 107, 110, 111]. This implies a value  $r_p = 3$  nm as the fully open pore radius in eq. 2.1 is the effective value seen by a diffusing lipid and so includes half the bilayer thickness, taken

to be 2nm (Supplementary Fig. **S1A**). Eq. 2.1 states that a flickering pore more often in the closed state (lower  $P_0$ ) releases lipids more slowly (larger  $\tau_{\text{release}}$ ).

For a given fusion event the vesicle area,  $A_{\text{ves}}$ , in eq. 2.1 is unknown as sizes varied significantly. The docked vesicle intensity  $I_{\text{dock}}$  (Fig. 2C) is the best measure of vesicle size, being the earliest and least affected by bleaching. The difficulty is that the relation between  $A_{\text{ves}}$  and  $I_{\text{dock}}$  is not a priori known, since the intensity of fluorescently labeled lipids in the vesicle is unknown. However, we directly measured  $I_{\text{lip}}$ , the single lipid intensity for lipids in the planar SBL (see below). Thus, we used the TIRFM curve for each event to determine the fluorescence intensity reduction factor  $\lambda_{\text{TIRF}}$ , namely the ratio of total intensities before and after lipid release. The area is then

$$A_{\text{ves}} = I_{\text{dock}} / (\lambda_{\text{TIRF}} I_{\text{lip}} 2\rho_{\text{lip}}). \quad 2.2$$

Here  $\rho_{\text{lip}}$  is the areal density of fluorophores in each leaflet of the vesicle membrane and  $\lambda_{\text{TIRF}} I_{\text{lip}}$  is the single labeled lipid intensity for a lipid in the vesicle, averaged over all locations in the vesicle membranes, including the reduction factor  $\lambda_{\text{TIRF}}$  relative to the value  $I_{\text{lip}}$  in the SBL. The reduction factor depends on vesicle size in a complex fashion (see below).

In practice, direct extraction of  $\tau_{\text{release}}$  and  $\lambda_{\text{TIRF}}$  from the measured fluorescence signal  $I_{\text{tot}}(t)$  is difficult due to bleaching of labelled lipids in the SBL, with bleaching time  $\tau_{\text{bleach}} \sim 3.5$  s (Fig. 2C and Supplementary Fig. **S2C**). Thus, we used the expression predicted by our model for the TIRFM signal, given by

$$\frac{I_{\text{tot}}(t)}{I_{\text{fus}}} = e^{-t/\tau_{\text{release}}} + \frac{(e^{-t/\tau_{\text{bleach}}} - e^{-t/\tau_{\text{release}}})}{\lambda_{\text{TIRF}} (1 - \tau_{\text{release}}/\tau_{\text{bleach}})} \quad 2.3$$

(see Appendix). We neglect the slower bleaching in the vesicle ( $\tau_{\text{bleach}} \sim 18$  s, Supplementary Fig. S2D) and quenching effects as our labeling densities are below the self-quenching threshold (Appendix). Our procedure was to fit the predicted expression, eq. 2.3, to the experimentally measured signal and determine the two crucial parameters  $\tau_{\text{release}}$  and  $\lambda_{\text{TIRF}}$  as best fit parameters.

**Permanently open pore.** In the above lipid release is limited by flickering and the fraction of labeled lipids remaining in the vesicle a time  $t$  after the instant of fusion (when the pore first opens) decays exponentially,  $\phi_{\text{ves}} = e^{-t/\tau_{\text{release}}}$  (Supplementary Eq. S8). We will see that our experiments show that a fraction of pores do not flicker, but are permanently open. In this case release is limited by diffusion, and our model shows that the decay has a qualitatively different inverse time dependence and the TIRFM intensity time course is different:

$$\frac{I_{\text{tot}}(t)}{I_{\text{fus}}} = e^{-t/\tau_{\text{bleach}}} \left[ \phi_{\text{ves}}(t) + \left( \frac{1 - \phi_{\text{ves}}(t)}{\lambda_{\text{TIRF}}} \right) \right], \phi_{\text{ves}}(t) = \tau_{\text{ves}}/t. \quad 2.4$$

### SNARE-mediated fusion pores flicker or are permanently open

We used the following procedure, which yielded the pore openness, the vesicle radius  $R_{\text{ves}}$  and the intensity reduction factor  $\lambda_{\text{TIRF}}$  for each fusion event. We first measured the bleaching time  $\tau_{\text{bleach}}$ , the diffusivity,  $D_{\text{lip}}$ , and the intensity,  $I_{\text{lip}}$ , of single fluorescently

labeled lipids in the SBL (Methods and Supplementary Fig. S2). (1) For each detected fusion event we extracted the docked fusion intensity  $I_{\text{dock}}$  and the intensity at the instant of fusion  $I_{\text{fus}}$  from the measured fluorescence intensity curve  $I_{\text{tot}}(t)$  (Fig. 2.1C). (2) We fit the predicted TIRF intensity curve  $I_{\text{tot}}(t)$ , eq. 2.3, to the experimental curve using the fluorescence reduction factor  $\lambda_{\text{TIRF}}$  and lipid release time  $\tau_{\text{release}}$  as fitting parameters. (3) We used eq. 2.2 to obtain the vesicle area and radius, and then eq. 2.1 to obtain the pore openess.

Applying this procedure to the fast SNARE-mediated fusion events we found that pores flickered with pore openess  $0.01 \lesssim P_o \lesssim 0.9$ , suggesting free energies of pore formation  $-2 \text{ kT} \lesssim \Delta F_{\text{pore}} \lesssim 5 \text{ kT}$  (Supplementary Fig. S1B). While most pores flickered, in many cases the analysis returned a nominal  $P_o$  value exceeding unity, indicating a fully open pore,  $P_o = 1$ . To reinforce this conclusion we tested these pores for inverse time release kinetics,  $\phi_{\text{ves}} \sim 1/t$ , the signature of a permanently open pore, eq. 2.4. Larger vesicles were used for this test,  $R_{\text{ves}} \geq 25 \text{ nm}$ , whose slower release kinetics were more accessible. The exponent of the best fit power law to the pooled release kinetics was close to that predicted ( $-0.99 \pm 0.22$ ), compared to a best fit exponent of  $-0.68 \pm 0.09$  for flickering pores with  $P_o < 0.15$  (Supplementary Fig. S3B).

To test our assumption that slow lipid release reflects flickering pores (eq. 2.3) rather than restricted lipid diffusion due to high curvature or protein crowding effects at the pore[160] we repeated experiments using a different label. We found statistically insignificant differences in pore openess values (Appendix and Fig. S6), suggesting that lipid diffusion through the pore was normal.

We note that a “permanently” open pore is one that remained open long enough to release all labelled lipids, approximately the lipid diffusion time for the vesicle size,  $\tau_{\text{ves}}$  (multiplied by a logarithmic factor of order unity involving the pore diameter[159]). Thus, such a pore could in fact be slowly flickering, with a frequency  $\lesssim 100$  Hz if we take a typical  $\tau_{\text{ves}} \sim 10$  ms. However, since neurotransmitter bulk diffusivities are  $\sim 500$ -fold greater[106] than the lipid diffusivities we measured (Supplementary Table **S3**), such a pore would be permanently open during the entire episode of contents release, which would occur within one flicker. Further, we found no vesicle size dependence in the fusion statistics (Appendix and Fig. **S4**) suggesting that such pores flickered at frequencies less than 20 Hz, the limit imposed by the largest vesicles ( $R_{\text{ves}} \sim 80$  nm).

### **Cholesterol promotes the open state of the fusion pore**

When pore statistics were classified according to the composition of the fusing membranes, a strong correlation of flickering pore openness with the presence of cholesterol emerged, Fig. 2.2B-D. For biologically motivated but cholesterol-free compositions, the mean flickering pore openness was  $\bar{P}_o = 0.04$  while only  $\sim 2\%$  were permanently open. With 45% (10%) cholesterol in the SUV (SBL) membranes, the mean  $P_o$  doubled but the permanently open fraction was unchanged. For physiological conditions with all membranes containing 45% cholesterol the effect was dramatic: relative to cholesterol-free membranes, the flickering pore openness and the permanently open fraction increased  $\sim 10$ -fold and  $\sim 20$ -fold, respectively.

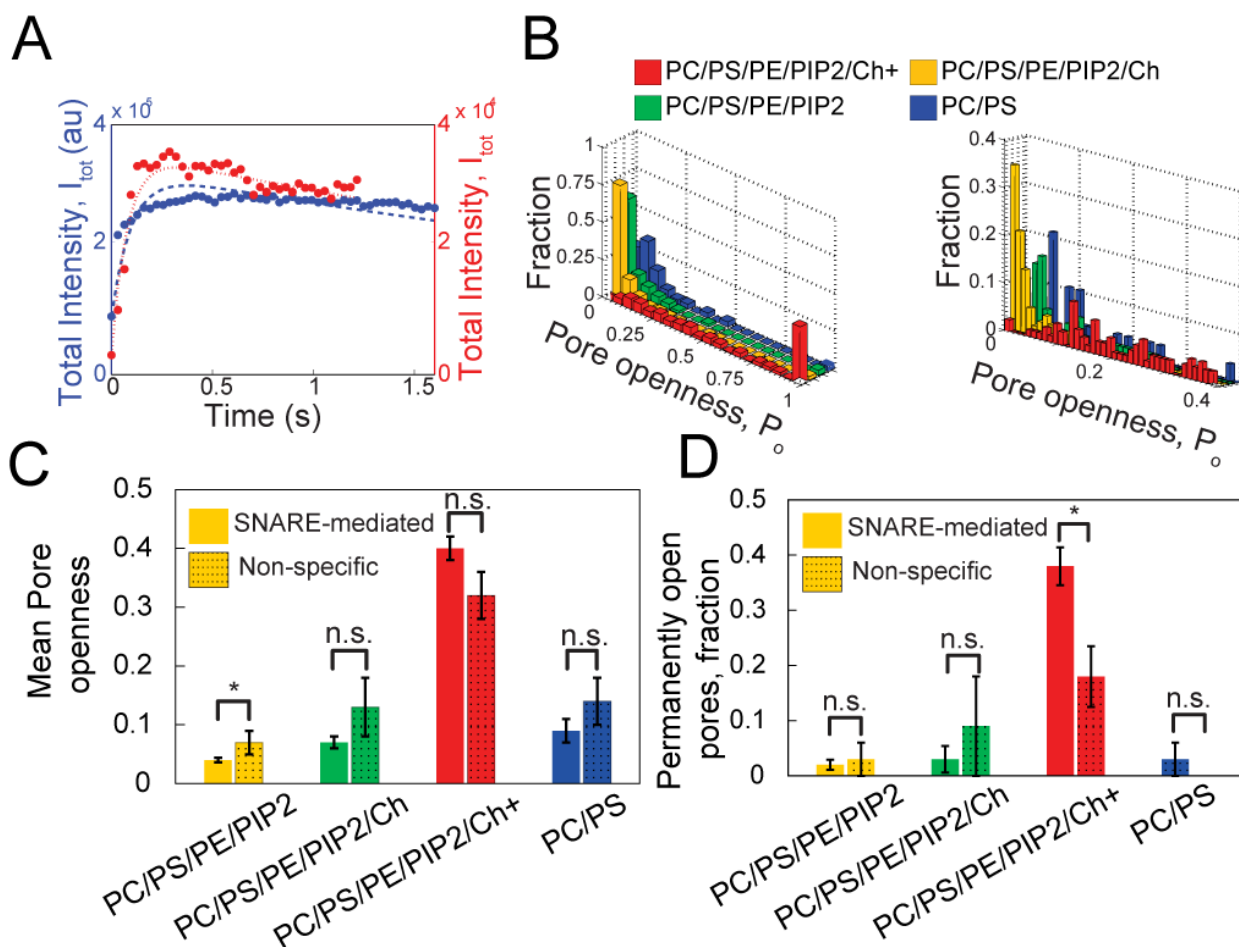


**Figure 2.2-**

Openness statistics of SNARE-mediated flickering fusion pores. (A) TIRF intensity versus time following fusion for two typical SNARE-mediated fusion events. Red (PC/PS): the time course is well fit by eq. 2.3 for a flickering pore, with openness  $P_o = 0.09$  (short-dashed curve). Blue (PC/PS/PE/PIP2/Ch+, 45% cholesterol): the fit from eq. 2.3 is poor, with nominal  $P_o = 3.48$  (long-dashed curve), flagging a permanently open pore, eq. 2.4. (B) SNARE-mediated fusion pores flicker and are dramatically opened by increasing cholesterol content. (left panel) Flickering pore openness  $P_o$  and the fraction of pores that are permanently open ( $P_o = 1$  column) for each of the four lipid compositions studied (Tables S1 & S2). Bin size 0.05. (right panel) Blowup of  $P_o \leq 0.4$  data (bin size 0.01). (C,D) SNAREs play little or no role in fusion pore flickering unless cholesterol content is high. Mean pore openness (C) and fraction of pores that are permanently open (D) versus composition for SNARE-mediated and SNARE-independent fusion pore dynamics. Error bars in C and D are standard errors of the mean. Asterisk denotes  $p < 0.05$ , student's t-test.

## **SNARE proteins have little effect on the fusion pore unless physiological levels of cholesterol are present**

To distinguish the respective roles of SNAREs and lipid bilayers in fusion pore dynamics we repeated the above analysis for the slow non-specific fusion events, for which we assumed the fusion pore dynamics are not SNARE-mediated [77]. Without cholesterol, and with 45% (10%) cholesterol in the SUV (SBL) membranes, these events showed pore openness and permanently open pore fractions statistically indistinguishable from SNARE-mediated events, other than a small increase in  $P_0$  with no cholesterol (n=353 SNARE-mediated events, m=68 non-specific events, Fig 2.3C, D). This suggests that the lipid bilayers themselves governed pore dynamics with little influence from SNARE proteins.

To test this conclusion we measured fusion between protein free SBLs and v-SNARE containing SUVs (Appendix, Fig. S2F). For the same compositions the delay times and openness were statistically indistinguishable from those for the slow component in the presence of v- and t-SNAREs. This supports the hypothesis that pore dynamics for the slow component reflect the physical properties of lipid bilayers only.

A qualitatively different picture emerged at physiological cholesterol levels in all membranes (45%): SNARE proteins then increased the fraction of open pores significantly, from 18% to 38% (Fig. 2.2D). Thus, at high concentrations cholesterol opens pores both indirectly, by activating SNARE-mediated pore opening, and directly through its influence on the lipid membranes.

**With physiological amounts of cholesterol fusion is so accelerated that there is insufficient time to recruit additional t-SNAREs to the fusion site after docking**

Next we examined the effect of cholesterol on the docking-to-fusion delay times for the fast SNARE-mediated fusion events, and we applied the model of ref. [77] that assumes fusion is limited by the diffusive recruitment of t-SNAREs to the fusion site once a vesicle has docked. Delays were ~2-fold greater in the presence of intermediate amounts of cholesterol (45% and 10% in the SUV and SBL membranes) and sufficient for 3-6 t-SNAREs to have been recruited, consistent with literature values for the number of SNAREs required for fusion [77, 85], see Fig. 2.3A and Appendix.

By contrast at physiological cholesterol levels (45% in all membranes) the delay times were ~3-fold smaller, too short for even one additional t-SNARE to have been diffusively recruited if one assumes a uniform spatial distribution of t-SNAREs. This was unexpected, since lipid diffusivity was reduced ~4-fold at these cholesterol levels (Supplementary Table S3) suggesting delay times would be greater. Thus, t-SNAREs were presumably already clustered at docking sites in sufficient numbers to trigger fusion, consistent with cholesterol-mediated t-SNARE clustering observed in cells [161-163].

Consistent with these results, the probability that a docked vesicle underwent SNARE-mediated fusion during the observation time increased ~3-fold at the highest cholesterol levels (Fig. 2.3B).

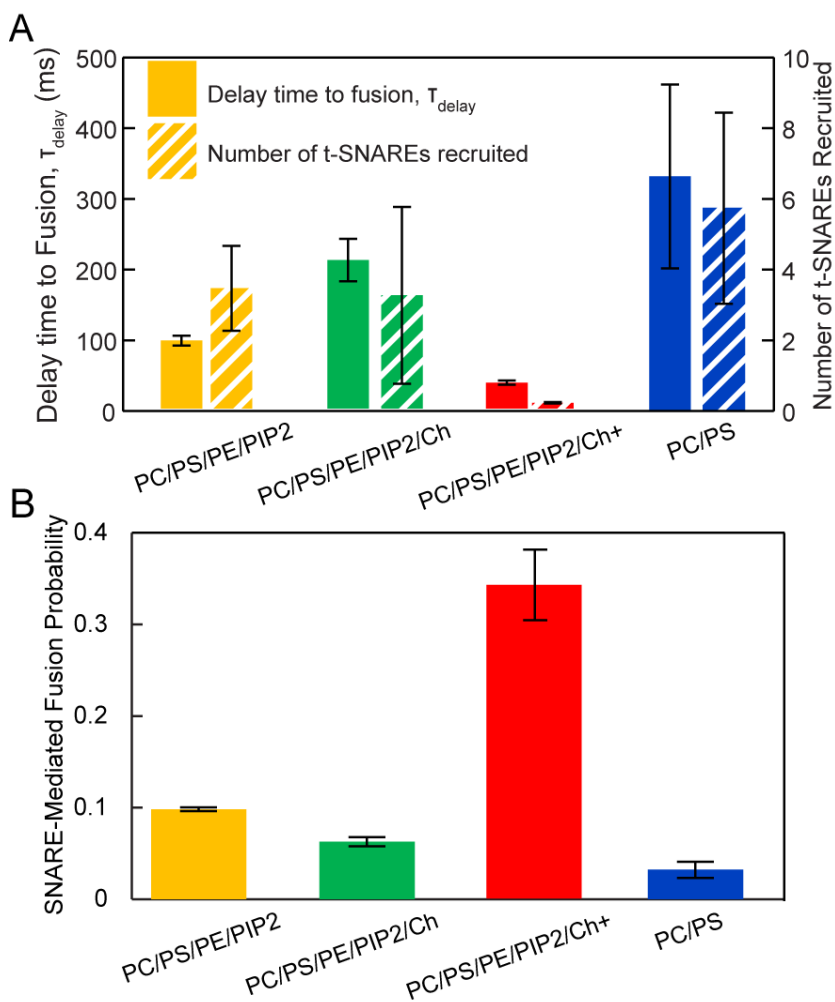


**Figure 2.3-**

Physiological amounts of cholesterol accelerate fusion by clustering t-SNAREs. (A) Delay times to SNARE-mediated fusion following vesicle docking versus membrane lipid composition (solid colors), and calculated number of t-SNAREs assumed recruited by diffusion to the fusion site during the delay time (striped). Lower amounts of cholesterol (yellow, green) increase delay times, consistent with the reduced lipid diffusivities, but the number of t-SNAREs recruited for fusion is unchanged. At physiological cholesterol (PC/PS/PE/PIP2/Ch+) fusion is so accelerated that there is insufficient time to recruit any additional t-SNAREs after docking, suggesting t-SNAREs are pre-clustered. (B) Physiological cholesterol levels increase the probability ~3-fold that a docked vesicle undergoes SNARE-mediated fusion (as opposed to non-specific fusion or no fusion) before complete bleaching (~20s).

## **Fluorescence reduction factor and vesicle size are unique functions of the docked vesicle intensity**

Our procedure entailed measuring the docked vesicle intensity  $I_{\text{dock}}$  for each fusion event and extracting the intensity reduction factor  $\lambda_{\text{TIRF}}$  by fitting our model to the fluorescence profile (Figs. 2.2C, 2.3A). An important self-consistency check is that  $\lambda_{\text{TIRF}}$  is a unique function of  $I_{\text{dock}}$ , since the value of  $I_{\text{dock}}$  fixes the vesicle size and hence the value of  $\lambda_{\text{TIRF}}$  (Fig. 5A). When we pooled the values for several compositions and included non-specific fusion events, the  $\lambda_{\text{TIRF}}$  vs.  $I_{\text{dock}}$  data collapsed around a definite curve (Fig. 2.4B). The  $R_{\text{ves}}$  vs.  $I_{\text{dock}}$  data collapsed similarly (Fig. 2.4C). Thus, our method satisfies this self-consistency check.

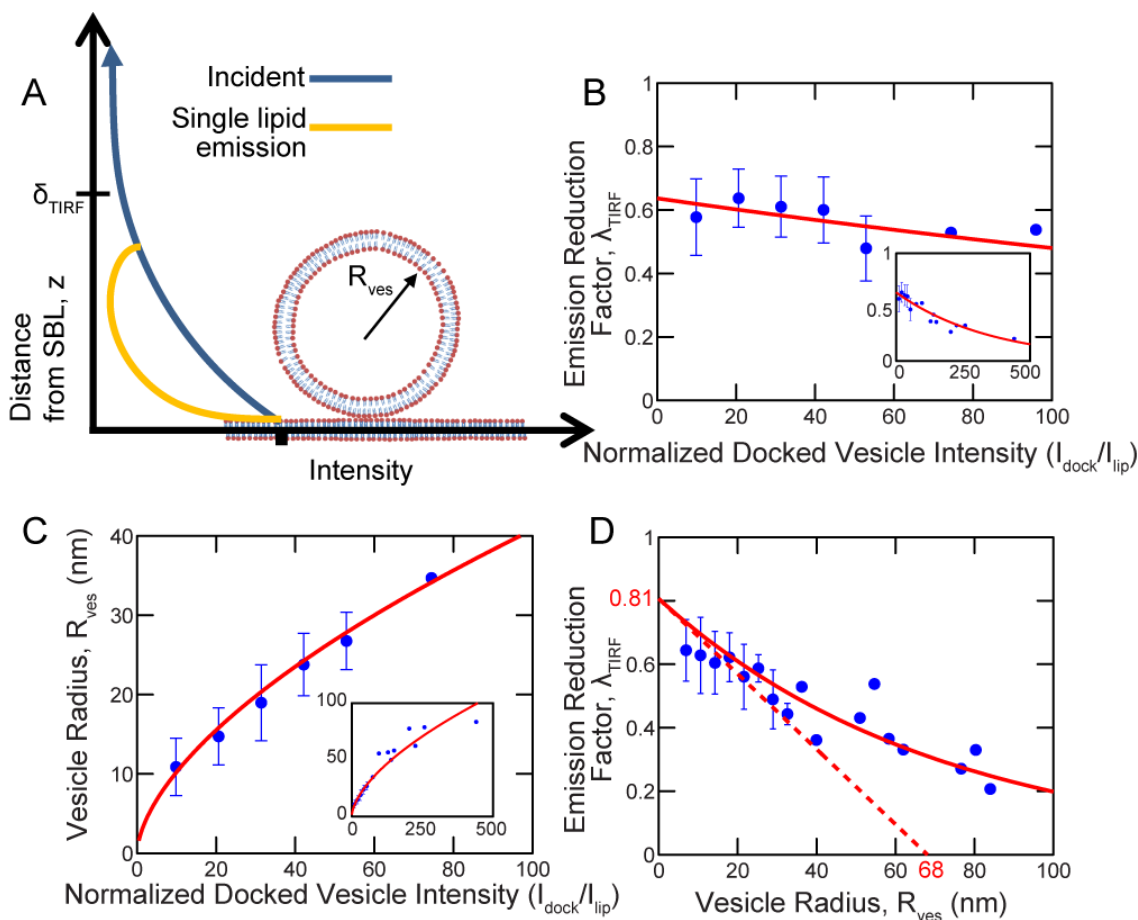


**Figure 2.4-**

In TIRFM the vesicle size and fluorescence reduction factor are unique functions of the docked vesicle intensity. (A) The fluorescence intensity of a labeled lipid distant  $z$  from the SBL in a vesicle of radius  $R_{ves}$  (yellow curve) is the product of the decaying incident evanescent wave intensity (blue curve) and a polarization factor due to lipid orientation. The net fluorescence reduction factor for the vesicle,  $\lambda_{TIRF}$ , is the average of the yellow curve weighted by the number of lipids at each height. (B,C)  $\lambda_{TIRF}$  and  $R_{ves}$  are uniquely determined by the docked vesicle intensity (139 fusion events, see Appendix). (B) Values of  $\lambda_{TIRF}$  versus docked vesicle intensity  $I_{dock}$  from this study follow a best fit exponential  $0.64 \exp(-I_{dock}/350 I_{lip})$  ( $p < 0.05$ ) (red curve). Bin size 10.7. (C) Values of  $R_{ves}$  versus  $I_{dock}$  are well described by the best fit power law  $R_{ves} = 2.6 (I_{dock}/I_{lip})^{0.61}$  nm ( $p < 0.05$ ). Bin size 10.7. (D) Values of  $\lambda_{TIRF}$  versus  $R_{ves}$  from this study. The tangent at the origin (red dashed line) is a linear fit to  $R_{ves} < 35$  nm points, constraining the intercept on the  $R_{ves}$  axis to be the TIRF decay length,  $\delta_{TIRF} = 68$  nm (Appendix, eq. S18) ( $p < 0.05$ ). This yielded  $\lambda_{TIRF}^0 = 0.81$  for the limiting value of  $\lambda_{TIRF}$  for small vesicles, a pure polarization effect. Bin size 3.6 nm. For (B)-(D) mean values (blue symbols)  $\pm$ SD are shown.

### **III-Discussion**

Single exocytotic fusion pores were first detected almost 30 years ago [116], shortly followed by observations of rapid flickering between the open and closed states [116, 117]. Neuroendocrine cells regulate hormone release by adapting the incidence and flickering dynamics of fusion pores to physiologic inputs [113]. Pores also flicker during synaptic vesicle release but the relevance is less established, in part because just a few rapid flickers would empty the vesicle of contents. “Whispering” synapses at which downstream receptors are not activated may be associated with slow release through flickering fusion pores [120], and neurotransmitter release through transient pores may facilitate rapid recycling of synaptic vesicles [106].

The underlying molecular mechanisms of fusion pore flickering remain poorly understood. Here we used TIRFM to study the dynamics of SNARE-mediated fusion pores *in vitro* for the first time.

#### **The size of a docked vesicle can be directly inferred from the docked vesicle intensity in TIRFM**

TIRFM is a powerful technique that selectively illuminates a small ~100 nm deep region adjacent to a substrate [154]. Ideally, one would like to use the method to directly infer the size or location of illuminated objects from the fluorescence intensity, but this relation is not a priori known. For a docked spherical vesicle the intensity results both from the decay of the evanescent field with distance from the substrate, and from the varied orientations of labelled lipids at different locations in the vesicle whose fluorophores thus interact differently with the polarized illuminating field (Fig. 2.4A).

Here, by tracking individual fusion events we measured this characteristic relationship, which for a given TIRFM setup quantifies the relative contributions of evanescent wave decay and polarization effects to the normalized fluorescence intensity  $\lambda_{\text{TIRF}}$  as a function of vesicle radius, Fig. 2.4D. It can be shown that the slope at the origin is  $-\lambda_{\text{TIRF}}^0/\delta_{\text{TIRF}}$  where  $\lambda_{\text{TIRF}}^0$  is the value at zero radius and  $\delta_{\text{TIRF}}$  the decay length of the evanescent excitation field, 68 nm here (see Appendix). The best fit tangent at the origin yielded  $\lambda_{\text{TIRF}}^0 = 0.81 \pm 0.03$ , a pure polarization contribution since evanescent field decay effects are absent as vesicle size tends to zero.  $\lambda_{\text{TIRF}}^0$  being less than unity shows that the evanescent field polarization is a worse match for labelled lipids in the vesicle, averaged over all lipid orientations in the spherical vesicle, than for lipids in the SBL.

### **Fusion pores mediated by SNARE proteins flicker rapidly**

When vesicles fused with the SBL, vesicle-to-SBL lipid release rates were up to two orders of magnitude slower than they would be through fully open pores (Supplementary Fig. S1C). We conclude that pores flickered at rates  $\gtrsim 100$  Hz, the resolution limit of our measurements set by the time for a lipid to diffuse a distance of order the vesicle size,  $\tau_{\text{ves}} \sim 10$  ms. The small release rates could not be explained by permanently open but narrow pores, as this would require invoking pore radii  $r_p$  for lipid release less than the minimum value  $\sim 2$  nm, the lipid monolayer thickness (see Supplementary Fig. S1A and eq. 2.1 and following). Thus, SNARE-mediated pores flicker rapidly in the absence of other fusion machinery components.

## **Lipid membranes alone sustain flickering pores**

We analyzed the population of slow non-specific fusion events[77] and fusion events with protein free SBLs, for both of which we assumed SNARE-independent fusion pore dynamics. For all compositions but those with the highest cholesterol levels studied, pores flickered with similar statistics to those of SNARE-mediated pores: the flickering pore openness, the fraction that were fully open and the cholesterol dependence were similar (Fig. 2.2C, D). This is consistent with previous observations of flickering pores in protein-free systems[105]. This also provides further evidence that lipid diffusion is not severely restricted at the fusion pore by SNARE transmembrane domains. Our results suggest that in cells a major component of the mechanism of fusion pore flickering derives from the biophysical properties of the phospholipid membranes themselves, independently of SNAREs or other fusion machinery.

## **Cholesterol opens fusion pores by lowering the pore bending energy**

Increasing amounts of cholesterol dramatically opened fusion pores (Fig. 2.2B-D). At physiological cholesterol levels flickering pores had a mean openness  $P_o \sim 0.4$ , similar to values  $P_o \sim 0.3 - 0.8$  we estimate for exocytotic pores from electrophysiological measurements [97, 102, 106, 108]. In addition,  $\sim 40\%$  of pores were permanently open, suggesting this may be true of exocytotic pores.

It follows that cholesterol lowers the free energy of pore formation,  $\Delta F_{\text{pore}}$ , closely related to  $P_o$ . This trend was consistent for SNARE-mediated and SNARE-independent pores, suggesting the origin lies in membrane energetics. Thus, adapting the model of ref. [153], we calculated the change in the fusion pore bending energy due to cholesterol, whose

negative spontaneous curvature favors the net negative curvature of the fusion pore. Cholesterol lowered  $\Delta F_{\text{pore}}$ , with a reduction of  $\sim 80 \text{ k}_B\text{T}$  at physiological levels, Supplementary Figure S5, signifying essentially open pores,  $P_o = 1$ . These results can qualitatively explain the experimental trend; however, we observed that a significant fraction of pores remained flickering, suggesting additional effects beyond this simple model.

### **Cholesterol promotes fusion by direct membrane effects and by indirect promotion of SNARE-mediated fusion**

We found that SNAREs play little role in pore flickering when cholesterol is absent or at intermediate concentrations (Fig. 2.2C, D), suggesting that cholesterol opens pores solely through its direct effect on membrane bending energy for these conditions. However at physiological cholesterol levels SNAREs exerted a pronounced pore-opening effect as their presence increased the fraction of permanently open pores  $\sim 2$ -fold (Fig. 3D). Moreover, at these cholesterol levels fusion occurred so rapidly after docking that there was insufficient time to recruit additional t-SNAREs, suggesting that t-SNAREs were pre-clustered at the docking site (Fig. 2.3A), consistent with previously reported cholesterol-mediated t-SNARE clustering [161-163].

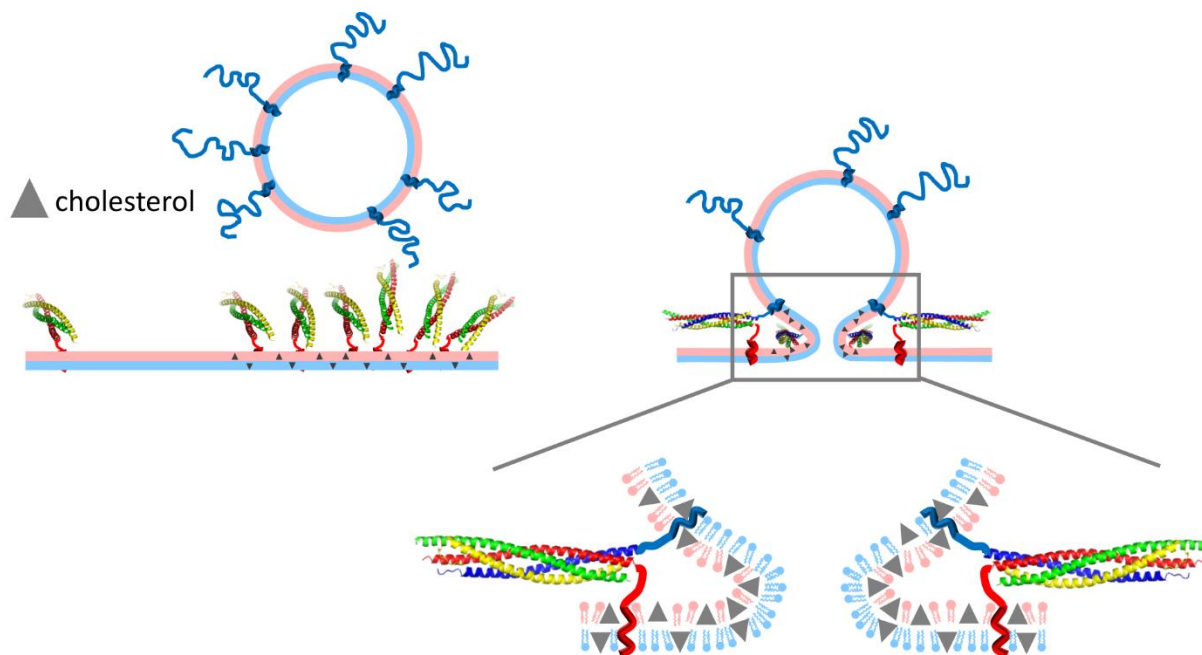


**Figure 2.5-**

Model of promotion of SNARE-mediated fusion by cholesterol. Cholesterol (gray triangles) clusters t-SNAREs in target membranes (left), increasing vesicle docking rates and providing multiple t-SNAREs that are instantly available for accelerated fusion (right). Once initiated, the openness of the flickering pore is increased by cholesterol: (i) directly, by lowering the bending energy of the pore (Fig. S5) whose negative curvature is compatible with cholesterol's large, negative spontaneous curvature  $\sim -0.4 \text{ nm}^{-1}$  [164] (blow up, right); (ii) indirectly, by increasing the number of SNAREpins at the fusion pore. Increased openness stabilizes the pore and may increase contents release rates and accelerate pore dilation (Fig. 1.1).

A growing body of evidence suggests that cholesterol opens pores and augments fusion rates [124, 127, 128]. Our results suggest that cholesterol facilitates exocytosis both directly, by lowering the energy to deform membranes into the severely bent shape of a fusion pore, and indirectly through its influence on SNARE proteins (Fig. 2.5). We propose that by clustering t-SNAREs in target membranes cholesterol increases vesicle docking rates and increases the number of SNAREpins that cooperate to create and maintain a fusion pore, thereby increasing the openness of the pore [85]. By increasing openness these

effects stabilize fusion pores, increase rates of content release and may accelerate pore dilation.

## Methods

**Recombinant protein expression and purification.** Recombinant VAMP2, Syntaxin-1, and SNAP25 were expressed, purified, and reconstituted into small unilamellar vesicles (SUVs) as described in detail previously [77, 132]. The membrane compositions tested in this study are shown in Tables **S1**, **S2**. 1-palmitoyl-2-oleoyl-sn-glycero-3-phosphocholine (POPC), 1,2-dioleoyl-sn-glycero-3-phosphocholine (DOPC), 1,2-dioleoyl-sn-glycero-3-phospho-(1'-myo-inositol-4',5'-bisphosphate) (PI(4,5)P<sub>2</sub>), 1,2-dioleoyl-sn-glycero-3-phosphoethanolamine-N-(lissamine rhodamine B sulfonyl) (LR-PE), 1,2-dioleoyl-sn-glycero-3-phosphoethanolamine-N-(7-nitro-2-1,3-benzoxadiazol-4-yl) (NBD-PE), 1,2-dioleoyl-sn-glycero-3-phosphoethanolamine-N- [methoxy(polyethylene glycol)-2000] (PEG2K-PE), and cholesterol were purchased from Avanti Polar Lipids, Inc. PI(4,5)P<sub>2</sub>, only found in plasma membranes [157], and NBD-PE, used to check SBL fluidity using fluorescence recovery after photobleaching [132], were included only in the t-SNARE SBLs.

We used lipid-to-protein ratios (L:P) of 200 and 20,000 for the v-SUVs and t-SBLs, respectively. Even for the smallest v-SUVs ( $R_{ves} = 10 - 20$  nm), this provides enough copy numbers (5-17) of externally facing v-SNAREs per SUV, because efficient fusion in this assay requires  $\geq 5$  SNARE complexes [77]. Thus, our results for the number of t-SNAREs recruited for fusion (Fig. 4A) are not limited by the number of v-SNAREs present on vesicles.

**Preparation of SUVs and SBLs.** We used the method of refs. [77, 132], but with different lipid compositions as in Tables S1 & S2.

**Microfluidic flow channels and microscopy.** Fabrication of microfluidic flow channels, formation and characterization of t-SNARE-reconstituted supported bilayers (SBLs) in the channels, and detection of fusion events are described in detail in Karatekin & Rothman [132]. In this assay, fusion of single v-SNARE reconstituted liposomes (v-SUVs) with t-SNARE bearing SBLs is observed with frame rates of 32/s (full frame) to 60/s (from a cropped region of interest). These correspond to frame durations of 31 and 17 ms, respectively. Frame durations shorter than ~15 ms resulted in lower signal-to-noise ratios that made tracking of single LR-PE fluorescently labeled lipids difficult. One pixel corresponded to 267 nm in the sample plane.

To determine the areal lipid density in the membranes,  $\rho_{lip} = 1/(f_{lip} a_{lip})$  where  $f_{lip}$  is the fraction of lipids that are labeled, we assumed a lipid head group area  $a_{lip} = 0.8 \text{ nm}^2$  for PC/PS/PE/PIP2 and PC/PS compositions and  $a_{lip} = 0.6 \text{ nm}^2$  for PC/PS/PE/PIP2/Ch+ and PC/PS/PE/PIP2/Ch compositions [165].

Some of the data was obtained using an inverted microscope (Olympus IX81) equipped with an EM-CCD camera (iXon Ultra, Andor) and the Olympus CellTIRF TIRFM accessory. The microscope and data acquisition were controlled by Micro-Manager (UCSF). A 100X / 1.49 NA oil TIRF objective (UAPO N, Olympus) was used. All experiments were carried at 32 °C (Thermo Plate, TOKAI HIT). Images were collected with a frame duration 17 ms (full frame). We used a 488 nm laser for FRAP measurements, a 561 nm laser for detecting LR-PE or DiI during fusion.

To estimate the evanescent field penetration depth, we measured the angle of incidence  $\theta$  of the excitation beam with respect to the normal to the imaging plane, and used the

expression  $\delta_{TIRF} = \lambda_o / 4\pi (n_g^2 \sin^2 \theta - n_w^2)^{-1/2}$  [154], where  $\lambda_o = 532$  nm is the laser wavelength, and  $n_g = 1.52$  and  $n_w = 1.33$  are the refractive indices of glass and water, respectively. For this, we coupled a 2 cm by 2 cm by 2cm BK7 glass cube (Thorlabs) to the TIRF objective using oil that matched the refractive index of glass. At angle  $\theta$  used to generate TIR in the fusion experiments, the beam went undeflected into the cube, emerged from one side refracted at the glass-air interface, and projected onto a wall. Simple geometry based on the beam position on the wall and the position of the objective, along with the known refraction at the cube-air interface allowed calculation of the incidence angle  $\theta = 73.5 - 77.4^\circ$  ( $\delta_{TIRF} = 65 - 71$  nm), with the highest intensity spot at  $75^\circ$ , corresponding to  $\delta_{TIRF} = 68$  nm. This value is used in section “*The size of a docked vesicle can be directly inferred from the docked vesicle intensity in TIRFM.*” and Fig. 5D.

**Single lipid-label measurements.** We tracked single lipids using ImageJ and Speckle TrackerJ, the tracking plugin described in ref. [155]. For details, see Appendix, Fig. S2A-C

**Analysis of single vesicle events.** We identified fusing vesicles by eye and tracked them using the ImageJ plugin Speckle TrackerJ [155]. We used fusing vesicle trajectories to train Speckle TrackerJ to track the remaining vesicles which dock. For each fusion event the total intensity in a region of interest was computed with Matlab from the trajectories obtained from SpeckleTrackerJ.

**Curve fitting.** We performed all curve fitting using the Curve Fitting Toolbox in Matlab with linear or nonlinear least squares optimization.

## Appendix- Chapter 2

### Lipid compositions used in this study (details)

Symbol	PC (%)	DOPS (%)	SAPE (%)	PIP2 (%)	Chol (%)	Label (%)	PEG-PE	Label
$\alpha_{\text{chol}}^+$	22.53	11.57	15.43	-	45.99	0.62	3.86	LR-PE
$\alpha_{\text{chol}}$	23.75	12	15	-	45	0.8	3.45	LR-PE
	23.55	12	15	-	45	1	3.45	DiI
$\alpha$	67.2	12	15	-	-	0.8	5	LR-PE
	67	12	15	-	-	1	5	DiI
	59.2	15	20	-	-	0.8	5	LR-PE
$\beta$	79.2	15	-	-	-	0.8	5	LR-PE

**Table S1-**

Lipid compositions for vesicle membranes. Symbols  $\alpha_{\text{chol}}^+$ ,  $\alpha_{\text{chol}}$ ,  $\alpha$ , and  $\beta$  denote PC/PS/PE/PIP2/Ch+, PC/PS/PE/PIP2/Ch, PC/PS/PE/PIP2, and PC/PS, respectively. PC denotes 1-palmitoyl-2-oleoyl-*sn*-glycero-3-phosphocholine, POPC, except for composition  $\beta$  where it denotes 1,2-dioleoyl-*sn*-glycero-3-phosphocholine, DOPC; DOPS denotes 1,2-dioleoyl-*sn*-glycero-3-phospho-L-serine; SAPE denotes 1-stearoyl-2-arachidonoyl-*sn*-glycero-3-phosphoethanolamine; PIP2 denotes phosphatidylinositol 4,5-bisphosphate; LR denotes the fluorescent group lissamine rhodamine B.

<b>Symbol</b>	<b>PC (%)</b>	<b>DOPS (%)</b>	<b>SAPE (%)</b>	<b>PIP2 (%)</b>	<b>Chol (%)</b>	<b>Label (%)</b>	<b>PEG-PE (%)</b>
$\alpha_{\text{chol}}^+$	18.91	11.57	15.43	3.86	45.99	0.38	3.86
$\alpha_{\text{chol}}$	54.9	12	15	3	10	0.5	4.6
$\alpha$	64.5	12	15	3	-	0.5	5
	54.5	15	20	5	-	0.5	5
$\beta$	79.5	15	-	-	-	0.5	5

**Table S2-**

Lipid compositions for SBL membranes. Symbols have same meaning as for Table S1. Label for SBL is NBD-PE, which denotes 1,2-dioleoyl-sn-glycero-3-phosphoethanolamine-N-(7-nitro-2-1,3-benzoxadiazol-4-yl).

## Decomposition of the docking-to-fusion delay time distribution into a fast and a slow component

For each fusion event, following docking of a vesicle onto the SBL fusion occurred after a delay time  $\tau_{\text{delay}}$  (Fig. 2.1B, C). We measured  $\tau_{\text{delay}}$  from the TIRF signal and for each lipid composition we constructed the distribution of delay times, represented as the survivor function  $S(\tau_{\text{delay}})$ , the probability fusion has not occurred after a time  $\tau_{\text{delay}}$  (Fig. S2E). From these distributions we found that there are two populations of fusion events: a fast-fusing population and a slowly fusing population with significantly longer delay times, similarly to ref. [77]. Following ref. [77] we interpreted the fast fusers as being SNARE-dependent, and the slow fusers as originating in non-specific events and involving fusion pores whose dynamics were not controlled by SNAREpins. This enabled us to measure the effects of SNARE proteins on flickering fusion pore dynamics, and to study by comparison the dynamics of fusion pores that are apparently controlled only by the lipid membranes independently of SNAREs, consistent with ref. [77].

The survivor distributions were well fit by mixed exponentials of the form  $S(\tau_{\text{delay}}) = a \exp(-\tau_{\text{delay}}/\bar{\tau}_{\text{delay}}) + (1 - a) \exp(-\tau_{\text{delay}}/\bar{\tau}_{\text{ns}})$  where  $a$  is the amplitude of the fast fusing component and is interpreted as the fraction of vesicles which fuse in a SNARE-mediated manner,  $\bar{\tau}_{\text{delay}}$  is the mean docking-to-fusion delay time for SNARE-mediated fusion, and  $\bar{\tau}_{\text{ns}}$  is the mean delay time for non-specific fusion. Fits were obtained using a maximum likelihood estimate using Matlab's Statistics Toolbox.  $\bar{\tau}_{\text{ns}}$  was in the range  $\sim 2 - 3$  s for all compositions,  $\sim 10$  times greater than typical mean delay times for specific SNARE-mediated events.

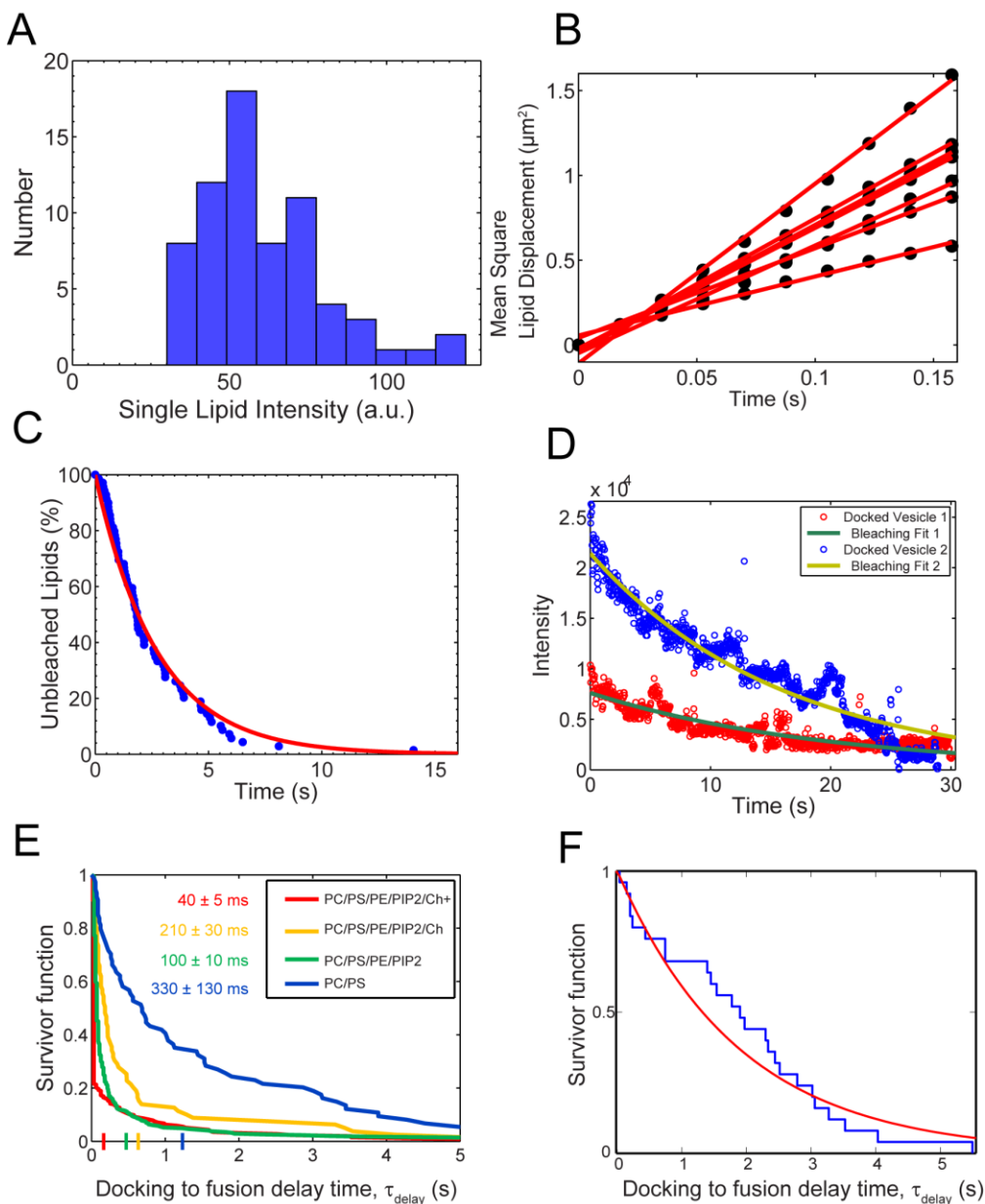


**Figure S1-**

Single lipid properties needed for fusion event analysis. (A-C) Single lipid resolution enables accurate measurement of diffusivity, bleaching time and single lipid emission. Plots shown for PC/PS membrane composition. (A) Distribution of measured single lipid intensities,  $I_{lip}$ , in a typical movie. (B) Mean square displacement versus time for seven lipid trajectories. (C) Digital measurement of bleaching time  $\tau_{bleach}$ . Labeled lipids in the SBL suddenly ceased fluorescing, indicating that these fluorescing spots were individual lipids. The survivor fraction is shown for a sample movie, fit to an exponential  $\exp -t/\tau_{bleach}$  (red curve). (D) Bleaching of lipids in vesicles is much slower than for lipids in the SBL. Emission intensity versus time for two representative unfused vesicles. Each is shown with a best fit curve to a decaying exponential  $I(t) = e^{-t/\tau_{bleach}^{ves}}$  where  $\tau_{bleach}^{ves}$  is the bleaching time in the vesicle. Both events are for PC/PS/PE/PIP2/Ch+ membrane composition. The bleaching time of the Docked Vesicle 1 (data: red points, best fit exponential: green curve) is 19.9 s. The bleaching time for Docked Vesicle 2 (data: blue points, best fit exponential: gold curve) is 16.0 s. Both values are much greater than  $3s \lesssim \tau_{bleach} \lesssim 5s$ ,

the bleaching time in the SBL. (E) Docking-to-fusion delay time distributions: measured survivor functions for all compositions. Mean delay times  $\bar{\tau}_{\text{delay}}$  for each composition are shown, along with 95% confidence interval. Colored ticks on the x-axis indicate the cutoff times used to separate the SNARE-mediated and non-specific fusion events. The cutoff times were obtained by fitting double exponentials to the survivor functions. (F) Docking-to-fusion delay time distributions for fusions between protein-free SBLs and v-SNARE containing SUVs, for lipid composition PC/PS/PE/PIP2/Ch that contains 45% (10%) cholesterol in the SUV (SBL) (see Tables **S1**, **S2**). Measured survivor function (blue curve) and best fit exponential (red curve) with delay time  $\bar{\tau}_{\text{pf}} = 1.9$  s are plotted. There is no statistically significant difference between this distribution and the long tail of the slow component of the delay time distribution for PC/PS/PE/PIP2/Ch fusion events ( $p > 0.05$ ), part (E).

**Method to identify events as fast or slow.** We determined a maximum cutoff time for the specific SNARE-mediated events, and defined all events with  $\tau_{\text{delay}}$  less (greater) than this time to be specific (non-specific) events. The cutoff time was determined as follows. As the parameter  $a$  represents the fraction of fusion events which are SNARE-mediated, we varied the cutoff time until the fraction of fusion events below this cutoff time matched  $a$  from the double exponential fit. For self-consistency, we checked that the cutoff time was larger than the mean value of the delay time for the fast fusers and smaller than the mean value of the delay time for the slow fusers. The cutoff times we find, ~70-600 ms (Fig. **S2E**), are ~2-6-fold greater than  $\bar{\tau}_{\text{delay}}$  and ~4-fold smaller than  $\bar{\tau}_{\text{ns}}$ .

**The statistics of fusion events between v-SUVs and protein-free SBLs are similar to those for the slow component of fusion events between v-SUVs and t-SBLs.** We also examined fusion events between protein-free SBLs (pf-SBLs) and v-SNARE containing SUVs (v-SUVs). To test that the slow component of the fusion events between t-SNARE containing SBLs (t-SBLs) and v-SUVs represented events for which the fusion pore dynamics were SNARE-independent, we compared  $\bar{\tau}_{\text{ns}}$  to  $\bar{\tau}_{\text{pf}}$ , the mean value of the delay time for pf-SBL/v-SUV fusion events. For membranes with 45% (10%) cholesterol in the

SUV (SBL) we found  $\bar{\tau}_{\text{pf}} \sim 2.9$  s, statistically indistinguishable from  $\bar{\tau}_{\text{ns}}$  for the same composition, Fig. 2.3A ( $p > 0.05$ ). Similarly, for the same composition the openness  $P_0 \sim 0.05 \pm 0.02$  of pf-SBL/v-SUVs fusion pores was statistically indistinguishable from the pore openness for the slow component of the t-SBL/v-SUV fusion events ( $P > 0.05$ , see non-specific events in Fig. 2.2C).

These observations are consistent with the hypothesis that the fusion pore dynamics of the slow component of t-SBL/v-SUV events are determined by the physical properties of the lipid bilayers.

### **Properties of single fluorescent lipids in the SBL**

In the main text (*SNARE-mediated fusion pores flicker or are permanently open*, in Results) we fit the predicted total intensity time course, eq. 2.3, to the measured integrated intensity time course  $I_{\text{tot}}(t)$  for each fusion event to determine the pore openness and vesicle size (Fig. 2.2). In order to perform this fit, we required three single lipid properties: the single fluorescent lipid intensity  $I_{\text{lip}}$  in the SBL, the fluorescent lipid bleaching time in the SBL  $\tau_{\text{bleach}}$ , and the single lipid diffusivity  $D_{\text{lip}}$  (Fig. S2). Almost all fluorescent spots released into the SBL upon fusion remained bright for a period and then suddenly darkened (bleached) in a single frame, consistent with these spots being single fluorescent lipids. In this way, for each lipid we made a ‘digital’ measurement of the bleaching time. We confined our single lipid analysis to those which bleached in one step in this manner. Fluorescent lipids were tracked using SpeckleTrackerJ [155], and further analysis was performed using Matlab.

**Measurement of single fluorescent lipid intensity,  $I_{lip}$ .** We measured the intensity of a single lipid by measuring the average change of intensity upon bleaching. We take the average of the total intensity of a lipid in an area  $3 \times 3$  pixels ( $0.80 \times 0.80 \mu m^2$ ) centered on the lipid, time-averaged over the final 15 frames for which the lipid fluoresced. We measured the background intensity in the same location where the lipid bleached, over the 15 frames following bleaching. The latter was subtracted from the former to determine the intensity of the individual lipid. We then averaged each of these individual lipid intensities over  $\sim 40$  lipids to determine the mean single lipid intensity  $I_{lip}$  for a given movie,  $\sim 1$  min in duration (i.e. Fig. S2A). All analysis of events from that movie used the measured single lipid intensity from that movie.

**Measurement of single lipid diffusion coefficient,  $D_{lip}$ .** We calculated the mean square displacement (MSD) for lipid trajectories lasting  $\geq 1.5$  seconds and determined the best fit linear relation of MSD vs.  $t$  over time windows ranging from one to 10 frames ( $t_{frame} \approx 17$  ms or 31 ms) to sample a full range of the trajectory. A sample of 7 of these MSD curves is shown in Fig. S2B. We then calculated the diffusion constant from  $MSD = MSD(0) + 4 D_{lip} t$  for each analyzed trajectory. We report a mean  $\pm$  SEM  $D_{lip}$  averaged from  $\sim 20$  analyzed lipid trajectories for each lipid composition, Table S3. The MSD was calculated in Matlab.

Symbol	$D_{\text{lip}}$ ( $\mu\text{m}^2/\text{s}$ )	Label
$\alpha_{\text{chol}}^+$	0.45	LR-PE
$\alpha$	1.17	LR-PE
	1.43	DiI
$\alpha_{\text{chol}}$	1.49	LR-PE
	2.39	DiI
$\beta$	1.7	LR-PE

**Table S3-**

Diffusion constants for each lipid membrane composition studied, and for each label used. Calculated from the measured mean square displacement curves for each composition (Fig. **S2B**).

**Measurement of lipid bleaching time in the SBL,  $\tau_{\text{bleach}}$ .** We measured the lipid bleaching time  $\tau_{\text{bleach}}$  by determining the total duration of single lipid trajectories and then calculating the survivor function  $f_{\text{fluor}}(t)$  describing many such trajectories. We fit a decaying exponential to the survivor function  $f_{\text{fluor}}(t) = e^{-t/\tau_{\text{bleach}}}$  (Fig. **S2C**). Approximately 50 bleaching episodes were used to calculate the survivor function in each movie. The uncertainty reported is the 95% confidence interval from the fitting routine.

**The bleaching rate in the vesicle is much slower than that in the SBL.** Our measurements of single lipid bleaching were for lipids in the SBL. To determine bleaching rates for lipids in vesicles (expected to be lower since the fluorescence emission is lower) we measured the bleaching time of entire vesicles  $\tau_{\text{bleach}}^{\text{ves}}$  for  $\sim 30$  vesicles that did not fuse per movie. We measured  $\tau_{\text{bleach}}^{\text{ves}}$  from the best fit exponential  $I_{\text{tot}}(t) = I_0 \exp(-t/\tau_{\text{bleach}}^{\text{ves}})$  (Fig. S2D).  $I_{\text{tot}}$  is the spatially integrated intensity over a box of size 15x15 pixels centered on the unfused vesicle, with the background subtracted off. Repeating this for each movie, we found that the bleaching time in vesicles is  $\sim 5$ - $8$ -fold greater than the bleaching time in the SBL. Thus, when we used our model to calculate the

fluorescence intensity versus time,  $I_{tot}(t)$ , we neglected fluorescent bleaching of lipids in the vesicle (eqs. 3, 4).

### **Analysis of individual fusion events.**

For each fusion event, we measured the total intensity versus time  $t$ ,  $I_{tot}(t)$  (Fig. 2.1B and C). To do this, we measured the integrated intensity by drawing a square region of interest of size 30x30 pixels. We use a box of this size to ensure that all of the lipids remain in the box for the duration of the measurement, 1.6 s. We analyzed fusion events with longer release times by manually drawing larger boxes based on the specific fusion event. Fusing vesicles were well spaced enough that we did not have to account for significant background lipid diffusion into the region of interest.

**In TIRFM the evolving fluorescence intensity following a SUV-SBL fusion event provides a high time resolution readout of lipid transfer.** As described in the main text, when lipids diffuse from a vesicle into the SBL through the walls of a fusion pore a rapid increase in fluorescence intensity is observed due to the spatial decay of the intensity of the incident evanescent wave, and the change in mean lipid orientation when a lipid transfers to the planar SBL from the spherical SUV which alters the coupling to the polarized evanescent wave. The increase in fluorescence is instantaneous upon transfer of a labeled lipid into the SBL and thus provides a very sensitive measure of the fraction of dye transferred between the fusing membranes as a function of time, with temporal resolution limited only by acquisition frame rates (~100 Hz, which is in turn limited by the exposure time needed to detect single fluorophores). In conjunction with a mathematical

model of release through a flickering pore, this enabled us to accurately measure SUV-to-SBL lipid release times  $\tau_{\text{release}}$ . A fitting procedure using the mathematical model was needed because the lipid release kinetics are convoluted with bleaching kinetics (Fig. 2.1C).

By comparison the spread of the dye from the fusion site to a distance larger than the optical resolution ( $\sim 250$  nm) would take 60 ms or longer (taking  $D_{\text{lip}}=1 \mu\text{m}^2\text{s}^{-1}$ ), too slow to measure typical release times. In a previous work where we employed the present SUV-SBL fusion assay, but used far-field fluorescence microscopy rather than TIRFM, the signal of fusion was taken to be this spread of lipids from the fusion site, quantified by the time course of the width of a two-dimensional Gaussian profile fit to the image sequence representing a fusing vesicle [77].

A different kind of resolution limit determines the minimum flickering frequency our method can access. When a flickering pore opens (Fig. S1A), if it remains open for longer than the time for all labelled lipids to diffuse out of the vesicle through the open pore, the signal will be lost before completion of a single flicker cycle. This diffusion time is approximately  $\tau_{\text{ves}}$ , the lipid diffusion time for a distance of order the vesicle size (multiplied by a logarithmic factor of order unity involving the pore diameter). Thus when we observe a pore openness  $<1$ , indicating that the release time exceeds  $\tau_{\text{ves}}$ , the most we can say is that the flickering frequency is higher than this lower limit. Given  $\tau_{\text{ves}} \sim 10\text{ms}$  for a typical vesicle size, it follows that the pores we measure flicker at frequencies  $\gtrsim 100$  Hz. A similar limitation holds for amperometry, once the contents have been released, the pore may continue to flicker without being observed.

## Dependence of fusion statistics on vesicle size

**Fusion pore statistics do not depend on vesicle size.** Over the vesicle size range ( $10 \lesssim R_{\text{ves}} \lesssim 80$  nm) and lipid compositions studied, our data did not reveal correlations between vesicle size and either docking-to-fusion delay times, pore openness  $P_o$  or the fraction of pores that were permanently open (Fig. S4A-C).

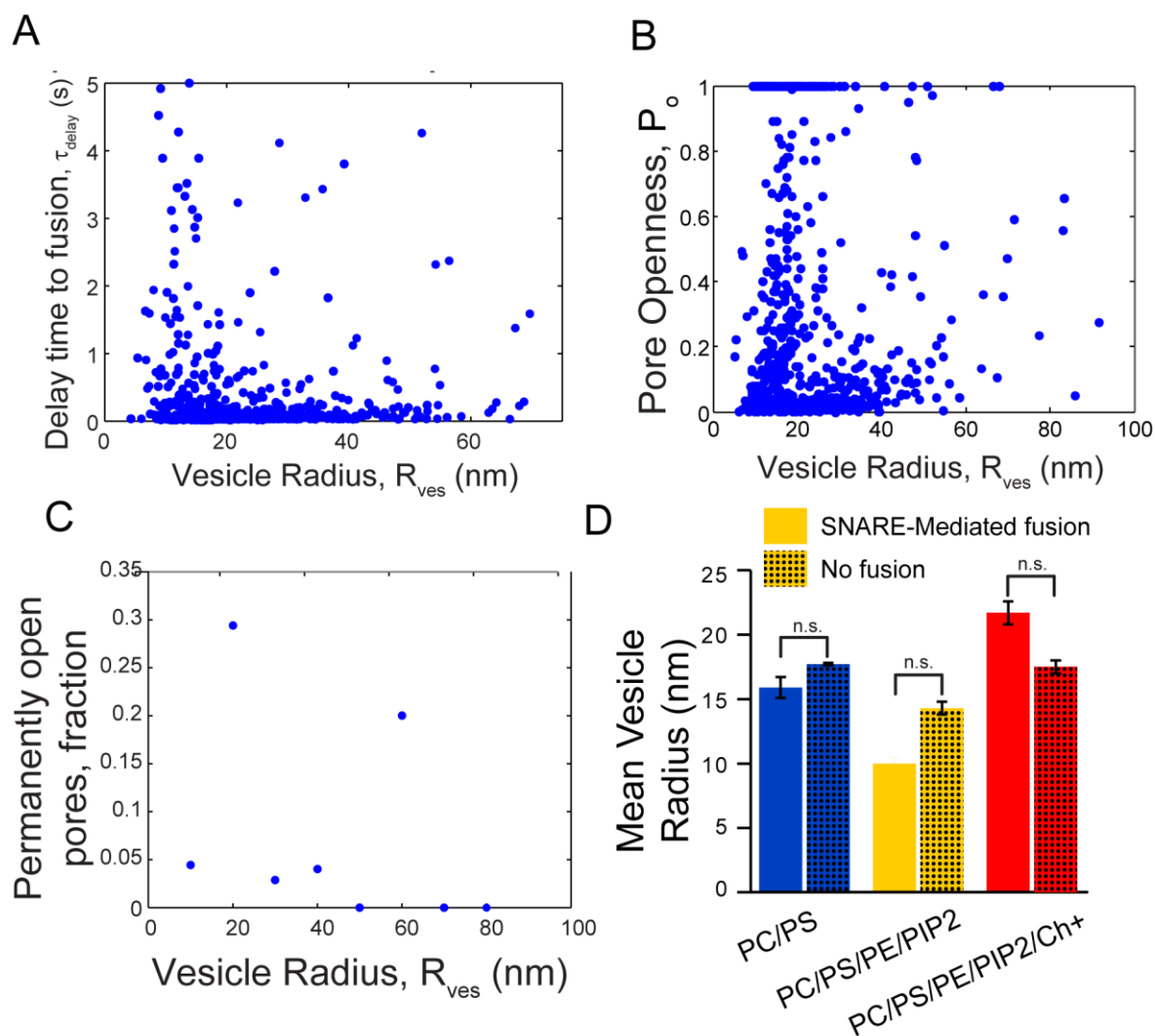


**Figure S2-**

Statistics of fusion reveal no dependence on vesicle size. (A) Docking-to-fusion delay times versus vesicle size showed no correlations ( $c_{\text{corr}} = -0.04$ ,  $n=772$ , SNARE-mediated and non-specific events). Data shown represents all fusion events measured in this study for which both SBL and SUV membranes contained SNAREs, for all compositions (Tables S1,S2). (B) Pore openness is not correlated with vesicle size, ( $c_{\text{corr}} =$

0.05, n=555 specific fusion events). Data shown represents all SNARE-mediated fusion events measured in this study (fast component of delay time distribution) for all compositions. (C) Fraction of pores that are permanently open is not correlated with vesicle size ( $c_{\text{corr}} = -0.04$ ). Bin size 10nm. Same fusion events as for (B). (D) Mean size of vesicles that undergo SNARE-mediated fusion (solid bars) is statistically indistinguishable from mean size of docked vesicles that do not fuse during the bleaching time (dotted bars),  $P > 0.05$ . The comparison is shown for three lipid membrane compositions.

**Fusion probability does not depend on vesicle size.** A fraction of vesicles dock but do not fuse within the time the labelled lipids in the vesicle have completely bleached. Thus we sought to determine whether these vesicles followed a different size distribution to vesicles that fused, as this would suggest size-dependence in the fusion mechanism.

For these events where fusion does not occur we could not use our usual procedure to measure vesicle size, which is based on fitting our model to a fluorescence intensity versus time curve  $I_{\text{tot}}(t)$  during a fusion event. Thus, to obtain the size distribution of such vesicles, we measured the docked vesicle intensity  $I_{\text{dock}}$  (Fig. 2.1C) and to deduce the vesicle radius  $R_{\text{ves}}$  we used the best fit power law relation  $R_{\text{ves}} = 2.6(I_{\text{dock}}/I_{\text{lip}})^{0.61}$  obtained from the assembled data from this study (Fig. 2.4C).

We then compared this distribution of non-fusers to the vesicle size distribution for vesicles that underwent SNARE-mediated fusion. The comparison showed that the size distributions were statistically indistinguishable (Fig. **S4D**).

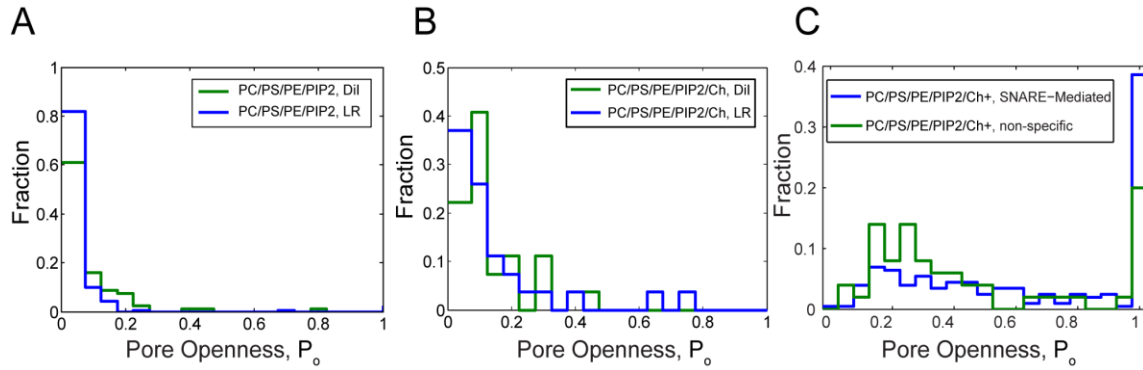


**Figure S3-**

(A, B). Measured distributions of pore openness were not significantly different ( $p > 0.05$ , student's t-test) for two distinct fluorescent lipid labels, lissamine-rhodamine-tagged PE (LR-PE) and the lipophilic dye DiI. This was true for both lipid compositions PC/PS/PE/PIP2 and PC/PS/PE/PIP2/Ch. These results suggest that LR-PE diffusion is not anomalously suppressed in the fusion pore and that the  $P_o$  values inferred from release kinetics of LR-PE through fusion pores are valid. (C) Distributions of fusion pore openness for SNARE-mediated and non-specific fusion events between membranes having high cholesterol content (lipid composition PC/PS/PE/PIP2/Ch+). The fraction of pores that were fully open was  $\sim 2$ -fold higher when SNAREs mediated the pores.

## Calculation of relation between pore openness and lipid release time

In the main text (“Fusion pore openness  $P_o$  is quantitatively related to lipid release time  $\tau_{\text{release}}$ ” in Results) we presented results to a mathematical model of diffusion of labeled lipids from the membrane of a vesicle through a flickering fusion pore into the SBL membranes, eqs. 1, 3, and 4. Here, we describe the derivation of these results, specifically the results for  $P_o$  as a function of vesicle area  $A_{\text{ves}}$  and lipid release time  $\tau_{\text{release}}$  (eq. 2.1), and the time dependent TIRF intensity emission  $I_{\text{tot}}(t)$  for both a flickering pore and a permanently open pore (eqs. 3 and 4 of the main text).

We will show below that  $\phi_{ves}(t)$  decays exponentially in time for a flickering pore. In parallel, we will show that for the special case of a fully open pore the release kinetics are instead of power law form,  $\phi_{ves} \sim 1/t$  (eq. 2.3).

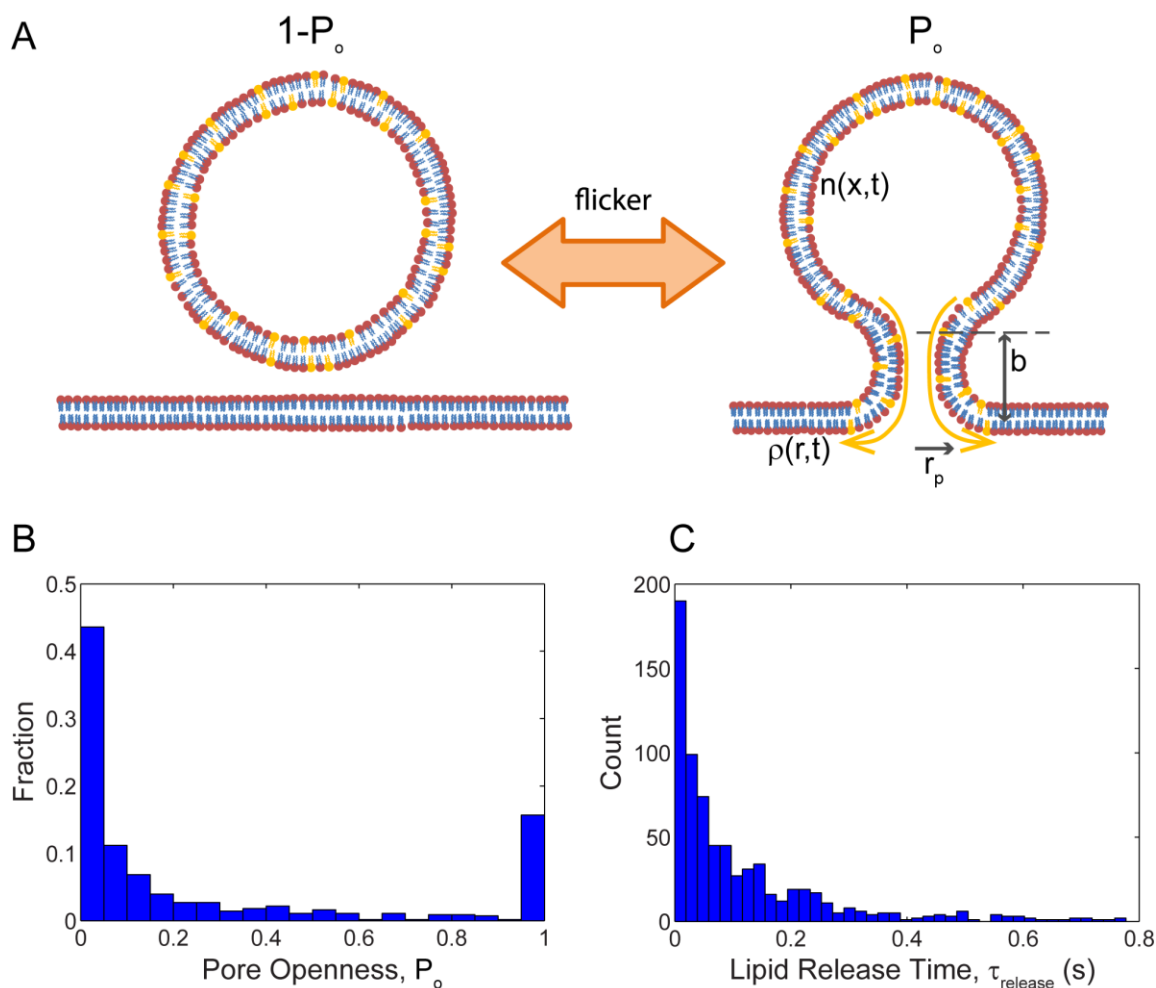


**Figure S4-**

(A) Model of lipid release from a vesicle through a flickering fusion pore. Schematic of model. The pore is centered at  $x = 0$  in the vesicle and  $r = 0$  in the SBL. The density of labelled lipids in the vesicle is  $n(x, t)$  and in the SBL is  $\rho(r, t)$ . Here, we model the pore as a cylinder of length  $b = 15$  nm and radius  $r_p = 3$  nm. The pore radius is measured from the center of the pore to the centerline of the bilayer. During open periods of the pore, lipids can diffuse through the membranes of the neck of the pore into the SBL membranes; the net current is proportional to the density difference across the pore multiplied by the fraction of the time the pore is open,  $P_o$  (eqs. S1 and S2). (B) Measured overall distribution of  $P_o$  values, for all compositions. Mean openness for flickering pores

is  $0.14 \pm 0.01$  and the fraction of pores that are permanently open is 15%. Bin size 0.05. (C) Measured distribution of lipid release times across all compositions. Bin size is 0.02 s.

The flickering pore is open for a fraction  $P_o$  of the time and closed for a fraction  $1 - P_o$  of the time. The starting point of the model is the time evolution of the density of labelled lipids in the vesicle,  $n(\mathbf{x}, t)$  and in the SBL,  $\rho(\mathbf{r}, t)$  (Fig. S1A).

$$\partial n / \partial t = D_{\text{lip}} \nabla^2 n - Q(t) \delta(\mathbf{x}), \partial \rho / \partial t = D_{\text{lip}} \nabla^2 \rho + Q(t) \delta(\mathbf{r}), \quad \text{S1}$$

where  $D_{\text{lip}}$  is the lipid diffusivity. From these fields, we calculate the fraction of labelled lipids remaining in the vesicle,  $\phi_{\text{ves}}(t)$ . The driving force for lipid release from the vesicle into the SBL is the density difference across the fusion pore,  $n_0(t) - \rho_0(t)$ . The lipid release rate  $Q(t)$  is the product of this density difference and the pore transmission coefficient  $k_{\text{pore}}$

$$Q(t) = k_{\text{pore}} \{n(0, t) - \rho(0, t)\}, d\phi_{\text{ves}}/dt = -Q(t)/n_0 A_{\text{ves}}, \quad \text{S2}$$

where  $k_{\text{pore}}$  is the pore transmission coefficient and  $n_0$  the initial density of labeled lipids in the vesicle of area  $A_{\text{ves}}$ . For simplicity, we take the pore as a cylinder of height  $b$  and radius  $r_p$ , commonly assumed in the interpretation of pore conductances [101, 107, 110, 111]. The release rate is then the flux through a cylindrical membrane tube of cross-sectional length  $2\pi r_p$ , i.e.

$$k_{\text{pore}} = P_o D_{\text{lip}} 2\pi r_p / b. \quad \text{S3}$$

Note that  $k_{\text{pore}}$  is reduced by the pore openness,  $P_o$ , which for a two-state (open/closed) pore is the fraction of the time the flickering pore is in the open state. More generally, for

a pore whose size changes continuously up to some maximum size in the fully open state,  $P_0$  is the mean pore radius relative to the maximum value.

We consider two cases: an infrequently open flickering pore (eq. 2.1) and a permanently open pore (eq. 2.3). We then calculate the total TIRF intensity as a function of time,  $I_{\text{tot}}(t)$ , for each case, allowing us to extract lipid release times  $\tau_{\text{release}}$ , vesicle sizes  $R_{\text{ves}}$ , and pore openness  $P_0$  for individual fusion events.

The solutions to eq. S1 can be written:

$$\begin{aligned} n(\mathbf{x}, \mathbf{t}) &= \mathbf{n}_a - \int_0^{\mathbf{t}} d\mathbf{t}' Q(\mathbf{t}') \mathbf{G}_s(\mathbf{0}, \mathbf{x}, \mathbf{t} - \mathbf{t}') \\ \rho(\mathbf{r}, \mathbf{t}) &= \int_0^{\mathbf{t}} d\mathbf{t}' Q(\mathbf{t}') \mathbf{G}(\mathbf{0}, \mathbf{r}, \mathbf{t} - \mathbf{t}') \end{aligned} \quad \text{S4}$$

where  $\mathbf{G}_s(\mathbf{x}', \mathbf{x}, \mathbf{t})$  is the Green's function of the diffusion equation in the vesicle, the probability a lipid in the vesicle at  $\mathbf{x}'$  diffuses to  $\mathbf{x}$  a time  $\mathbf{t}$  later, and  $\mathbf{G}(\mathbf{r}', \mathbf{r}, \mathbf{t})$  is the same for the SBL. Setting  $\mathbf{r} = \mathbf{x} = 0$  and including eq. S1 and S2 gives:

$$\begin{aligned} n_0(t) &= n_a - \int_0^t dt' g(t - t') \\ \rho_0(t) &= \int_0^t dt' Q(t') S(t - t') \\ Q(t) &= k_{\text{pore}} (n_0(t) - \rho_0(t)) \end{aligned} \quad \text{S5}$$

where  $g$  and  $S$  are the return probabilities for the vesicle and the SBL respectively, namely the Green's functions evaluated at  $\mathbf{x} = \mathbf{x}'$  and  $\mathbf{r} = \mathbf{r}'$ , respectively, and  $n_0, \rho_0$  denote the densities at  $\mathbf{x}=0$  and  $\mathbf{r}=0$ , respectively. In general,  $k_{\text{pore}}$  fluctuates with time. However, since measured flickering timescales are far less than the lipid release time we assumed that  $k_{\text{pore}}$  can be treated as a constant, the effective time-averaged value.

Laplace transforming  $t \rightarrow E$ , the solution is:

$$\begin{aligned}
Q &= \frac{k_{\text{pore}} n_a}{E[1+k_{\text{pore}}(g(E)+S(E))]}, \\
\rho_0 &= \frac{k_{\text{pore}} n_a S}{E[1+k_{\text{pore}}(g(E)+S(E))]}, \\
n_0/n_a &= \frac{k_{\text{pore}} S}{E[1+k_{\text{pore}}(g(E)+S(E))]},
\end{aligned}
\tag{S6}$$

where  $Q(E), \rho_0(E), n_0(E), g(E), S(E)$  are all functions of  $E$ . Note that  $G$  is a simple 2D Gaussian describing free lipid diffusion in the SBL. Thus,  $S(t) = 1/4\pi D_{\text{lip}} t$ , and a crude approximation of its Laplace transform is  $S(E) \approx (1/D_{\text{lip}}) \ln(1/E t_b)$  where  $t_b = b^2/D_{\text{lip}}$  and  $b$  is a pore cut-off scale.

**Lipid release through a flickering fusion pore.** If  $k_{\text{pore}} \ll D_{\text{lip}}$ , then  $S(E) \ll 1/k_{\text{pore}}$  for any  $E > t_b^{-1} e^{1/\epsilon}$ , where  $\epsilon = k_{\text{pore}}/D_{\text{lip}}$ . Thus for small enough  $\epsilon$ , for all relevant  $E$  we can delete the  $k_{\text{pore}} S$  terms in eq. S3. In addition, we can replace  $g(E) \approx 1/E A_{\text{ves}}$  with its form for small  $E$  ( $E < 1/\tau_{\text{ves}}$ ) reflecting the fact that on time scales greater than  $\tau_{\text{ves}}$  a point source uniformly covers the vesicle. We justify this below. Thus, eq. S5 gives:

$$\begin{aligned}
n_0 &= \frac{n_a}{E+k_{\text{pore}}/A_{\text{ves}}} \\
\rho_0 &= \frac{k_{\text{pore}} n_a S}{E+k_{\text{pore}}/A_{\text{ves}}} \\
Q &= k_{\text{pore}} n_0
\end{aligned}
\tag{S7}$$

The solution is  $n_0(t) = n_a \exp(-t/\tau_{\text{release}})$  where  $\tau_{\text{release}} = A_{\text{ves}}/k_{\text{pore}}$ . Using the expression for  $k_{\text{pore}}$  in eq. S3, we arrive at the expression for pore openness  $P_0$  in terms of  $\tau_{\text{release}}$  and  $A_{\text{ves}}$  of eq. 2.1 of the main text. Using the expression for  $Q$  in eq. S7 in eq. S2 gives

$$\phi_{\text{ves}} = \exp(-t/\tau_{\text{release}}) \quad \text{S8}$$

In this limit,  $n(x, t) \approx n_0(t)$  is uniform because the release time greatly exceeds the vesicle diffusion time (since  $\tau_{\text{release}}/\tau_{\text{ves}} = 1/\epsilon \gg 1$ ). Further, the fraction released by time  $\tau_{\text{ves}}$  is thus very small. Since  $g(t)$  assumes its long time form ( $1/A_{\text{ves}}$ ) for times  $t > \tau_{\text{ves}}$ , this justifies our replacing  $g(E)$  with its long time form to obtain eq. **S8**: these are the only time scales relevant to the decay of  $\phi_{\text{ves}}$ .

**TIRF intensity time course through a flickering fusion pore.** In this subsection we derive the expression of eq. 2.2 in the main text for the time-dependent total fluorescence intensity of labelled lipids during a fusion event. The total intensity  $I_{\text{tot}}$  is the sum of the intensity of lipids in the vesicle and the intensity of lipids released into the SBL. The calculation of this quantity rests on three principal features. (i) When a lipid in a SUV is released into the SBL its emission increases by a factor  $1/\lambda_{\text{TIRF}}$ . (ii) We ignore lipid bleaching in SUVs, being significantly slower than for lipids in the SBL (Figs. **S3C, D**). (iii) When a lipid is released through a flickering pore into the SBL, in this small  $k_{\text{pore}}$  limit that defines a flickering pore it is very unlikely to diffuse back into the vesicle. This follows from the fact that  $n_0 \ll \rho_0$  in this flickering pore limit, for which  $k_{\text{pore}} S \ll 1$  (see eq. S7), so the current of lipids is almost completely unidirectional from SUV to SBL (see eq. 2.2 of main text).

The total intensity for a vesicle is the sum of the contributions of fluorescent lipids which remain in the vesicle, and those that are in the SBL and have not yet bleached. The initial number of lipids in the vesicle is  $N_{\text{ves}}^{\text{a}} = n_{\text{a}}A_{\text{ves}}$ . The number of lipids in the vesicle decays as eq. S8, that is  $N_{\text{ves}}(t) = N_{\text{ves}}^{\text{a}} \exp(-t/\tau_{\text{release}})$ . The rate of fluorescent lipid addition to

the SBL is the same magnitude as the rate of lipid release from the vesicle. Thus, the number of fluorescent lipids in the SBL,  $N_{\text{SBL}}(t)$ , obeys

$$\frac{dN_{\text{SBL}}}{dt} = \frac{N_{\text{ves}}(t)}{\tau_{\text{release}}} - \frac{N_{\text{SBL}}(t)}{\tau_{\text{bleach}}},$$

where we used the fact that for this flickering pore case spatial variations in density in the vesicle can be ignored ( $n(x, t) \approx n_0(t) = N_{\text{ves}}(t)/A_{\text{ves}}$ ). The solution is

$$N_{\text{SBL}}(t) = \frac{N_{\text{ves}}^a (e^{-t/\tau_{\text{bleach}}} - e^{-t/\tau_{\text{release}}})}{(1 - \tau_{\text{release}}/\tau_{\text{bleach}})}. \quad \text{S9}$$

Hence the total intensity is given by

$$I_{\text{tot}}(t) = I_{\text{lip}} \lambda_{\text{TIRF}} N_{\text{ves}}(t) + I_{\text{lip}} N_{\text{SBL}}(t) \quad \text{S10}$$

where  $N_{\text{SBL}}(t)$  is given by eq. S9 and  $N_{\text{ves}}(t) = N_{\text{ves}}^a \exp(-t/\tau_{\text{release}})$ . As the vesicle intensity at the instant of fusion is  $I_{\text{fus}} = I_{\text{lip}} \lambda_{\text{TIRF}} N_{\text{ves}}^a$ , we obtain  $I_{\text{tot}}(t)$  in terms of  $\tau_{\text{release}}$ ,  $\lambda_{\text{TIRF}}$ , and  $\tau_{\text{bleach}}$  of eq. 2.2 in the main text by plugging eq. S9 and the expression for  $N_{\text{ves}}(t)$  above into eq. S8.

**The case of a permanently open pore.** For a fully open pore,  $P_0 = 1$ , eq. S3 tells us that  $k_{\text{pore}} = D_{\text{lip}} 2\pi r_p / b$ . Thus  $k_{\text{pore}}$  is of order  $D_{\text{lip}}$  ( $\epsilon \approx 1$ ), and  $k_{\text{pore}} S(E) \gg 1$  for all  $E \gg t_b^{-1}$ , ie for all relevant  $E$ . Thus from eq. S6

$$\rho_o \approx n_o \approx n_a A_{\text{ves}} S(E) \quad \text{S11}$$

Consider the behavior for  $E \ll 1/\tau_{\text{ves}}$ . On these time scales  $ES < 1/A_{\text{ves}}$  and we have

$$\rho_o(E) \approx n_o(E) \approx n_a A_{\text{ves}} S(E), (E < 1/\tau_{\text{ves}}) \quad \text{S12}$$

Thus  $n_0(t)$  decays as  $S(t) = 1/(4\pi D_{\text{lip}}t)$ , and  $\phi_{\text{ves}}(t) \approx n_0(t)/n_a = A_{\text{ves}}S(t)$ . Hence we obtain eq. 2.4 of the main text  $\phi_{\text{ves}}(t) = \tau_{\text{ves}}/t$ . The form of the net TIRF signal  $I_{\text{tot}}(t)$  is modified from eq. 2.3 of the main text. Unlike flickering pores, reverse diffusion is significant through an open pore: typical lipids transit the fusion pore many times and lipids which have bleached will reenter the vesicle, just as fluorescing lipids will. Thus, all lipids have equal probability of bleaching and the predicted TIRF fluorescence intensity  $I_{\text{tot}}(t)$  for permanently open pores is thus eq. 2.4 of the main text.

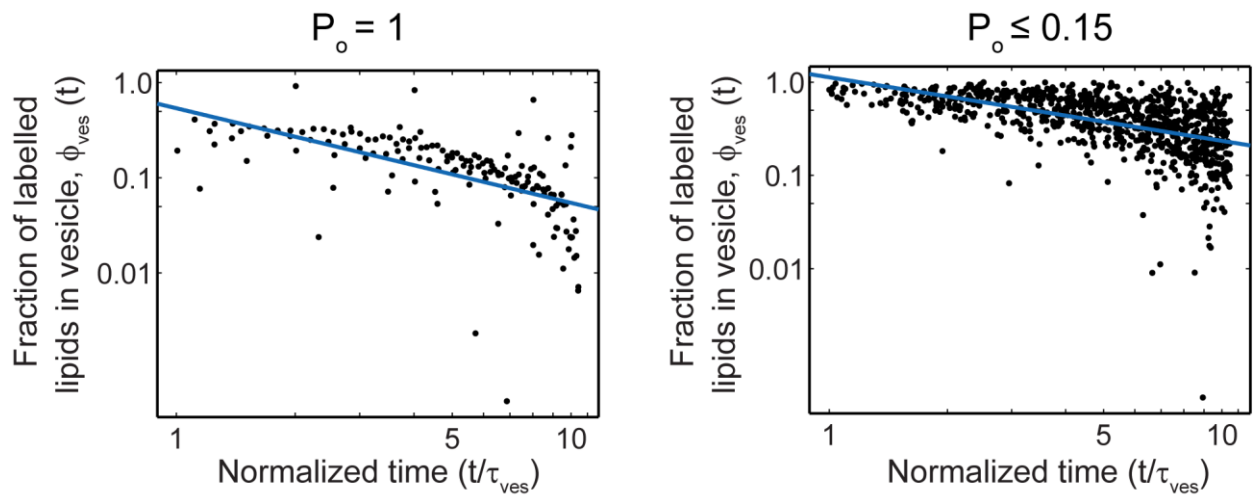


**Figure S5-**

Vesicle-to-SBL lipid release kinetics through permanently open pores have power law dependence on time. Our model predicts that the number of lipids remaining in the vesicle decays as  $\phi_{\text{ves}}(t) \sim \tau_{\text{ves}}/t$  for a fully open fusion pore where  $\tau_{\text{ves}}$  is the diffusion time on the scale of the vesicle and depends on vesicle size (see main text). The pooled  $\phi_{\text{ves}}(t)$  data that we measured for all fully open fusion pores ( $P_o = 1$ , left panel) collapsed onto a single power law relation when plotted against time scaled with  $\tau_{\text{ves}}$ . The best fit power law (blue line) was  $t^{-\alpha}$  with  $\alpha = -0.99 \pm 0.22$ , very close to the model prediction. The same procedure applied to flickering pores with relatively small openness ( $P_o \leq 0.15$ , right panel) produced a best fit power law exponent  $\alpha = -0.68 \pm 0.09$ .

## Calculation of the number of SNARE complexes at the fusion pore using the t-SNARE recruitment model of ref. [77]

In the main text (“At high cholesterol levels fusion is so accelerated that there is insufficient time to recruit t-SNAREs to the fusion site,” Fig. 2.3A) we report the number of t-SNAREs recruited during the docking-to-fusion delay time by vesicle v-SNAREs using the SNARE recruitment model that we previously developed in ref. [77]. This procedure provides an estimate of the number of SNAREpins involved in fusion for each membrane composition, reported in Fig. 2.3A of the main text.

**t-SNARE recruitment model.** In ref. [77], we developed a t-SNARE recruitment model to determine the number of t-SNAREs,  $N^*$ , recruited to the vesicle a time  $\tau$  after the vesicle is docked by formation of the first SNARE complex. The key model assumptions were: (1) t-SNAREs are homogeneously and randomly distributed throughout the SBL with density  $\Gamma_S$  and diffuse independently with diffusivity  $D_S$ ; (2) when a t-SNARE diffuses into the “reaction sink” region of radius  $b$  beneath the vesicle, it immediately binds an available vesicle v-SNARE to form a SNAREpin; (3) fusion occurs instantly when  $p$  SNAREpins have formed. Thus solving the reaction-diffusion equation governing t-SNARE diffusion and binding with v-SNAREs, the model-predicted mean number of t-SNAREs recruited after time  $\tau$  is

$$N^*(\tau) = \frac{4\pi\Gamma_S D_S \tau}{\ln(c_1 \tau / \tau_b)}, \tau_b = b^2 / D_S, \quad \text{S13}$$

where the numerical constant  $c_1 = 1.247$ . Here we evaluate eq. **S13** at the measured mean delay time to fusion ( $\tau = \bar{\tau}_{\text{delay}}$ ). Thus after accounting for the initial SNAREpin which

docks the vesicle, the total number of SNAREpins  $p$  participating in the fusion process for that vesicle is

$$p = \frac{4\pi\Gamma_s D_s \bar{\tau}_{\text{delay}}}{\ln(c_1 \bar{\tau}_{\text{delay}}/\tau_b)} + 1 \quad \text{S14}$$

Below we estimate the values of the parameters in eq. **S14** and thus estimate the number of SNAREpins recruited for each membrane composition,  $p - 1$ .

**Parameter values.** To evaluate the t-SNARE diffusivity, we assumed the ratio  $D_s/D_{\text{lip}}$  remained constant across different compositions and equal to 0.10, the value of this ratio that was used in ref. [77] based on the SNARE diffusivity measured by Wagner and Tamm [166]. Using the single lipid diffusivity values of Table **S3** for all SBL compositions gives t-SNARE diffusivities of 0.17, 0.12, 0.15, and  $0.04 \mu\text{m}^2/\text{s}$ . Assuming that the mobile, active fraction of t-SNAREs in the SBL is 0.5 [77, 166], the density of mobile t-SNAREs is  $\Gamma_s = 41.67/\mu\text{m}^2$  for our lipid to protein ratio (t-L:P=20,000). We take the sink size  $b=10$  nm as in ref. [77].

**Recruitment model predictions.** Let us define  $n = p - 1$  to be the number of t-SNAREs recruited to the fusion site before fusion occurs. Using the parameter estimates above in eq. **S14** predicts  $n = 6 \pm 3$  and  $n = 3 \pm 1$  for the model composition and the cholesterol free physiological composition PC/PS and PC/PS/PE/PIP2, respectively, and  $n = 3 \pm 2$  for physiological compositions with 45% cholesterol in the SUV membranes and 10% cholesterol in the SBL membranes. (Note the reported uncertainties in  $n$  are lower-bounds estimated by propagating only the uncertainty in  $\tau_{\text{delay}}$  values.) These  $n$  values are consistent with the range  $n \sim 3-10$  reported in refs. [77, 85]. In clear contrast, the same

procedure when applied to physiological compositions with 46% cholesterol in both the SUV and SBL membranes predicted that only  $n = 0.15 \pm 0.02$  SNAREpins are recruited during the delay to fusion, suggesting that there is insignificant time for even a single additional t-SNARE to be recruited to the fusion site after docking.

As discussed in the main text, this could indicate that t-SNAREs are preclustered at docking sites with high densities.

### **Dependence of the TIRF fluorescence reduction factor $\lambda_{\text{TIRF}}$ on vesicle radius $R_{\text{ves}}$ : coupled contributions from incident evanescent intensity decay and polarization effects**

In Fig. 2.4D of the main text we plotted values of  $\lambda_{\text{TIRF}}$  versus  $R_{\text{ves}}$  obtained from our analyses of many fusion events. Here, we discuss the theoretical relationship between these two quantities based on the known characteristics of TIRF microscopy. From this relation we determined the tangent of the relation at zero vesicle radius and we fit the tangent to the data of Fig. 2.4D.

Consider a vesicle of radius  $R_{\text{ves}}$  docked at the SBL as in Fig. 2.4A. The total TIRF fluorescence emission intensity of the vesicle is a sum over all lipid orientations  $\theta$  in the spherical vesicle membrane

$$I_{\text{dock}} = \epsilon I_{\text{inc}}^0 \rho_{\text{lip}} \mu_{\text{Q}} \int_0^\pi d\theta 2\pi R_{\text{ves}}^2 \sin \theta \alpha_{\text{p}}(\theta) e^{-R_{\text{ves}}[1+\cos \theta]/\delta_{\text{TIRF}}} . \quad \text{S15}$$

Here  $I_{\text{inc}}^0$  is the incident TIRF intensity at the SBL ( $z = 0$ ),  $\epsilon$  is the single fluorescent lipid emissivity,  $\delta_{\text{TIRF}}$  is the TIRF decay length and  $\mu_{\text{Q}} < 1$  is the fluorescence quenching factor

due to a higher labeled lipid density in the vesicle. The mean polarization factor per lipid,  $\alpha_p(\theta)$ , is the factor by which the lipid intensity is reduced (or enhanced) due to its orientation, for a segment of the vesicle bilayer with outward normal oriented at angle  $\theta$  relative to the SBL normal. We define this factor relative to the situation when the lipid resides in the SBL ( $\theta = 0$ ): hence  $\alpha_p(0) \equiv 1$ . It arises because the evanescent TIRF wave is polarized, and preferentially excites fluorescent labels whose excitation dipoles align with its polarization[167].  $\alpha_p$  is the mean value per lipid, and is a weighted average over all labeled lipids in the inner and outer monolayers of the local vesicle segment. In general it is expected to depend on bilayer curvature, labeled and unlabeled lipid density and the partitioning of labeled lipids between the two monolayers.

Following fusion of the vesicle, the labeled lipids will be released into the SBL and after sufficient time will have diffused to be dilute enough for full dequenching to have occurred,  $\mu_Q < 1$ . The polarization factor for the lipids is then unity. Thus, the total intensity of the released lipids in the SBL is given by:

$$I_{\text{dock}} = \epsilon I_{\text{inc}}^0 \rho_{\text{lip}} 4\pi R_{\text{ves}}^2 \quad \text{S16}$$

The fluorescence reduction factor is the ratio of the total intensities before and after fusion:

$$\lambda_{\text{TIRF}}(R_{\text{ves}}) = \frac{I_{\text{dock}}}{I_{\text{SBL}}} = \frac{\mu_Q}{2} \int_0^\pi d\theta \sin \theta \alpha_p(\theta) e^{-R_{\text{ves}}[1+\cos \theta]/\delta_{\text{TIRF}}} \quad \text{S17}$$

We are interested in the form of  $\lambda_{\text{TIRF}}$  as a function of  $R_{\text{ves}}$ . It is clear from the integral in eq. **S17** that this dependence is complex, as the effects of exponential TIRF intensity fall off and polarization are intimately coupled. Both effects are important. The only practical

way to establish this crucial function,  $\lambda_{\text{TIRF}}(R_{\text{ves}})$ , is to directly measure it as described in the main text (Fig. 1.5D).

**Determining the pure polarization effect.** Now taking the derivative of  $\lambda_{\text{TIRF}}(R_{\text{ves}})$  with respect to  $R_{\text{ves}}$  and setting  $R_{\text{ves}} = 0$ , one obtains a sum of two terms,  $-\lambda_{\text{TIRF}}(0)/\delta_{\text{TIRF}} + (\mu_{\text{Q}}/2) \int_0^\pi d\theta \sin \theta \cos \theta \alpha_{\text{p}}(\theta)$ . The second term vanishes, however, from the up-down symmetry of the polarization factor,  $\alpha_{\text{p}}(\theta) = \alpha_{\text{p}}(\pi - \theta)$ . Thus

$$\left(\frac{\partial \lambda_{\text{TIRF}}}{\partial R_{\text{ves}}}\right)_{R_{\text{ves}}=0} = \frac{-\lambda_{\text{TIRF}}(0)}{\delta_{\text{TIRF}}}, \quad \lambda_{\text{TIRF}}(0) = \left(\frac{\mu_{\text{Q}}}{2}\right) \int_0^\pi d\theta \sin \theta \alpha_{\text{p}}(\theta). \quad \text{S18}$$

This shows that, at zero vesicle radius,  $\lambda_{\text{TIRF}}$  and its slope are determined by a simple moment of the polarization factor  $\alpha_{\text{p}}(\theta)$ . To obtain  $\lambda_{\text{TIRF}}(0)$ , in principle one could measure  $\lambda_{\text{TIRF}}$  versus vesicle radius (as described in this paper) and extrapolate to zero radius. In the main text we outlined an alternative procedure to obtain  $\lambda_{\text{TIRF}}^0 \equiv \lambda_{\text{TIRF}}(0)$  which is based on the slope at the origin, and is preferable because our data is noisiest for small vesicles, whose small lipid release times are covered by fewest time frames in our intensity profiles. For small  $R_{\text{ves}}$  (we used data points with  $R_{\text{ves}} < 35$  nm) we fit our  $\lambda_{\text{TIRF}}$  versus  $R_{\text{ves}}$  data to a linear relation with the correct slope, as given by eq. S18 (dashed red line, Fig. 2.4D). Constraining this tangent to have intercept  $R_{\text{ves}} = \delta_{\text{TIRF}} = 68$  nm, the experimentally measured evanescent field penetration depth (see Materials and Methods), and extrapolating to zero vesicle size we could read off  $\lambda_{\text{TIRF}}^0 = 0.81 \pm 0.03$ .

## **Quantitative model of the effect of cholesterol on the fusion pore bending energy**

A number of theoretical studies have analyzed the energetics of the membrane fusion pore [153, 168]. Here we estimated the reduction by cholesterol of the bending energy of the highly bent fusion pore using a simple extension of a mathematical model developed in ref. [153]. This is a strong effect because cholesterol has negative spontaneous curvature, and the fusion pore has a net negative curvature. The model quantifies the elastic properties of the lipid leaflets that constitute the pore. Our aim is to predict the influence of cholesterol on the free energy of pore formation,  $\Delta F_{\text{pore}}$ , which is closely related to pore openness  $P_0$  (see main text).

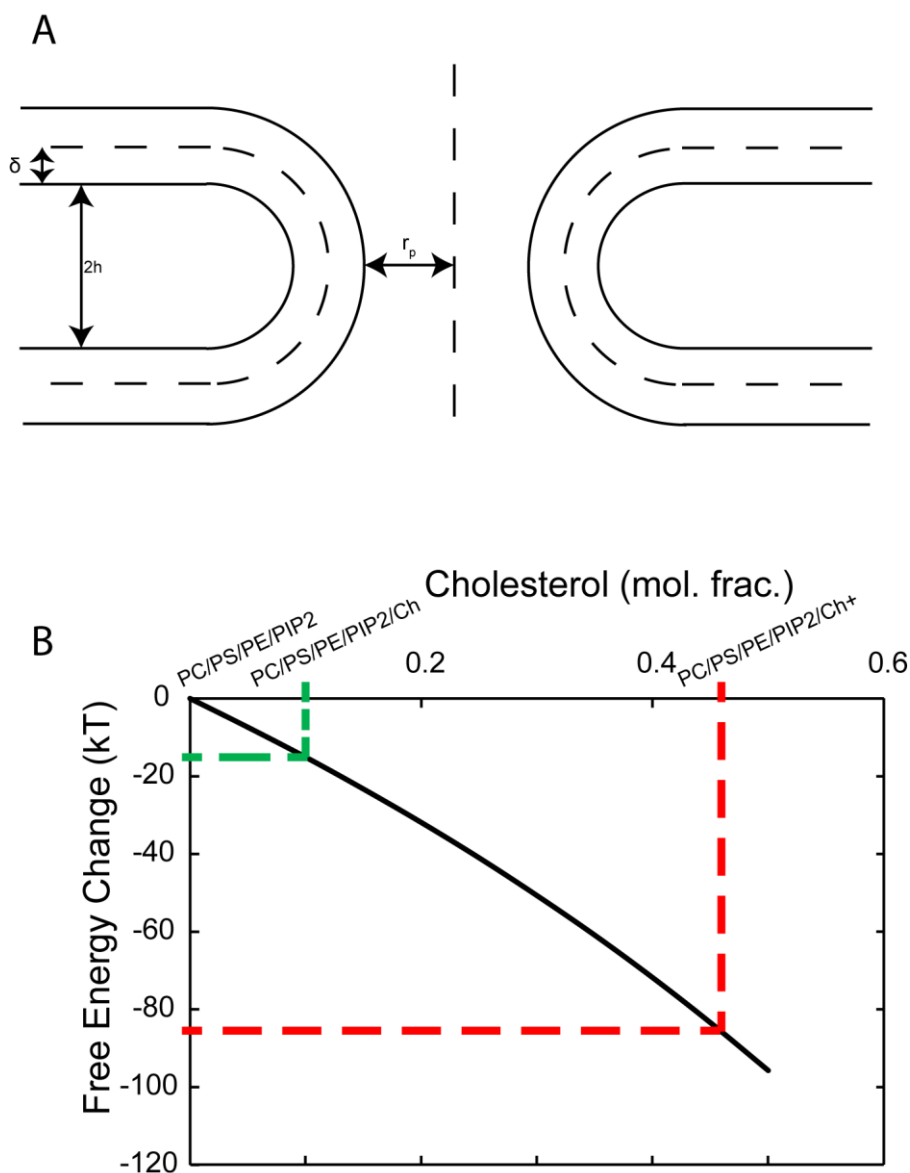


**Figure S6-**

Cholesterol lowers the bending energy of fusion pores: calculation of pore bending energy using an elastic model of the fusion pore. (A) Schematic of a fusion pore, side view. The membranes have asymptotic separation  $2h$  and the pore radius is  $r_p$ . Each leaflet has thickness  $\delta$ . (B) Free energies were calculated for the biologically motivated family of lipid compositions (Tables S1, S2) using eq. S20. The change in free energy of pore formation relative to zero cholesterol (PC/PS/PE/PIP2) is plotted versus cholesterol content. Values for the two cholesterol-rich compositions studied (PC/PS/PE/PIP2/Ch, PC/PS/PE/PIP2/Ch+) are indicated. High cholesterol levels produce enormous free energy decreases, indicating a powerful stabilizing effect on the open state of the pore.

Consider two planar bilayers, separated by distance  $2h$  (Fig. **S5A**). We assume each bilayer is symmetric and we will consider each of the physiologically motivated compositions that we treated in our experimental study (PC/PS/PE/PIP2, PC/PS/PE/PIP2/Ch, PC/PS/PE/PIP2/Ch+, Tables **S1**, **S2**). What is the free energy to create a fusion pore,  $\Delta F_{\text{pore}}$ ? How is this free energy change affected by the addition of cholesterol? Here we have extended the simple elastic theory based on the work of Chizmadahev et al.[153] by taking each leaflet into account individually to provide quantitative answers. The overall bending energy of one leaflet of the fusion pore is[169]:

$$F_{\text{leaflet}} = \frac{\kappa}{2} \int dA \left( \frac{1}{h} + \frac{1}{r_p} - C_o \right)^2 - 2\kappa C_o^2 \int dA \quad \text{S19}$$

where  $h$  and  $r_p$  are the asymptotic membrane separation and the minimal radius of the fusion pore assumed toroidal in shape,  $\kappa$  is the leaflet bending modulus of elasticity, and  $C_o$  is the mean spontaneous curvature of the leaflet. Integrating over the surface of the pore, it can be shown that [153]

$$F_{\text{leaflet}} = 2\pi\kappa \left\{ \frac{2(h + r_p)^2}{h\sqrt{r_p(r_p + 2h)}} \text{atan} \sqrt{\frac{r_p + 2h}{r_p}} + 2C_o[\pi(r_p + h) - 4h] - 4 \right\} \quad \text{S20}$$

Here we take  $\kappa = 12 \text{ kT}$ [164], we fix the membrane separation at 3.5 nm, and we calculate the spontaneous curvature  $C_o$  by taking the weighted average of all  $C_o$  values for the individual lipid species in the bilayer. The centerlines of individual leaflets are separated by a distance  $\delta = 2 \text{ nm}$ , half the bilayer thickness. Thus, to analyze a bilayer fusion pore of a given radius we need to sum the energies of two leaflets, each with a distinct value of  $h$  and  $r_p$ . Additionally,  $r_p$  and  $h$  are defined as separations between the outermost points on

each head group. The calculation of bending energy for each leaflet was based on the centerline of each leaflet, 1 nm from the outer edge of the head group. To calculate the energy of pore formation relative to two flat bilayers we determined  $\Delta F_{\text{pore}} = F_{\text{leaflet}}^{\text{outer}} + F_{\text{leaflet}}^{\text{inner}}$ . To determine membrane shape, we allowed the pore radius to anneal, and we found that the pore radius corresponding to the lowest free energy of the fusion pore was independent of the spontaneous curvature of the individual leaflets.

To examine the mechanisms by which cholesterol may promote the open state of the fusion pore, we calculated the free energy advantage of adding cholesterol to the leaflets. In eq. **S20**, the different amounts of cholesterol had the effect of changing  $C_0$  (we assumed bending modulus  $\kappa$  was unaffected). To calculate the spontaneous curvature  $C_0$  for each level of cholesterol, we took the weighted average of the spontaneous curvature of each of the components. We took the spontaneous radius of curvatures of PC, PS, PE, and cholesterol to be -9.9, 14.4, -2.8, and -2.7 nm, respectively [164, 170]. We find that the addition of moderate levels of cholesterol to physiological mimic compositions (45% and 10% cholesterol in SUV and SBL membranes, respectively, composition PC/PS/PE/PIP2/Ch) lowers the free energy of pore formation by ~10 kT, while with physiological cholesterol levels (46% in all membranes PC/PS/PE/PIP2/Ch+) the free energy of pore formation was lowered by ~80 kT (Fig. **S5B**).

## **Chapter 3- Study of the phospholipid membrane interactions in the presence of SNAREpins.**

### **I-Background**

Despite years of study of SNARE-mediated fusion both in live cells and in vitro, the mechanisms by which SNAREs mediate fusion are unknown. Thus, we sought to interrogate these mechanisms. At the synapse, fusion and neurotransmitter release occur within a millisecond of the arrival of the action potential [4], but in vitro studies which only involved reconstituted SNAREs have shown that the delay between docking and fusion ranges from ~25 ms to several seconds [77-79, 81, 171]. This raises two questions. First, can SNAREs truly drive fast fusion on their own, and second, if so, how are SNAREs able to mediate fusion.

Different models have been proposed to explain the mechanism of SNARE-mediated fusion. It has been suggested that ~10-140 kT is required to merge two phospholipid bilayers [140, 172-175]. The formation of a SNAREpin releases 56-70 kT upon zippering [16]. Using this criteria, it would appear that ~2-3 SNAREpins would be sufficient to drive fusion. This is consistent with bulk fusion assays that indicate that 1-3 SNAREs are sufficient for fusion [85, 176]. However, bulk assays are unable to measure the kinetics of individual fusion events, and biological fusion occurs on the millisecond timescale. Additionally, single vesicle studies have suggested that ~5-11 SNAREpins are necessary for fast fusion [77, 171, 177]. Additionally, it seems unlikely that several SNAREs could simultaneously zipper and harness their combined energy. Thus, this type of energy criterion is an extremely unlikely mechanistic candidate.

Several models have suggested that either the linker domain or the TMD of the SNAREs plays a critical role in inducing SNARE-mediated fusion [178-180]. It has been proposed that SNAREs form a continual helix, resulting in a stiff linker domain which transduces the energy of SNARE zippering in the form of a force that could bend the bilayer and perturb it [1, 181-183]. However, EPR has suggested that the linker domains may exhibit flexibility [184], and when flexible residues are added to the linker domain either in vivo or in vitro fusion efficiency is progressively reduced, rather than abolished [185-187]. When SNARE TMDs are replaced with lipid anchors in either yeast vacuole fusion [188] or at the synapse [189] fusion was either rescued upon the addition of SNARE disassembly machinery [188] or was not abolished [189], indicating that the TMD is not essential for SNARE-mediated fusion.

Thus, it is necessary to develop a new mechanistic model of SNARE-mediated fusion which might explain the disparate experimental results. We thus asked the following questions:

- By what mechanism do SNAREs drive fusion?
- How many SNAREs are required for fusion, or is there a definite number?

To answer these questions I quantified the membrane-membrane, SNAREpin-SNAREpin, and SNAREpin-membrane interactions in the simplest of fusion assays, the reconstituted SNARE SUV-SBL fusion. This has frequently been studied on the single event basis using either epifluorescence or total internal reflection fluorescence microscopy (TIRF) [13, 47, 78-82]. In collaborative work with Hakhamanesh Mostafavi, Dr. Jason Warner, and Prof. Ben O'Shaughnessy, we developed a model of SNARE-mediated fusion using these

interactions, the experimentally measured SNARE zipping energy, and other experimentally measured properties of the SNAREs to predict fusion rates using a Monte Carlo simulation. We then compared the results of our combined model to those from experiment to attempt to answer these critical questions.

## II-SNAREpin and Membrane Interactions

There is a long history of the study of membrane-membrane interactions [190]. Through x-ray diffraction, surface force apparatus (SFA), AFM and other experimental methods, the interactions between large, planar membranes have been well characterized. These interactions include the steric-hydration force [191], the van der Waals force [192], the electrostatic force [192], and undulation or Helfrich forces [169]. The Helfrich forces are relevant when both of the interacting membranes are very large. Here we consider SUVs, which are ~50 nm in diameter, and thus we are able to ignore Helfrich forces in our calculations. Both the electrostatic and van der Waals forces are long ranged and dominate at separations between ~2-7 nm. Steric-hydration forces are very short ranged and dominate at separations  $\lesssim 2$  nm.

**The steric-hydration force.** When membranes are forced to very small separations, very high strength repulsions are observed, regardless of the ionic strength of the membranes which are interacting. These forces are well-described by an exponential fit to experimentally measured separations  $h$  at known osmotic pressures [191]

$$P_{SH} = P_0 e^{-h/\lambda_{SH}} \quad 3.1$$

where  $\lambda_{SH}$  is the steric-hydration decay length. Values of  $P_0$  and  $\lambda_{SH}$  has been reported for various membrane compositions with  $\lambda_{SH}$  in the range of 0.1-0.3 nm for all lipid species

considered whereas the prefactor  $P_0$  largely depends on the nature of the head group [193]. The total steric-hydration energy is the integral of the pressure  $P_{SH}$  over the surface of the vesicle multiplied by the interaction area on the vesicle. The resulting total steric-hydration free energy  $F_{SH}$  energy is

$$F_{SH} = 2\pi P_0 R_{ves} \lambda_{SH}^2 e^{-h/\lambda_{SH}} \quad 3.2$$

where  $R_{ves}$  is the vesicle radius.

**The van der Waals forces.** Another well-established force is the van der Waals force. This arises from induced dipoles interacting in opposing surfaces. As the distance between the induced dipoles becomes smaller, their orientation becomes more correlated, giving rise to the attractive van der Waals force. For a spherical vesicle interacting with a planar membrane the van der Waals interaction  $F_{vdw}$  energy is given by

$$F_{vdw} = \frac{AR_{ves}}{6h} \quad 3.3$$

where  $A$  is the experimentally measured Hamaker constant [192].

**The electrostatic forces.** Electrostatic repulsive forces arise because each membrane contains a small amount (~10-15 %) of negatively charged lipids. The salt content of the water results in electrical screening. For a spherical vesicle interacting with a planar membrane the electrostatic interaction free energy  $F_{es}$  is given by:

$$F_{es} = R_{ves} Z_{mb} e^{-h/\lambda_D} \quad 3.4$$

Where  $\lambda_D$  is the Debye screening length, which depends on the salt concentration of the solution ( $\lambda_D = 0.3/[\text{NaCl}]^{1/2}$  nm for monovalent cation salts), and  $Z_{mb}$  is the electrostatic interaction constant which depends only on the properties of the surface, the charge density or the surface potential. At 37°C and for monovalent salts such as NaCl,  $Z$  is given by:

$$Z = (9.38 \times 10^{-11}) \tanh^2(\psi_0/107) \text{ J/m} \quad 3.5$$

where  $\psi_0$  is the surface potential in millivolts (mV) [192]. Surface potential is related to the surface charge density, which can be determined from the concentration of charged lipids in the membranes  $\sigma'_m$  by the Graham equation [192]:

$$\sigma'_m = 0.116 \sinh(\psi_0/53.4) [\text{NaCl}]^{0.5} \text{ C m}^{-2} \quad 3.6$$

Using this equation with eq. 3.5 gives the electrostatic interaction constant for membranes  $Z_{\text{mb}} = 2.1 \text{ kT/nm}$ .

**SNAREpin-SNAREpin interaction energy.** Each SNAREpin was coarse-grained into 5 beads with 1 nm radius,  $r_{\text{bead}}$ , and surface potential,  $\psi_0$ , of 3 kT/e in the range of the electrostatic potentials reported for a neuronal SNARE complex [194]. For two similarly charged surfaces in solution electrostatic energy decays exponentially with their separation,  $d$  [192]. The electrostatic energy of two beads is calculated by:

$$E_{\text{bead-bead}} = \frac{r_{\text{bead}}}{2} Z_{\text{snare}} e^{-d/\lambda_D} \quad 3.7$$

where  $\lambda_D$  is the same as for the membrane-membrane electrostatic interactions in eq. 3.4, and  $Z_{\text{snare}} = 8.8 \text{ kT/nm}$  is the interaction coefficient using the surface potential of the SNAREpins  $\sim 3 \text{ kT/e}$  [194].

**Membrane-SNAREpin interaction energy.** The electrostatic interactions between SNAREpins and membranes were calculated by

$$F_{\text{snves}} = Z_{\text{combined}} \left( \frac{R_{\text{ves}} r_{\text{bead}}}{R_{\text{ves}} + r_{\text{bead}}} \right) e^{-d/\lambda_D}, \quad 3.8$$

where  $Z_{\text{combined}} = (Z_{\text{mb}} Z_{\text{snare}})^{1/2}$  is the geometric mean of the  $Z$  value of both the membrane and the SNARE beads.

**Membrane compositions and parameter value estimation.** We calculated the composition weighted average of the prefactor  $P_0$  and steric-hydration decay length based on the experimentally measured values of pure substances [191]. The Hamaker constant was also estimated based on the lipid composition to be  $6 \times 10^{-21}$  J. The surface charge density is given by the density of phosphatidylserine (PS) in the bilayers. We took the physiological salt concentration 0.15 M NaCl, giving  $\lambda_D = 0.7$  nm. Membranes considered in this study contained 35% phosphatidylcholine (PC), 25% phosphatidylethanolamine (PE), 15% PS and 30% cholesterol mimicking a typical synaptic plasma membrane [195] unless stated otherwise.

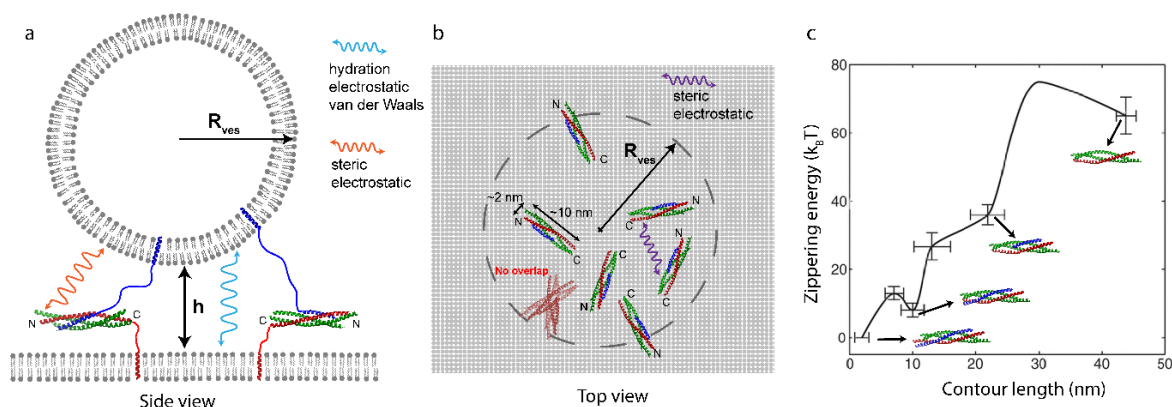


**Figure 3.1-**

Model of a cluster of SNAREpins connecting a vesicle to a planar membrane. a) Membranes interact via steric-hydration, van der Waals and electrostatic forces. SNAREpins experience steric and electrostatic interactions with the membranes (a) and one another (b). c) Energy landscape of SNAREpin zippering from ref. [16], local minimum at SNAREpin full assembly. The contour length of the SNAREpin between the C-termini of syntaxin and VAMP is the reaction coordinate.

**Calculation of the pressure between membranes.** A pressure is generated between two interacting membranes which increases with decreasing separation. For curved membranes the generated pressure is not uniform on the membranes and has a maximum at the point of closest approach (Fig 1B). We calculated the pressure at the point of closest approach

on the target membrane (planar membrane or vesicle) interacting with the vesicle,  $P_{\max}$ , as the sum of the three membrane-membrane interactions discussed: van der Waals (VDW), electrostatic (ES), and steric-hydration (SH) forces

$$P_{\max} = P_{\text{VDW}} + P_{\text{ES}} + P_{\text{SH}} \quad 3.9$$

*Electrostatic and van der Waals pressures.* The net VDW and electrostatic pressure at the point of interest on the target membrane is obtained by pressure generated at that point per unit area of the membrane integrated over the surface area of the vesicle. The pressure per unit area of the vesicle resulting from VDW attraction between lipid tails,  $f_{\text{VDW}}$ , is approximated from:

$$f_{\text{VDW}} = C_{\text{VDW}} \sigma_m \sigma_v n^2 \left( \frac{1}{r^7} \right) \quad 3.10$$

where  $\sigma_m$  and  $\sigma_v$  are the areal density of lipids in the target membrane and vesicle membrane, respectively, both taken as ( $\sim 1.25$  lipid/nm<sup>2</sup>), and  $r$  is the distance of any point on the vesicle from the point of closest approach on target membrane.  $C_{\text{VDW}}$  is the VDW energy coefficient which we take as  $1.8 \times 10^{-23}$  J nm<sup>6</sup>. This is the value for hydrocarbons interacting through a water medium which we use as a model for lipid tails as the specific values for lipid tails are not available, and  $n$  is the number of CH<sub>2</sub> groups constituting lipid tails estimated as 18. The pressure per unit area of the vesicle resulting from electrostatic interaction between charged head groups,  $f_{\text{ES}}$ , is calculated from:

$$f_{\text{ES}} = \frac{\sigma'_m \sigma'_v}{4\pi\epsilon\epsilon_0} \left( \frac{1}{r^2} \right) e^{-r/\lambda_D} \quad 3.11$$

where  $\sigma'_m$  and  $\sigma'_v$  are areal charge density on the target membrane and vesicle, respectively.  $\lambda_D = 0.7$  nm is the Debye screening length for physiological salt concentrations of 0.15 M NaCl [192]. The ES and VDW pressures can be calculated by integrating the pressure per unit area over the surface of the vesicle using

$$P_{\text{interact}} = \int_{\theta=0}^{\pi} \sigma_v R_{\text{ves}} d\theta 2\pi R_{\text{ves}} \sin(\theta) (f_{\text{interact}}) \cos(\alpha) \quad 3.12$$

Where the subscript “interact” is either the ES or the VDW pressure per unit area.

### III-Collaborative Results

In collaboration with Hakhamanesh Mostafavi, Dr. Jason Warner, and Prof. Ben O’Shaughnessy, we used these forces, in concert with experimental results to develop a Monte Carlo simulation of SNARE-mediated fusion. First we addressed the issue of how SNAREs can mediate fusion between a planar membrane and a SUV, finding that they form a ring-like structure at the site of fusion and that the size of the SNAREpin ring depends on both the vesicle size and the number of SNAREpins in the ring. We also find that the SNAREpin-SNAREpin and SNAREpin-membrane interactions are most important for fusion.

**Distribution of membrane separations.** At temperature  $T$ , the probability distribution of membrane separations,  $p(s, h)$ , depends on the free energy,  $F(h)$ , according to the Boltzmann distribution:

$$p(s, h) \sim e^{-F(s, h)/k_B T} = e^{-[E_{\text{mb}}(h) + E_{\text{snare}}(s, h) + (E_{\text{snare, mb}}(s, h))]/k_B T} \quad 3.13$$

The sum is over all SNARE configurations  $s$ , at membrane separation  $h$ .  $F(h)$  is the total free energy of the system where  $E_{\text{mb}}(h) = F_{\text{es}}(h) + F_{\text{vdw}}(h) + F_{\text{sh}}(h)$  is the total membrane-membrane interaction free energy at separation  $h$  calculated using eqs. 3.2-3.4. The sum of  $E_{\text{snare}}(s, h) + E_{\text{snare,mb}}(s, h)$  is the total SNARE-SNARE interaction and SNARE-membrane interaction free energy, respectively, calculated using eqs. 3.7 and 3.8.

**Calculation of fusion statistics: Monte Carlo simulation.** A Monte Carlo simulation was used to calculate the distribution of membrane separations  $h$  for a given vesicle size  $R_{\text{ves}}$  and number of SNAREpins  $N_{\text{snare}}$  connecting the vesicle to the planar membrane. From this distribution we calculated the distribution of membrane interaction energies  $E_{\text{mb}}$  and membrane pressures at the point of closest approach  $\langle P_{\text{max}} \rangle$ , and the relative waiting time to fusion  $\tau_{\text{fus}}$ .

Simulated clusters of SNAREpins between two membranes were generated with randomly positioned half-zippered SNAREpins. SNAREpins were allowed to zipper and unzipper according to the energy landscape of ref. [16] (**Figure 3. C**), move by both lateral and radial motion of the TMDs, and by motion of the SNAREpin bundle in all directions of space. Membrane separation was allowed to change. Overlaps of the SNAREpins, the membranes, and the SNAREpins with the membranes were prohibited.

**SNAREpin clusters form a ring between the membranes whose size depends on the vesicle radius  $R_{\text{ves}}$  and the number of SNAREpins in the cluster  $N_{\text{snare}}$ .** We performed simulations with vesicles of 20 nm radius and 2-11 SNAREpins. We found that for all numbers of SNAREpins, the cluster forms a ring with radius  $R_{\text{ring}}$  which increases with  $N_{\text{snare}}$ . Additionally, we find that the membrane separation  $h$  is correlated with  $R_{\text{ring}}$ , thus

as the ring radius increases separation gets smaller and the membrane energy  $E_{mb}$  and the pressure between the membranes increases. Because of the exponential nature of the membrane interactions, it is expected that for small reductions in membrane separation, the membrane energy increases dramatically, as is clear in **Figure 3.2**. This is due to the nature of the steric-hydration forces, which are exponential and have a very short decay length,  $\sim 0.2$  nm [191].

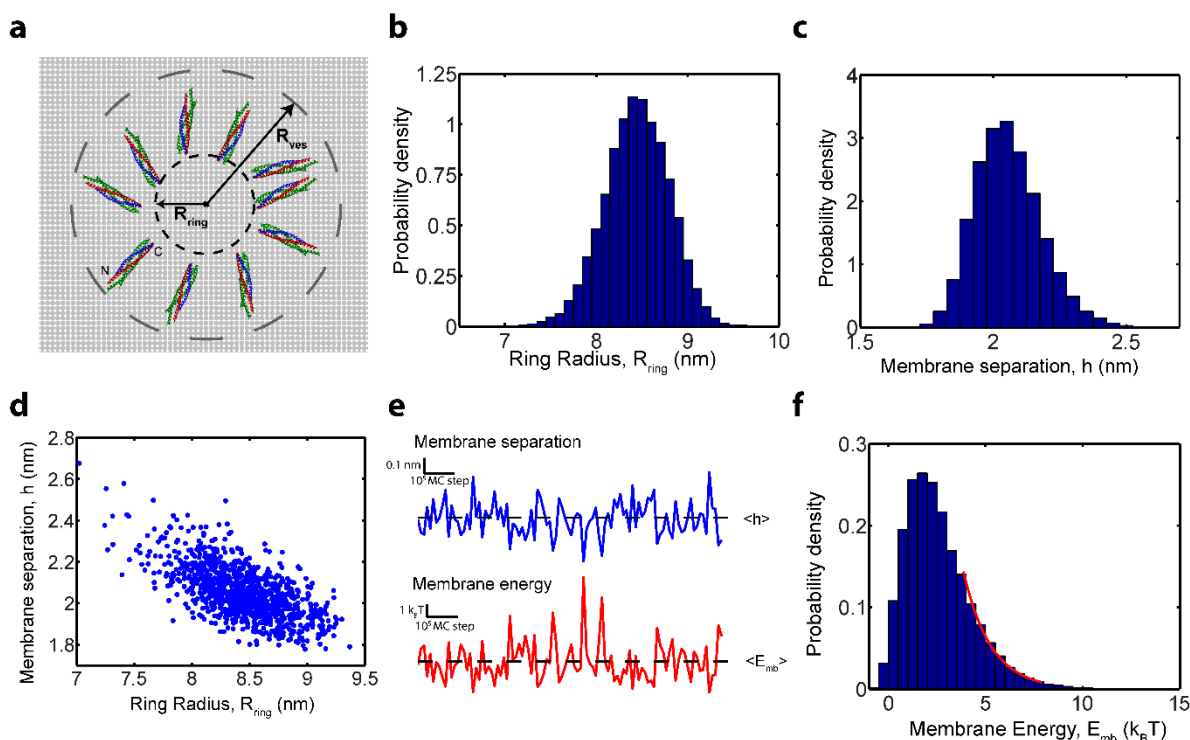


**Figure 3.2-**

A ring of fully assembled SNAREpins forces membranes into close contact. a) a snap-shot of the simulations showing ring organization of SNAREpins. b) Distribution of ring sizes (bin width = 0.1 nm). c) Distribution of membrane separations (bin width = 0.05 nm). d) Correlation between ring size and membrane separation. e) Monte Carlo time traces of membrane separation (top) and membrane energy (bottom). f) Distribution of membrane energies (bin width = 0.5  $k_B T$ ), red line shows an exponential fit to the tail of the distribution, eqs. 3.2-3.4.  $R_{ves} = 20$  nm, and  $N_{snare} = 10$ .

**The pressure generated by a ring of SNAREpins is comparable to those seen to drive fusion and hemifusion.** We find that, according to eq. 3.9, the maximum pressure between the membranes also depends on the number of SNAREpins in the cluster. The pressure increases from  $\sim 2 \pm 2$  atm to  $\sim 25 \pm 15$  atm as the number of SNAREpins increases from 2 to 11. Using polymer cushioned membranes on mica substrates, SFA experiments have shown that  $\sim 5$ -10 atm is sufficient to drive hemifusion, where only the outer leaflets of the opposing membranes have fused, and  $\sim 50$  atm will drive the hemifused state to full fusion [196]. Thus, the pressures that we see here are comparable, and we could expect to see fusion occur. However, as the range of pressures seems to vary greatly with changing lipid composition and vesicle size, we only take the pressures observed here as a guide to confirm that fusion is possible.

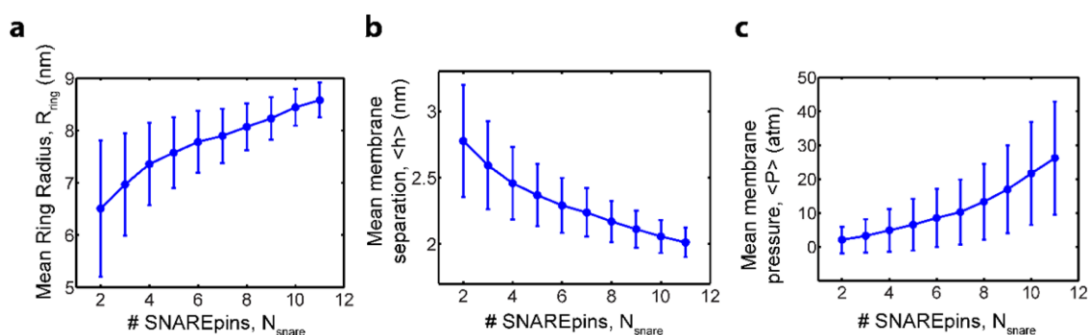


**Figure 3.3-**

Efficiency of SNARE-mediated fusion increases with the number of SNAREpins at the fusion site, and decreases with vesicle size and linker length. Ring size increases (a), membrane separation decreases (b) and the pressure generated between the membranes increases (c) with the number of SNAREpins in the ring.  $R_{\text{ves}} = 20$  nm. All error bars show standard deviation.

**Steric and electrostatic interactions induce membrane fusion, not SNARE motifs zippering.** It is thought that SNARE zippering brings the membranes to close contact. However, the detailed mechanism whereby SNAREs produce fusion remains unknown.

The energy released during complexation of SNARE motifs (~56-70 kT) has been suggested to provide the free energy required for fusion [16]. Upon initiation of zippering from N-termini the membranes can be up to 20-30 nm apart, and bringing membranes into close contact is expected to dissipate a large fraction of the zippering energy. However, studies of SNARE assembly kinetics [197] and the fact that SNAREpins can assemble without fusing membranes [198], suggest that SNAREpins may assemble before fusion after dissipating zippering energy.

Our results suggest that in the absence of regulatory proteins, the SNARE domain fully assembles prior to fusion. We find that fully assembled SNAREpins self-organize into a ring driven by SNAREpin-membrane and inter-SNAREpin steric and electrostatic interactions. The ring size is geometrically coupled to membrane separation. Thus, inter-SNAREpin and SNAREpin-membrane forces tending to expand the ring, forcing the membranes together and enabling close contact and fusion. This suggests that steric and electrostatic interactions, not necessarily SNARE zippering, play a key role in providing the free energy required for fusion.

## Bibliography

1. Jahn, R. and R.H. Scheller, *SNAREs—engines for membrane fusion*. Nature Reviews Molecular Cell Biology, 2006. **7**(9): p. 631-643.
2. Jahn, R., T. Lang, and T.C. Sudhof, *Membrane fusion*. Cell, 2003. **112**(4): p. 519-533.
3. Chen, Y. and R. Scheller, *SNARE-mediated membrane fusion*. Nature Reviews Molecular Cell Biology, 2001. **2**(2): p. 98-106.
4. Südhof, Thomas C., *Neurotransmitter Release: The Last Millisecond in the Life of a Synaptic Vesicle*. Neuron, 2013. **80**(3): p. 675-690.
5. *Principles of Neural Science*. 5 ed. 2013: McGraw Hill Medical.
6. Chandler, D.E. and J. Heuser, *MEMBRANE-FUSION DURING SECRETION - CORTICAL GRANULE EXOCYTOSIS IN SEA-URCHIN EGGS AS STUDIED BY QUICK-FREEZING AND FREEZE-FRACTURE*. Journal of Cell Biology, 1979. **83**(1): p. 91-108.
7. Burgoyne, R.D. and A. Morgan, *Secretory granule exocytosis*. Physiological reviews, 2003. **83**(2): p. 581-632.
8. Ashcroft, Frances M. and P. Rorsman, *Diabetes Mellitus and the  $\beta$  Cell: The Last Ten Years*. Cell, 2012. **148**(6): p. 1160-1171.
9. Das, K., et al., *Structures of influenza A proteins and insights into antiviral drug targets*. Nature Structural & Molecular Biology, 2010. **17**(5): p. 530-538.
10. Söllner, T., et al., *SNAP receptors implicated in vesicle targeting and fusion*. Nature, 1993. **362**(6418): p. 318-324.
11. Sutton, R.B., et al., *Crystal structure of a SNARE complex involved in synaptic exocytosis at 2.4 angstrom resolution*. Nature, 1998. **395**(6700): p. 347-353.
12. Takamori, S., et al., *Molecular Anatomy of a Trafficking Organelle*. Cell, 2006. **127**(4): p. 831-846.
13. Weber, T., et al., *SNAREpins: minimal machinery for membrane fusion*. Cell, 1998. **92**(6): p. 759-772.
14. Rizo, J. and C. Rosenmund, *Synaptic vesicle fusion*. Nature Structural & Molecular Biology, 2008. **15**(7): p. 665-674.
15. Stein, A., et al., *Helical extension of the neuronal SNARE complex into the membrane*. Nature, 2009. **460**(7254): p. 525-528.
16. Gao, Y., et al., *Single Reconstituted Neuronal SNARE Complexes Zipper in Three Distinct Stages*. Science, 2012.
17. Fasshauer, D., et al., *Identification of a minimal core of the synaptic SNARE complex sufficient for reversible assembly and disassembly*. Biochemistry, 1998. **37**(29): p. 10354-10362.
18. Poirier, M.A., et al., *Protease resistance of syntaxin· SNAP-25· VAMP complexes*. Journal of Biological Chemistry, 1998. **273**(18): p. 11370-11377.
19. Hayashi, T., et al., *Synaptic vesicle membrane fusion complex: action of clostridial neurotoxins on assembly*. EMBO journal, 1994. **13**(21): p. 5051.
20. Yang, B., et al., *SNARE interactions are not selective implications for membrane fusion specificity*. Journal of Biological Chemistry, 1999. **274**(9): p. 5649-5653.

21. Söllner, T., et al., *A protein assembly-disassembly pathway in vitro that may correspond to sequential steps of synaptic vesicle docking, activation, and fusion.* Cell, 1993. **75**(3): p. 409-418.
22. Mayer, A., W. Wickner, and A. Haas, *Sec18p (NSF)-driven release of Sec17p ( $\alpha$ -SNAP) can precede docking and fusion of yeast vacuoles.* Cell, 1996. **85**(1): p. 83-94.
23. Veit, M., T.H. Söllner, and J.E. Rothman, *Multiple palmitoylation of synaptotagmin and the t-SNARE SNAP-25.* FEBS letters, 1996. **385**(1-2): p. 119-123.
24. Hess, D.T., et al., *The 25 kDa synaptosomal-associated protein SNAP-25 is the major methionine-rich polypeptide in rapid axonal transport and a major substrate for palmitoylation in adult CNS.* The Journal of neuroscience, 1992. **12**(12): p. 4634-4641.
25. Gonzalo, S. and M.E. Linder, *SNAP-25 palmitoylation and plasma membrane targeting require a functional secretory pathway.* Molecular biology of the cell, 1998. **9**(3): p. 585-597.
26. Lane, S.R. and Y. Liu, *Characterization of the Palmitoylation Domain of SNAP-25.* Journal of neurochemistry, 1997. **69**(5): p. 1864-1869.
27. Sudhof, T. and J. Rothman, *Membrane fusion: grappling with SNARE and SM proteins.* Science, 2009. **323**(5913): p. 474.
28. Misura, K.M.S., R.H. Scheller, and W.I. Weis, *Three-dimensional structure of the neuronal-Sec1-syntaxin 1a complex.* Nature, 2000. **404**(6776): p. 355-362.
29. Margittai, M., et al., *The Habc domain and the SNARE core complex are connected by a highly flexible linker.* Biochemistry, 2003. **42**(14): p. 4009-4014.
30. Margittai, M., et al., *Single-molecule fluorescence resonance energy transfer reveals a dynamic equilibrium between closed and open conformations of syntaxin 1.* Proceedings of the National Academy of Sciences, 2003. **100**(26): p. 15516.
31. Rizo, J. and T. Sudhof, *Snares and Munc18 in synaptic vesicle fusion.* Nature Reviews Neuroscience, 2002. **3**(8): p. 641-653.
32. Gallwitz, D. and R. Jahn, *The riddle of the Sec1/Munc-18 proteins—new twists added to their interactions with SNAREs.* Trends in biochemical sciences, 2003. **28**(3): p. 113-116.
33. Maximov, A. and T.C. Südhof, *Autonomous function of synaptotagmin 1 in triggering synchronous release independent of asynchronous release.* Neuron, 2005. **48**(4): p. 547-554.
34. Malsam, J., et al., *Complexin arrests a pool of docked vesicles for fast Ca<sup>2+</sup>-dependent release.* EMBO Journal, 2012. **31**(15): p. 3270-3281.
35. Giraudo, C.G., et al., *A clamping mechanism involved in SNARE-dependent exocytosis.* Science, 2006. **313**(5787): p. 676.
36. Li, F., et al., *Complexin activates and clamps SNAREpins by a common mechanism involving an intermediate energetic state.* Nature Structural & Molecular Biology, 2011. **18**(8): p. 941-946.
37. Krishnakumar, S.S., et al., *A conformational switch in complexin is required for synaptotagmin to trigger synaptic fusion.* Nature Structural & Molecular Biology, 2011. **18**(8): p. 934-940.
38. Kümmel, D., et al., *Complexin cross-links prefusion SNAREs into a zigzag array.* Nature Structural & Molecular Biology, 2011. **18**(8): p. 927-933.

39. Yoon, T.Y., et al., *Complexin and Ca<sup>2+</sup> stimulate SNARE-mediated membrane fusion*. *Nature Structural & Molecular Biology*, 2008. **15**(7): p. 707-713.
40. Hobson, R.J., et al., *Complexin maintains vesicles in the primed state in C. elegans*. *Current Biology*, 2011.
41. Diao, J., et al., *Synaptic proteins promote calcium-triggered fast transition from point contact to full fusion*. *eLife Sciences*, 2012. **1**.
42. Huntwork, S. and J.T. Littleton, *A complexin fusion clamp regulates spontaneous neurotransmitter release and synaptic growth*. *Nature neuroscience*, 2007. **10**(10): p. 1235-1237.
43. Bai, J., et al., *Fusion pore dynamics are regulated by synaptotagmin-t-SNARE interactions*. *Neuron*, 2004. **41**(6): p. 929-942.
44. Chapman, E.R., *Synaptotagmin: A Ca<sup>2+</sup> sensor that triggers exocytosis?* *Nature reviews Molecular cell biology*, 2002. **3**(7): p. 498-508.
45. Chapman, E.R., *How does synaptotagmin trigger neurotransmitter release?* *Annual Reviews of Biochemistry*, 2008. **77**: p. 615-641.
46. Jackson, M.B. and E.R. Chapman, *Fusion pores and fusion machines in Ca<sup>2+</sup>-triggered exocytosis*. *Annual Review of Biophysics and Biomolecular Structures*, 2006. **35**: p. 135-160.
47. Tucker, W.C., T. Weber, and E.R. Chapman, *Reconstitution of Ca<sup>2+</sup>-regulated membrane fusion by synaptotagmin and SNAREs*. *Science*, 2004. **304**(5669): p. 435.
48. Wang, C.T., et al., *Synaptotagmin–Ca<sup>2+</sup> triggers two sequential steps in regulated exocytosis in rat PC12 cells: fusion pore opening and fusion pore dilation*. *The Journal of Physiology*, 2006. **570**(2): p. 295-307.
49. Brunger, A., et al., *Single-molecule studies of the neuronal SNARE fusion machinery*. *Annual review of biochemistry*, 2009. **78**: p. 903-928.
50. Yoshihara, M. and J.T. Littleton, *Synaptotagmin I functions as a calcium sensor to synchronize neurotransmitter release*. *Neuron*, 2002. **36**(5): p. 897-908.
51. Sutton, R.B., J.A. Ernst, and A.T. Brunger, *Crystal Structure of the Cytosolic C2a-C2b Domains of Synaptotagmin III*. *The Journal of Cell Biology*, 1999. **147**(3): p. 589.
52. Kasai, H., N. Takahashi, and H. Tokumaru, *Distinct Initial SNARE Configurations Underlying the Diversity of Exocytosis*. *Physiological Reviews*, 2012. **92**(4): p. 1915-1964.
53. Schiavo, G., et al., *A POSSIBLE DOCKING AND FUSION PARTICLE FOR SYNAPTIC TRANSMISSION*. *Nature*, 1995. **378**(6558): p. 733-736.
54. Fernández-Chacón, R., et al., *Synaptotagmin I functions as a calcium regulator of release probability*. *Nature*, 2001. **410**(6824): p. 41-49.
55. Wang, C.T., et al., *Synaptotagmin modulation of fusion pore kinetics in regulated exocytosis of dense-core vesicles*. *Science*, 2001. **294**(5544): p. 1111.
56. Wang, C.T., et al., *Different domains of synaptotagmin control the choice between kiss-and-run and full fusion*. *Nature*, 2003. **424**(6951): p. 943-947.
57. Tang, J., et al., *A complexin/synaptotagmin I switch controls fast synaptic vesicle exocytosis*. *Cell*, 2006. **126**(6): p. 1175-1187.
58. Martens, S., M.M. Kozlov, and H.T. McMahon, *How Synaptotagmin Promotes Membrane Fusion*. *Science*, 2007. **316**(5828): p. 1205-1208.

59. Stein, A., et al., *Synaptotagmin activates membrane fusion through a Ca<sup>2+</sup>-dependent trans interaction with phospholipids*. Nature Structural & Molecular Biology, 2007. **14**(10): p. 904-911.
60. Radhakrishnan, A., et al., *The Ca<sup>2+</sup> Affinity of Synaptotagmin 1 Is Markedly Increased by a Specific Interaction of Its C2B Domain with Phosphatidylinositol 4, 5-Bisphosphate*. Journal of Biological Chemistry, 2009. **284**(38): p. 25749.
61. Jorquera, R.A., et al., *Complexin Controls Spontaneous and Evoked Neurotransmitter Release by Regulating the Timing and Properties of Synaptotagmin Activity*. The Journal of neuroscience, 2012. **32**(50): p. 18234-18245.
62. Lee, J., et al., *Genetic Analysis of Synaptotagmin C2 Domain Specificity in Regulating Spontaneous and Evoked Neurotransmitter Release*. The Journal of neuroscience, 2013. **33**(1): p. 187-200.
63. Seven, A.B., et al., *Prevalent mechanism of membrane bridging by synaptotagmin-1*. Proceedings of the National Academy of Sciences, 2013.
64. Borisovska, M., et al., *v-SNAREs control exocytosis of vesicles from priming to fusion*. EMBO journal, 2005. **24**(12): p. 2114-2126.
65. Whyte, J.R.C. and S. Munro, *Vesicle tethering complexes in membrane traffic*. Journal of cell science, 2002. **115**(13): p. 2627.
66. Sudhof, T.C., *The synaptic vesicle cycle*. Annual review of neuroscience, 2004. **27**: p. 509.
67. Wang, Y., et al., *Rim is a putative Rab3 effector in regulating synaptic-vesicle fusion*. Nature, 1997. **388**(6642): p. 593-598.
68. Kaeser, P. and T. Sudhof, *RIM function in short-and long-term synaptic plasticity. mammalian genome*, 2005. **4**: p. 5.
69. Burkhardt, P., et al., *Munc18a controls SNARE assembly through its interaction with the syntaxin N-peptide*. EMBO journal, 2008. **27**(7): p. 923-933.
70. Shen, J., et al., *Selective activation of cognate SNAREpins by Sec1/Munc18 proteins*. Cell, 2007. **128**(1): p. 183-195.
71. Yu, H., et al., *Comparative studies of Munc18c and Munc18-1 reveal conserved and divergent mechanisms of Sec1/Munc18 proteins*. Proceedings of the National Academy of Sciences, 2013.
72. Nakata, Y., et al., *Accumulation of  $\alpha$ -synuclein triggered by presynaptic dysfunction*. The Journal of Neuroscience, 2012. **32**(48): p. 17186-17196.
73. Kramer, M.L. and W.J. Schulz-Schaeffer, *Presynaptic  $\alpha$ -Synuclein Aggregates, Not Lewy Bodies, Cause Neurodegeneration in Dementia with Lewy Bodies*. The Journal of Neuroscience, 2007. **27**(6): p. 1405-1410.
74. Hackmann, Y., et al., *Syntaxin binding mechanism and disease-causing mutations in Munc18-2*. Proceedings of the National Academy of Sciences, 2013. **110**(47): p. E4482-E4491.
75. Andersson, S.A., et al., *Reduced insulin secretion correlates with decreased expression of exocytotic genes in pancreatic islets from patients with type 2 diabetes*. Molecular and cellular endocrinology, 2012. **364**(1): p. 36-45.
76. Scarr, E., et al., *Increased levels of SNAP-25 and synaptophysin in the dorsolateral prefrontal cortex in bipolar I disorder*. Bipolar Disorders, 2006. **8**(2): p. 133-143.

77. Karatekin, E., et al., *A fast, single-vesicle fusion assay mimics physiological SNARE requirements*. Proceedings of the National Academy of Sciences, 2010. **107**(8): p. 3517-3521.
78. Fix, M., et al., *Imaging single membrane fusion events mediated by SNARE proteins*. Proceedings of the National Academy of Sciences of the United States of America, 2004. **101**(19): p. 7311.
79. Bowen, M., et al., *Single-molecule studies of synaptotagmin and complexin binding to the SNARE complex*. Biophysical journal, 2005. **89**(1): p. 690-702.
80. Liu, T., et al., *Productive hemifusion intermediates in fast vesicle fusion driven by neuronal SNAREs*. Biophysical journal, 2008. **94**(4): p. 1303-1314.
81. Liu, T.T., et al., *SNARE-driven, 25-millisecond vesicle fusion in vitro*. Biophysical journal, 2005. **89**(4): p. 2458-2472.
82. Kiessling, V., M.K. Domanska, and L.K. Tamm, *Single SNARE-Mediated Vesicle Fusion Observed In Vitro by Polarized TIRFM*. Biophysical journal, 2010. **99**(12): p. 4047-4055.
83. Yoon, T.Y., et al., *Multiple intermediates in SNARE-induced membrane fusion*. Proceedings of the National Academy of Sciences, 2006. **103**(52): p. 19731.
84. Hua, Y. and R.H. Scheller, *Three SNARE complexes cooperate to mediate membrane fusion*. Proceedings of the National Academy of Sciences of the United States of America, 2001. **98**(14): p. 8065.
85. Shi, L., et al., *SNARE proteins: one to fuse and three to keep the nascent fusion pore open*. Science Signalling, 2012. **335**(6074): p. 1355.
86. Bean, B.P., *The action potential in mammalian central neurons*. Nature Reviews Neuroscience, 2007. **8**(6): p. 451-465.
87. Sabatini, B. and W. Regehr, *Timing of synaptic transmission*. Annual Review of Physiology, 1999. **61**(1): p. 521-542.
88. Stuart, G., et al., *Action potential initiation and backpropagation in neurons of the mammalian CNS*. Trends in neurosciences, 1997. **20**(3): p. 125-131.
89. Ghosh, A. and M. Greenberg, *Calcium signaling in neurons: molecular mechanisms and cellular consequences*. Science, 1995. **268**(5208): p. 239-247.
90. Clapham, D.E., *Calcium Signaling*. Cell, 2007. **131**(6): p. 1047-1058.
91. Borst, J.G.G. and B. Sakmann, *Calcium influx and transmitter release in a fast CNS synapse*. Nature, 1996. **383**(6599): p. 431-434.
92. Katz, B., *The release of neural transmitter substances*. The release of neural transmitter substances. 1969: Sherrington Lectures No.10, Liverpool University Press. i-xi, 1-60.
93. Jackson, M.B. and E.R. Chapman, *The fusion pores of Ca<sup>2+</sup>-triggered exocytosis*. Nature Structural & Molecular Biology, 2008. **15**(7): p. 684-689.
94. Lindau, M. and G. Alvarez de Toledo, *The fusion pore*. Biochimica et Biophysica Acta (BBA)-Molecular Cell Research, 2003. **1641**(2-3): p. 167-173.
95. Chow, R.H., L. von Rüden, and E. Neher, *Delay in vesicle fusion revealed by electrochemical monitoring of single secretory events in adrenal chromaffin cells*. Nature, 1992. **356**: p. 60-63.
96. Sombers, L., et al., *The effects of vesicular volume on secretion through the fusion pore in exocytotic release from PC12 cells*. The Journal of neuroscience, 2004. **24**(2): p. 303.

97. De Toledo, G.A., R. Fernandez-Chacon, and J. Fernandez, *Release of secretory products during transient vesicle fusion*. *Nature*, 1993. **363**(6429): p. 554-558.
98. Han, X., et al., *Transmembrane segments of syntaxin line the fusion pore of Ca<sup>2+</sup>-triggered exocytosis*. *Science*, 2004. **304**(5668): p. 289.
99. Graham, M.E., J.W. Barclay, and R.D. Burgoyne, *Syntaxin/Munc18 interactions in the late events during vesicle fusion and release in exocytosis*. *Journal of Biological Chemistry*, 2004. **279**(31): p. 32751.
100. Lam, A.D., et al., *SNARE-catalyzed fusion events are regulated by Syntaxin1A-lipid interactions*. *Molecular biology of the cell*, 2008. **19**(2): p. 485.
101. Monck, J.R. and J.M. Fernandez, *The exocytotic fusion pore*. *The Journal of Cell Biology*, 1992. **119**(6): p. 1395.
102. Monck, J.R., G. Alvarez de Toledo, and J.M. Fernandez, *Tension in secretory granule membranes causes extensive membrane transfer through the exocytotic fusion pore*. *Proceedings of the National Academy of Sciences*, 1990. **87**(20): p. 7804.
103. McNally, J.M., D.J. Woodbury, and J.R. Lemos, *Syntaxin 1A drives fusion of large dense-core neurosecretory granules into a planar lipid bilayer*. *Cell biochemistry and biophysics*, 2004. **41**(1): p. 11-23.
104. Woodbury, D.J. and K. Rognlien, *The t-SNARE syntaxin is sufficient for spontaneous fusion of synaptic vesicles to planar membranes*. *Cell biology international*, 2000. **24**(11): p. 809-818.
105. Chanturiya, A., L.V. Chernomordik, and J. Zimmerberg, *Flickering fusion pores comparable with initial exocytotic pores occur in protein-free phospholipid bilayers*. *Proceedings of the National Academy of Sciences*, 1997. **94**(26): p. 14423.
106. Staal, R.G.W., E.V. Mosharov, and D. Sulzer, *Dopamine neurons release transmitter via a flickering fusion pore*. *Nature neuroscience*, 2004. **7**(4): p. 341-346.
107. Breckenridge, L. and W. Almers, *Final steps in exocytosis observed in a cell with giant secretory granules*. *Proceedings of the National Academy of Sciences*, 1987. **84**(7): p. 1945.
108. Zhou, Z., S. Misler, and R.H. Chow, *Rapid fluctuations in transmitter release from single vesicles in bovine adrenal chromaffin cells*. *Biophysical journal*, 1996. **70**(3): p. 1543-1552.
109. He, L. and L.-G. Wu, *The debate on the kiss-and-run fusion at synapses*. *Trends in neurosciences*, 2007. **30**(9): p. 447-455.
110. He, L., et al., *Two modes of fusion pore opening revealed by cell-attached recordings at a synapse*. *Nature*, 2006. **444**(7115): p. 102-105.
111. Klyachko, V.A. and M.B. Jackson, *Capacitance steps and fusion pores of small and large-dense-core vesicles in nerve terminals*. *Nature*, 2002. **418**(6893): p. 89-92.
112. Albillos, A., et al., *The exocytotic event in chromaffin cells revealed by patch amperometry*. *Nature*, 1997. **389**(6650): p. 509-512.
113. Fulop, T., S. Radabaugh, and C. Smith, *Activity-Dependent Differential Transmitter Release in Mouse Adrenal Chromaffin Cells*. *The Journal of Neuroscience*, 2005. **25**(32): p. 7324-7332.

114. An, S. and D. Zenisek, *Regulation of exocytosis in neurons and neuroendocrine cells*. Current opinion in neurobiology, 2004. **14**(5): p. 522-530.
115. Mohrmann, R., et al., *Fast vesicle fusion in living cells requires at least three SNARE complexes*. Science, 2010. **330**(6003): p. 502.
116. Breckenridge, L. and W. Almers, *Currents through the fusion pore that forms during exocytosis of a secretory vesicle*. Nature, 1987. **328**(6133): p. 814-817.
117. Spruce, A., et al., *Properties of the fusion pore that forms during exocytosis of a mast cell secretory vesicle*. Neuron, 1990. **4**(5): p. 643-654.
118. Alabi, A.A. and R.W. Tsien, *Perspectives on Kiss-and-Run: Role in Exocytosis, Endocytosis, and Neurotransmission*. Annual Review of Physiology, 2013. **75**(1): p. 393-422.
119. Wightman, R.M. and C.L. Haynes, *Synaptic vesicles really do kiss and run*. Nature neuroscience, 2004. **7**(4): p. 321-321.
120. Lisman, J.E., S. Raghavachari, and R.W. Tsien, *The sequence of events that underlie quantal transmission at central glutamatergic synapses*. Nature Reviews Neuroscience, 2007. **8**(8): p. 597-609.
121. Fang, Q.H., et al., *The role of the C terminus of the SNARE protein SNAP-25 in fusion pore opening and a model for fusion pore mechanics*. Proceedings of the National Academy of Sciences of the United States of America, 2008. **105**(40): p. 15388-15392.
122. Breckenridge, W.C., G. Gombos, and I.G. Morgan, *The lipid composition of adult rat brain synaptosomal plasma membranes*. Biochimica et Biophysica Acta (BBA) - Biomembranes, 1972. **266**(3): p. 695-707.
123. Traynor, A.E., D. Schubert, and W.R. Allen, *Alterations of Lipid Metabolism in Response to Nerve Growth Factor*. Journal of Neurochemistry, 1982. **39**(6): p. 1677-1683.
124. Linetti, A., et al., *Cholesterol reduction impairs exocytosis of synaptic vesicles*. Journal of cell science, 2010. **123**(4): p. 595-605.
125. Wang, N., et al., *Influence of cholesterol on catecholamine release from the fusion pore of large dense core chromaffin granules*. The Journal of Neuroscience, 2010. **30**(11): p. 3904-3911.
126. Zhang, Z. and M.B. Jackson, *Membrane Bending Energy and Fusion Pore Kinetics in Ca<sup>2+</sup>-Triggered Exocytosis*. Biophysical journal, 2010. **98**(11): p. 2524-2534.
127. Tong, J., et al., *A scissors mechanism for stimulation of SNARE-mediated lipid mixing by cholesterol*. Proceedings of the National Academy of Sciences, 2009. **106**(13): p. 5141.
128. Biswas, S., et al., *Cholesterol Promotes Hemifusion and Pore Widening in Membrane Fusion Induced by Influenza Hemagglutinin*. The Journal of General Physiology, 2008. **131**(5): p. 503-513.
129. Ritchie, T., et al., *Reconstitution of membrane proteins in phospholipid bilayer nanodiscs*. Methods in enzymology, 2009. **464**: p. 211-231.
130. Frauenfeld, J., et al., *Cryo-EM structure of the ribosome–SecYE complex in the membrane environment*. Nature structural & molecular biology, 2011. **18**(5): p. 614-621.

131. Katayama, H., et al., *Three-dimensional structure of the anthrax toxin pore inserted into lipid nanodiscs and lipid vesicles*. Proceedings of the National Academy of Sciences, 2010. **107**(8): p. 3453-3457.
132. Karatekin, E. and J.E. Rothman, *Fusion of single proteoliposomes with planar, cushioned bilayers in microfluidic flow cells*. Nature Protocols, 2012. **7**(5): p. 903-920.
133. Ginsberg, L., *Does Ca<sup>2+</sup> cause fusion or lysis of unilamellar lipid vesicles?* Nature, 1978. **275**(5682): p. 758-760.
134. Ohki, S., *A mechanism of divalent ion-induced phosphatidylserine membrane fusion*. Biochimica et Biophysica Acta (BBA) - Biomembranes, 1982. **689**(1): p. 1-11.
135. Ohki, S. and H. Ohshima, *Divalent cation-induced phosphatidic acid membrane fusion. Effect of ion binding and membrane surface tension*. Biochimica et Biophysica Acta (BBA)-Biomembranes, 1985. **812**(1): p. 147-154.
136. Wilschut, J. and D. Papahadjopoulos, *Ca<sup>2+</sup>-induced fusion of phospholipid vesicles monitored by mixing of aqueous contents*. Nature, 1979. **281**(5733): p. 690-692.
137. Bentz, J., et al., *On the correlation between HII phase and the contact-induced destabilization of phosphatidylethanolamine-containing membranes*. Proceedings of the National Academy of Sciences, 1985. **82**(17): p. 5742-5745.
138. Akabas, M.H., F.S. Cohen, and A. Finkelstein, *Separation of the osmotically driven fusion event from vesicle-planar membrane attachment in a model system for exocytosis*. The Journal of Cell Biology, 1984. **98**(3): p. 1063-1071.
139. Chernomordik, L., et al., *The hemifusion intermediate and its conversion to complete fusion: regulation by membrane composition*. Biophysical journal, 1995. **69**(3): p. 922-929.
140. Kozlovsky, Y. and M.M. Kozlov, *Stalk Model of Membrane Fusion: Solution of Energy Crisis*. Biophysical journal, 2002. **82**(2): p. 882-895.
141. Kachar, B., N. Fuller, and R. Rand, *Morphological responses to calcium-induced interaction of phosphatidylserine-containing vesicles*. Biophysical journal, 1986. **50**(5): p. 779-788.
142. Nikolaus, J., et al., *Direct Visualization of Large and Protein-Free Hemifusion Diaphragms*. Biophysical journal, 2010. **98**(7): p. 1192-1199.
143. Rand, R., B. Kachar, and T.S. Reese, *Dynamic morphology of calcium-induced interactions between phosphatidylserine vesicles*. Biophysical Journal, 1985. **47**(4): p. 483-489.
144. Evans, E., et al., *Dynamic tension spectroscopy and strength of biomembranes*. Biophysical journal, 2003. **85**(4): p. 2342-2350.
145. Miklavc, P., et al., *Existence of exocytotic hemifusion intermediates with a lifetime of up to seconds in type II pneumocytes*. Biochemical Journal, 2009. **424**: p. 7-14.
146. Reese, C., F. Heise, and A. Mayer, *Trans-SNARE pairing can precede a hemifusion intermediate in intracellular membrane fusion*. Nature, 2005. **436**(7049): p. 410-414.
147. Zampighi, G.A., et al., *Conical Electron Tomography of a Chemical Synapse: Vesicles Docked to the Active Zone are Hemi-Fused*. Biophysical Journal, 2006. **91**(8): p. 2910-2918.

148. Wong, J.L., et al., *Membrane hemifusion is a stable intermediate of exocytosis*. *Developmental cell*, 2007. **12**(4): p. 653-659.
149. Da Silva, P.P. and M.L. Nogueira, *Membrane fusion during secretion*. *Journal of Cell Biology*, 1977. **73**: p. 161-181.
150. Palade, G. and R. Bruns, *Structural modulations of plasmalemmal vesicles*. *The Journal of Cell Biology*, 1968. **37**(3): p. 633-649.
151. Curran, M.J., et al., *Exocytotic fusion pores exhibit semi-stable states*. *The Journal of Membrane Biology*, 1993. **133**(1): p. 61-75.
152. Yifrach, O. and R. MacKinnon, *Energetics of Pore Opening in a Voltage-Gated K<sup>+</sup> Channel*. *Cell*, 2002. **111**(2): p. 231-239.
153. Chizmadzhev, Y.A., et al., *Membrane mechanics can account for fusion pore dilation in stages*. *Biophysical journal*, 1995. **69**(6): p. 2489-2500.
154. Axelrod, D., *Total Internal Reflection Fluorescence Microscopy*, in *Methods in Cell Biology*, J.C. Dr. John and Dr. H. William Detrich, III, Editors. 2008, Academic Press. p. 169-221.
155. Smith, M.B., et al., *Interactive, Computer-Assisted Tracking of Speckle Trajectories in Fluorescence Microscopy: Application to Actin Polymerization and Membrane Fusion*. *Biophysical journal*, 2011. **101**(7): p. 1794-1804.
156. Chernomordik, L.V., G.B. Melikyan, and Y.A. Chizmadzhev, *Biomembrane fusion: a new concept derived from model studies using two interacting planar lipid bilayers*. *Biochimica et biophysica acta*, 1987. **906**(3): p. 309-352.
157. Cremona, O. and P. De Camilli, *Phosphoinositides in membrane traffic at the synapse*. *Journal of Cell Science*, 2001. **114**(6): p. 1041-1052.
158. Honigsmann, A., et al., *Phosphatidylinositol 4,5-bisphosphate clusters act as molecular beacons for vesicle recruitment*. *Nature Structural & Molecular Biology*, 2013. **20**(6): p. 679-686.
159. Durning, C. and B. O'Shaughnessy, *Diffusion controlled reactions at an interface*. *The Journal of chemical physics*, 1988. **88**(11): p. 7117-7128.
160. Razinkov, V.I., G.B. Melikyan, and F.S. Cohen, *Hemifusion between cells expressing hemagglutinin of influenza virus and planar membranes can precede the formation of fusion pores that subsequently fully enlarge*. *Biophysical journal*, 1999. **77**(6): p. 3144-3151.
161. Lang, T., et al., *SNAREs are concentrated in cholesterol-dependent clusters that define docking and fusion sites for exocytosis*. *EMBO journal*, 2001. **20**(9): p. 2202-2213.
162. Barg, S., et al., *Syntaxin clusters assemble reversibly at sites of secretory granules in live cells*. *Proceedings of the National Academy of Sciences*, 2010. **107**(48): p. 20804-20809.
163. van den Bogaart, G., et al., *Membrane protein sequestering by ionic protein-lipid interactions*. *Nature*, 2011. **479**(7374): p. 552-555.
164. Chen, Z. and R. Rand, *The influence of cholesterol on phospholipid membrane curvature and bending elasticity*. *Biophysical journal*, 1997. **73**(1): p. 267-276.
165. Hung, W.-C., et al., *The Condensing Effect of Cholesterol in Lipid Bilayers*. *Biophysical journal*, 2007. **92**(11): p. 3960-3967.

166. Wagner, M.L. and L.K. Tamm, *Reconstituted syntaxin1a/SNAP25 interacts with negatively charged lipids as measured by lateral diffusion in planar supported bilayers*. Biophysical journal, 2001. **81**(1): p. 266-275.
167. Axelrod, D., *Total internal reflection fluorescence microscopy*. Methods in cell biology, 1989. **30**: p. 245-270.
168. Jackson, M.B., *Minimum membrane bending energies of fusion pores*. Journal of Membrane Biology, 2009. **231**(2-3): p. 101-115.
169. Helfrich, W., *Elastic properties of lipid bilayers: theory and possible experiments*. Z. Naturforsch. c, 1973. **28**(11): p. 693-703.
170. Fuller, N., C.R. Benatti, and R. Peter Rand, *Curvature and bending constants for phosphatidylserine-containing membranes*. Biophysical journal, 2003. **85**(3): p. 1667-1674.
171. Domanska, M., et al., *Single vesicle millisecond fusion kinetics reveals number of SNARE complexes optimal for fast SNARE-mediated membrane fusion*. Journal of Biological Chemistry, 2009. **284**(46): p. 32158.
172. Cohen, F. and G. Melikyan, *The energetics of membrane fusion from binding, through hemifusion, pore formation, and pore enlargement*. Journal of Membrane Biology, 2004. **199**(1): p. 1-14.
173. Lee, J.K. and B.R. Lentz, *Secretory and viral fusion may share mechanistic events with fusion between curved lipid bilayers*. Proceedings of the National Academy of Sciences, 1998. **95**(16): p. 9274-9279.
174. Lee, J.Y. and M. Schick, *Calculation of Free Energy Barriers to the Fusion of Small Vesicles*. Biophysical Journal, 2008. **94**(5): p. 1699-1706.
175. Siegel, D.P., *The Gaussian Curvature Elastic Energy of Intermediates in Membrane Fusion*. Biophysical Journal, 2008. **95**(11): p. 5200-5215.
176. van den Bogaart, G., et al., *One SNARE complex is sufficient for membrane fusion*. Nature Structural & Molecular Biology, 2010. **17**(3): p. 358-364.
177. Hernandez, J.M., et al., *Variable cooperativity in SNARE-mediated membrane fusion*. Proceedings of the National Academy of Sciences, 2014. **111**(33): p. 12037-12042.
178. McNew, J.A., et al., *Close Is Not Enough*. The Journal of Cell Biology, 2000. **150**(1): p. 105.
179. Risselada, H.J., C. Kutzner, and H. Grubmüller, *Caught in the Act: Visualization of SNARE-Mediated Fusion Events in Molecular Detail*. ChemBioChem, 2011. **12**(7): p. 1049-1055.
180. Langosch, D., et al., *Peptide mimics of SNARE transmembrane segments drive membrane fusion depending on their conformational plasticity*. Journal of molecular biology, 2001. **311**(4): p. 709-721.
181. Knecht, V. and H. Grubmüller, *Mechanical coupling via the membrane fusion SNARE protein syntaxin 1A: a molecular dynamics study*. Biophysical journal, 2003. **84**(3): p. 1527-1547.
182. Hanson, P.I., J.E. Heuser, and R. Jahn, *Neurotransmitter release—four years of SNARE complexes*. Current opinion in neurobiology, 1997. **7**(3): p. 310-315.
183. Sutton, R.B., et al., *Crystal structure of a SNARE complex involved in synaptic exocytosis at 2.4 Å resolution*. Nature, 1998. **395**(6700): p. 347-353.

184. Kim, C.S., D.-H. Kweon, and Y.-K. Shin, *Membrane topologies of neuronal SNARE folding intermediates*. *Biochemistry*, 2002. **41**(36): p. 10928-10933.
185. McNew, J.A., et al., *The length of the flexible SNAREpin juxtamembrane region is a critical determinant of SNARE-dependent fusion*. *Molecular cell*, 1999. **4**(3): p. 415-421.
186. Kesavan, J., M. Borisovska, and D. Bruns, *v-SNARE Actions during Ca<sup>2+</sup>-Triggered Exocytosis*. *Cell*, 2007. **131**(2): p. 351-363.
187. Guzman, R.E., et al., *SNARE force synchronizes synaptic vesicle fusion and controls the kinetics of quantal synaptic transmission*. *The Journal of Neuroscience*, 2010. **30**(31): p. 10272-10281.
188. Xu, H., et al., *A lipid-anchored SNARE supports membrane fusion*. *Proceedings of the National Academy of Sciences*, 2011. **108**(42): p. 17325-17330.
189. Zhou, P., et al., *Lipid-anchored SNAREs lacking transmembrane regions fully support membrane fusion during neurotransmitter release*. *Neuron*, 2013. **80**(2): p. 470-483.
190. Israelachvili, J.N., *Intermolecular and surface forces: revised third edition*. 2011: Academic press.
191. Rand, R. and V. Parsegian, *Hydration Forces Between Phospholipid Bilayers*. *Biochimica et Biophysica Acta*, 1989. **988**(3): p. 351-376.
192. Leckband, D. and J. Israelachvili, *Intermolecular forces in biology*. *Quarterly Reviews of Biophysics*, 2001. **34**(02): p. 105.
193. Rand, R. and V. Parsegian, *Hydration forces between phospholipid bilayers*. *Biochimica et Biophysica Acta (BBA)-Reviews on Biomembranes*, 1989. **988**(3): p. 351-376.
194. Guo, T., L.-C. Gong, and S.-F. Sui, *An electrostatically preferred lateral orientation of SNARE complex suggests novel mechanisms for driving membrane fusion*. *PloS one*, 2010. **5**(1): p. e8900.
195. Cotman, C.W., et al., *Lipid composition of synaptic plasma membranes isolated from rat brain by zonal centrifugation*. *Biochemistry*, 1969. **8**(11): p. 4606-4612.
196. Wong, J.Y., et al., *Polymer-Cushioned Bilayers. II. An Investigation of Interaction Forces and Fusion Using the Surface Forces Apparatus*. *Biophysical journal*, 1999. **77**(3): p. 1458-1468.
197. Zhang, F., et al., *SNARE assembly and membrane fusion, a kinetic analysis*. *Journal of Biological Chemistry*, 2004. **279**(37): p. 38668-38672.
198. Shin, J., et al., *Multiple conformations of a single SNAREpin between two nanodisc membranes reveal diverse pre-fusion states*. *Biochemical Journal*, 2014. **459**(1): p. 95-102.